Supporting Information

Template-Directed Synthesis of a Conjugated Zinc Porphyrin Nanoball

Jonathan Cremers,[†] Renee Haver,[†] Michel Rickhaus,[†] Juliane Q. Gong,[‡] Ludovic Favereau,[†] Martin D. Peeks,[†] Tim D. W. Claridge,[†] Laura M. Herz,[‡] and Harry L. Anderson*,[†]

[‡]Clarendon Laboratory, Department of Physics, University of Oxford, Oxford, OX1 3PU, United Kingdom

[†]Chemistry Research Laboratory, Department of Chemistry, University of Oxford, Oxford, OX1 3TA, United Kingdom

*harry.anderson@chem.ox.ac.uk

Table of Contents

A. General Methods

Dry toluene and THF were obtained by passing the solvents through columns of alumina, under nitrogen. Diisopropylamine (i-Pr$_2$NH) was distilled from CaH$_2$ and kept over activated molecular sieves (3 Å, 8–12 mesh). Unless specified otherwise, all other solvents were used as commercially supplied. Flash chromatography was carried out on silica gel 60 under positive pressure. Analytical thin-layer chromatography was carried out on aluminum-backed silica gel 60 F254 plates. Visualization was achieved using UV light when necessary.

All UV-vis-NIR spectra were recorded in solution using a Perkin-Lambda 20 spectrometer (1 cm path length quartz cell). Chloroform (containing ca. 0.5% ethanol as stabilizer) or toluene was used for all titrations without any further purification.

Unless stated otherwise, ^{1}H/^{13}C NMR spectra were recorded at 298 K using a Bruker AV400 (400/100 MHz) or Bruker AV700 (700/175 MHz) instrument. ^{1}H and ^{13}C NMR spectra are reported in ppm; coupling constants are given in Hertz, to the nearest 0.1 Hz. The solvent used was CDCl$_3$ which was calibrated to residual CHCl$_3$ at 7.27 ppm. Diffusion coefficients were measured at 298 K in CDCl$_3$ using a double stimulated echo sequence for convection compensation. The hydrodynamic radius was estimated from the diffusion coefficient using the Stoke-Einstein equation with a viscosity for CDCl$_3$ at 298 K of 5.28×10^{-4} Kg m^{-1} s^{-1}.

MALDI-ToF spectra were measured at the EPSRC National Mass Spectrometry service (Swansea) using the Applied Biosystems Voyager DE-STR or at the University of Oxford using Waters MALDI Micro MX spectrometer utilizing dithranol as a matrix.

Size exclusion chromatography (SEC) was carried out using Bio-Beads S-X1, 200-400 mesh (Bio Rad). Analytical GPC was carried out using JAIGEL-3H-A (8φ×500) and JAIGEL-4H-A (8φ×500) columns in THF/1% pyridine or toluene as eluent with a flow rate of 1.0 mL/min. Analytical and semi-preparative GPC were also carried out on a Shimadzu Recycling GPC system equipped with a LC-20 AD pump, SPD-20A UV detector and a set of JAIGEL 3H (20 × 600 mm) and JAIGEL 4H (20 × 600 mm) columns in toluene/1% pyridine as the eluent at a flow rate of 3.5 mL/min.

B. Synthetic Procedures

Porphyrin ring (2)
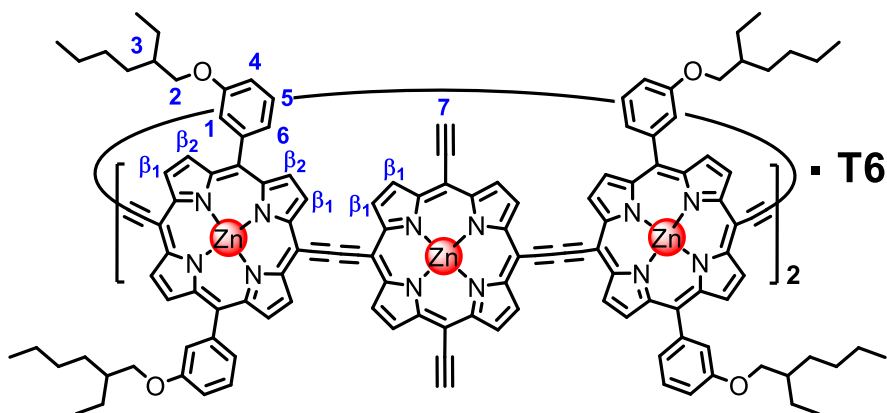
Porphyrin ring *c*-P6·T6 (1)[1,2] (15.0 mg, 2.56 μmol) was dissolved in CH_2Cl_2 (3 mL). Tetra-*n*-butylammonium fluoride (0.41 mL, 1.0 M solution in THF, 0.41 mmol) was added and the reaction mixture was stirred for 15 min. The crude reaction mixture was purified by silica column chromatography ($CHCl_3$) followed by size exclusion chromatography on Biobeads SX-1 (toluene, 1% pyridine) to yield the title compound as a red solid (11.7 mg, 87%).

¹H NMR (400 MHz, $CDCl_3$, 298 K): δ_H (ppm) 9.60-9.53 (16H, m, β_1), 9.51 (8H, d, *J* = 4.5 Hz, β_1), 9.47 (8H, d, *J* = 4.5 Hz, β_1), 8.86-8.78 (16H, m, β_2), 7.82-7.16 (32H, m, H1, H4, H5 and H6), 5.57-5.34 (24H, m, T6), 5.04-4.88 (12H, m, T6), 4.18 (4H, s, H7), 4.17-3.97 (16H, m, H2), 2.32-2.17 (12H, m, T6), 1.93-0.79 (112H, m, H3).

MALDI-TOF: *m/z* = 5245 ($C_{336}H_{268}N_{30}O_8Zn_6$, M^+ requires 5246).
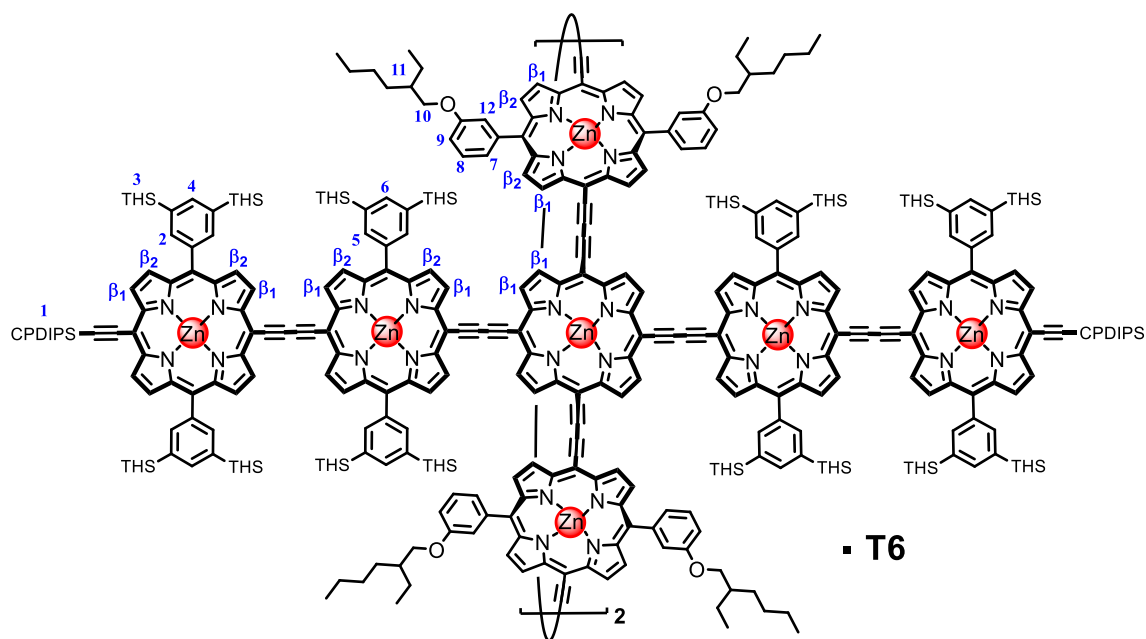
λ_{max} **($CHCl_3$) / nm log(ε)**: 489 (5.44), 757 (5.24), 792 (5.38), 833 (5.39).

Mono-protected THS-dimer (3)
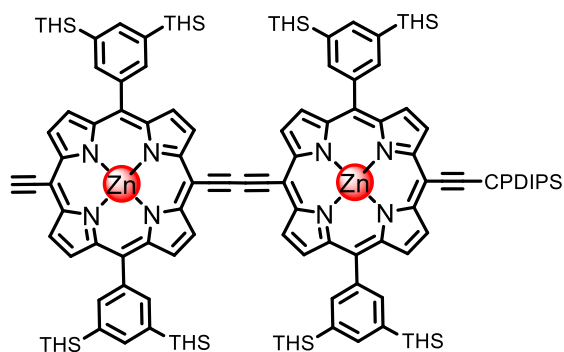
The mono-deprotected THS-dimer was prepared as reported previously.[3] Structure shown above for clarification.

Ball precursor *c*-P6(*l*-P2)₄·T6 (4)

Porphyrin ring **2** (6.6 mg, 1.26 μmol) and dimer (**3**) (181.5 mg, 50.59 μmol) were dissolved in toluene (10 mL). A catalyst solution was prepared by dissolving PdCl$_2$(PPh$_3$)$_2$ (4.2 mg, 5.94 μmol), CuI (4.2 mg, 21.88 μmol) and 1,4-benzoquinone (12.3 mg, 0.114 mmol) in toluene (3 mL) and *i*-Pr$_2$NH (0.25 mL). The catalyst solution was added to the porphyrin solution and the reaction mixture was stirred at room temperature for 35 min. The crude reaction mixture was purified by silica column chromatography (toluene), size exclusion column on Biobeads SX-1 (toluene, 1% pyridine) and finally recycling GPC (toluene, 1% pyridine) to yield the title compound as a red solid (10.0 mg, 41%).

^{1}H NMR (400 MHz, CDCl$_3$, 298 K): δ$_H$ (ppm) 9.99-9.90 (24H, m, β$_1$), 9.79-9.54 (40H, m, β$_1$), 9.08-8.78 (48H, m, β$_2$), 8.38 (16H, m, H2 or H5), 8.30 (16H, m, H2 or H5), 8.09 (8H, m, H4 or H6), 8.04 (8H, m, H4 or H6), 7.78 (8H, m, H9 or H12), 7.66-7.54 (16H, m, (H9 or H12) and H8), 7.31 (8H, m, H7), 5.67-5.46 (24H, m, T6), 5.17 (4H, m, T6), 5.04 (8H, m, T6), 4.16-3.96 (16H, m, H10), 2.68 (4H, m, T6), 2.58 (8H, t, J = 6.7 Hz, H1), 2.30 (8H, m, T6), 2.24 (8H, m, H1), 1.91-0.63 (1424H, m, H1 and H3 and H11).

MALDI-TOF: m/z = 19600 (C$_{1240}$H$_{1704}$N$_{66}$O$_8$Si$_{36}$Zn$_{14}$, M$^+$ requires 19590).

λ_{max} **(CHCl$_3$) / nm log(ε)**: 456 (6.25), 493 (6.08), 768 (5.79), 806 (5.93), 847 (5.93).
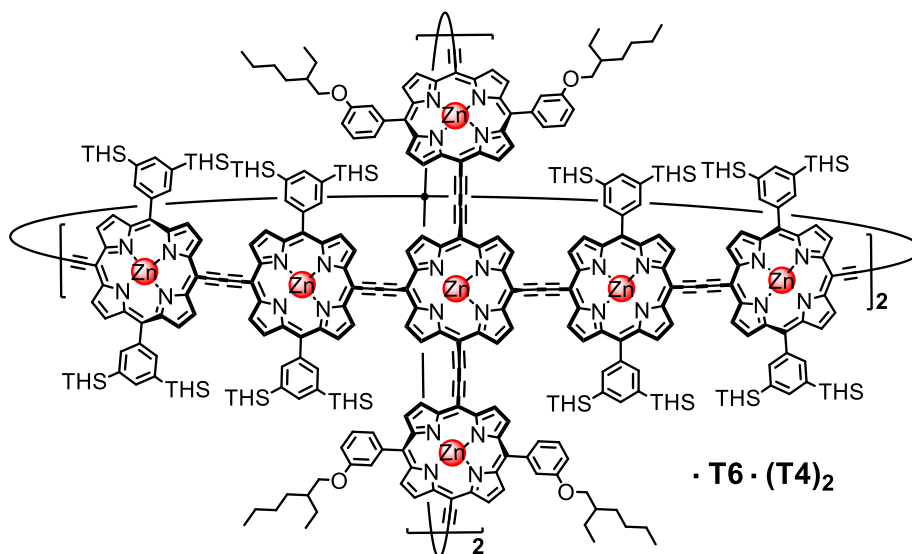
Ball precursor (5)
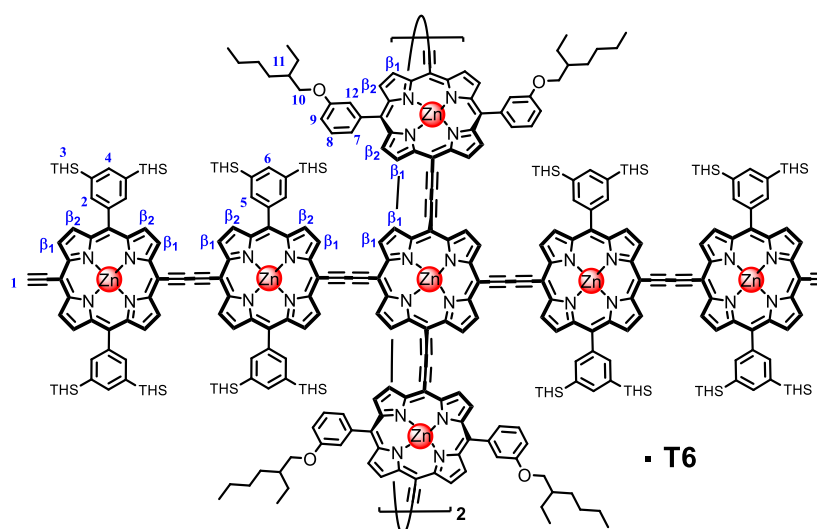
Ball precursor 4 (10.0 mg, 0.51 μmol) was dissolved in CH$_2$Cl$_2$ (2 mL). Tetra-*n*-butylammonium fluoride (82 μL, 1.0 M solution in THF, 82 μmol) was added and the reaction was stirred for 15 min. The crude reaction mixture was purified by silica column chromatography (CHCl$_3$) followed by size exclusion chromatography on Biobeads SX-1 (toluene, 1% pyridine) to yield the title compound as a red solid (9.6 mg, 97%).

^{1}H NMR (400 MHz, CDCl$_3$, 298 K): δ$_H$ (ppm) 9.99-9.88 (24H, m, β$_1$), 9.78-9.53 (40H, m, β$_1$), 9.08-8.77 (48H, m, β$_2$), 8.38 (16H, m, H2 or H5), 8.31 (16H, m, H2 or H5), 8.09 (8H, m, H4 or H6), 8.04 (8H, m, H4 or H6), 7.78 (8H, m, H9 or H12), 7.66-7.54 (16H, m, (H9 or H12) and H8), 7.31 (8H, m, H7), 5.68-5.45 (24H, m, T6), 5.16 (4H, m, T6), 5.04 (8H, m, T6), 4.20 (4H, s, H1), 4.15-3.95 (16H, m, H10), 2.68 (4H, m, T6), 2.31 (8H, m, T6), 1.91-0.63 (1360H, m, H3 and H11).

MALDI-TOF: m/z = 18899 (C$_{1200}$H$_{1628}$N$_{62}$O$_8$Si$_{32}$Zn$_{14}$, M$^+$ requires 18864).

λ_{max} **(CHCl$_3$) / nm log(ε)**: 455 (5.98), 493 (5.85), 768 (5.53), 806 (5.69), 846 (5.70).

Porphyrin ball *b*-P14·T6·(T4)$_2$

· T6 · (T4)$_2$

Ball precursor **5** (9.6 mg, 0.51 μmol) and template **T4** (0.86 mg, 1.02 μmol) were dissolved in CHCl$_3$ (4.4 mL). UV-vis indicated the formation of the desired 1:2 complex. A catalyst solution was prepared by dissolving Pd(PPh$_3$)$_2$Cl$_2$ (0.88 mg, 1.25 μmol), CuI (1.20 mg, 6.28 μmol) and 1,4-benzoquinone (2.78 mg, 25.74 μmol) in CHCl$_3$ (0.6 mL) and freshly distilled *i*-Pr$_2$NH (8.3 μL). This solution was added to the reaction mixture, which was stirred vigorously at room temperature for 16 h. The crude reaction mixture was purified by silica column chromatography (CHCl$_3$), size exclusion column on Biobeads SX-1 (toluene, 1% pyridine) and finally recycling GPC (toluene, 1% pyridine) to yield the title compound as a red solid (5.3 mg, 51%).

^{1}H NMR (700 MHz, CDCl$_3$, 298 K): δ$_H$ (ppm) 9.79 (8H, s, **l**), 9.66 (8H, m, **g**), 9.65 (16H, m, **f+m**), 9.63 (8H, m, **a**), 9.59 (5H, m, **o***), 9.57 (11H, m, **n+o**) 9.51 (8H, s, **w+w***), 8.95 (8H, s, **k**), 8.86 (8H, m, **h**), 8.83 (16H, m, **b+e**), 8.80 (8H, m, **p+p***), 8.76 (8H, m, **v+v***), 8.47 (8H, s, **c**), 8.43 (8H, m, **i**), 8.20 (8H, m, **i'**), 8.11 (8H, m, **j**), 8.06 (16H, s, **c'+d**), 7.71 (5H, m, **q***), 7.66-7.60 (9H, m, **q+r+u**), 7.55 (5H, m, **u***), 7.51 (5H, m, **r***),

7.29 (8H, m, **s+s***), 5.85 (44H, m, **δ1+δ2+γ2+Ph**), 5.68 (8H, m, **γ1**), 5.30 (32H, m, **β2+γ3+γ4+δ3+δ4**), 5.17 (8H, m, **β1**), 4.93 (4H, m, **β4**), 4.83 (8H, m, **β3**), 4.01 (16H, m, **t**), 2.61 (8H, m, **α2**), 2.45 (12H, m, **α1+α4**), 2.20 (8H, m, **α3**), 1.98-0.38 (1,368H, m, **THS+EtH**).

MALDI-TOF: m/z = 18861 ($C_{1200}H_{1624}N_{62}O_8Si_{32}Zn_{14}$ (***b*-P14·T6**), M$^+$ requires 18861), 17865 ($C_{1128}H_{1576}N_{56}O_8Si_{32}Zn_{14}$ (***b*-P14**), M$^+$ requires 17863).

λ_{max} **(toluene) / nm log(ε)**: 436 (5.87), 490 (6.00), 520 (5.91), 731 (5.44), 773 (5.73), 812 (5.85), 857 (5.96), 883 (6.16).
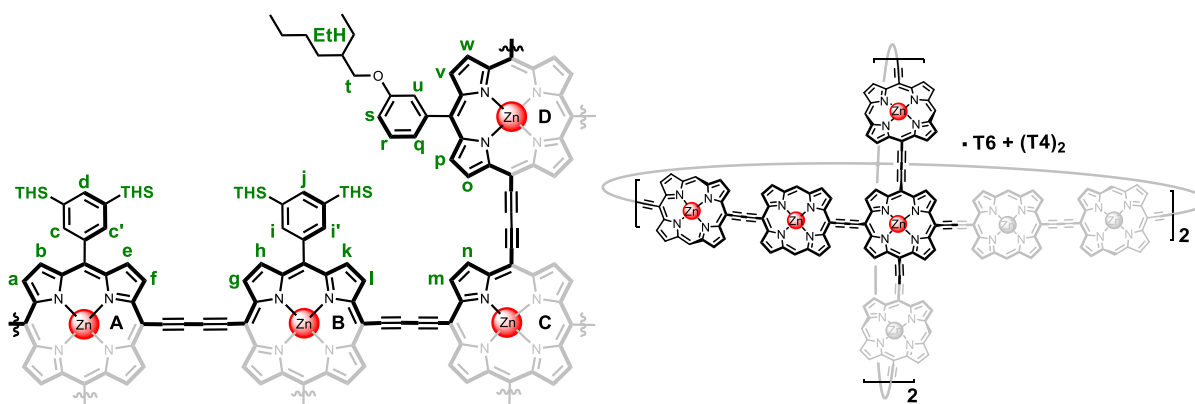

Figure S1: Symmetric unit of the porphyrins in *b*-P14·T6·(T4)₂ with proton labeling. Templates are not shown for clarity. Protons c and i point towards the center of the ball whereas c' and i' point outwards. There are two diastereomers of porphyrin D. As drawn the EtH chain is pointing towards the center of the ball, the signals with the EtH chain pointing outwards will be denoted with a *. (THS = trihexylsilyl; EtH = ethylhexyl).
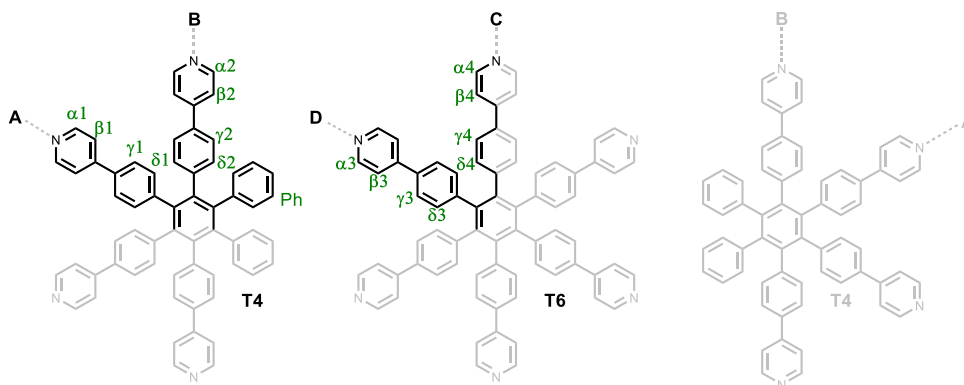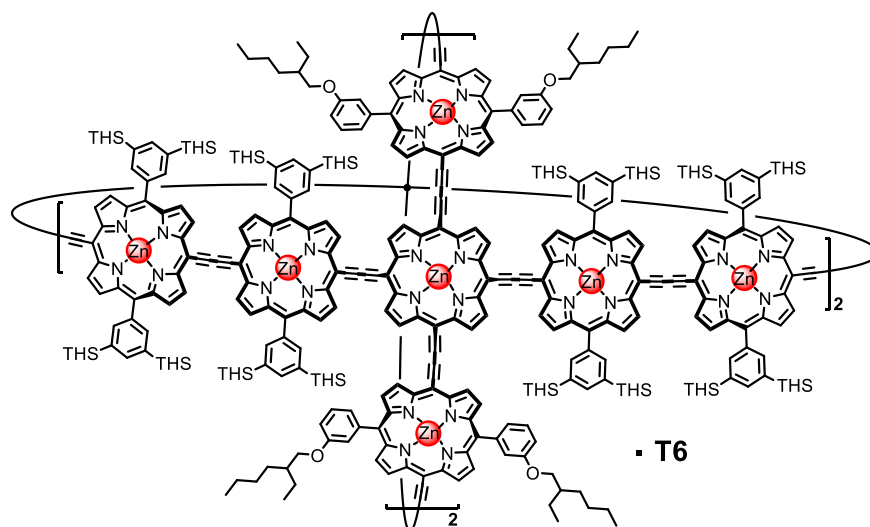

Figure S2: Symmetric unit of the templates within *b*-P14·T6·(T4)₂ with proton labeling.

Porphyrin ball *b*-P14·T6

Ball **b-P14·T6·(T4)₂** (2.0 mg, 0.10 μmol) was dissolved in toluene (0.4 mL) and pyridine (0.6 mL). The solution was passed over a size exclusion column with Biobeads SX-1 (toluene 40%, pyridine 60%). The colored porphyrin band was collected to yield the title compound as a red solid (1.8 mg, 98%).

^{1}H NMR (700 MHz, CDCl₃, 298 K): δ_H (ppm) 9.84 (8H, m, **l**), 9.76 (8H, m, **g**), 9.75 (8H, m, **f**), 9.70 (8H, m, **a**), 9.66 (8H, m, **m**), 9.55 (16H, m, **n+o**), 9.50 (8H, m, **w**), 8.95 (8H, m, **k**), 8.89 (8H, m, **h**), 8.87 (8H, m, **b+e**), 8.86 (8H, m, **b+e**), 8.76 (16H, m, **p+v**), 8.28 (16H, m, **i**), 8.24 (16H, m, **c**), 8.05 (8H, s, **j**), 8.03 (8H, s, **d**), 7.73-7.61 (8H, m, **q**), 7.61-7.46 (16H, m, **r+u**), 7.32-7.19 (8H, m, **s**), 5.41-5.26 (24H, m, **γ1+γ2+δ1+δ2**), 4.98 (4H, d, *J* = 7.5Hz, **β2**), 4.87 (8H, m, **β1**), 4.05-3.80 (16H, m, **t**), 2.53 (4H, m, **α2**), 2.22 (8H, m, **α1**), 1.88-0.32 (1,368H, m, **THS+EtH**).

MALDI-TOF: *m/z* = 18852 (C₁₂₀₀H₁₆₂₄N₆₂O₈Si₃₂Zn₁₄, M⁺ requires 18861).

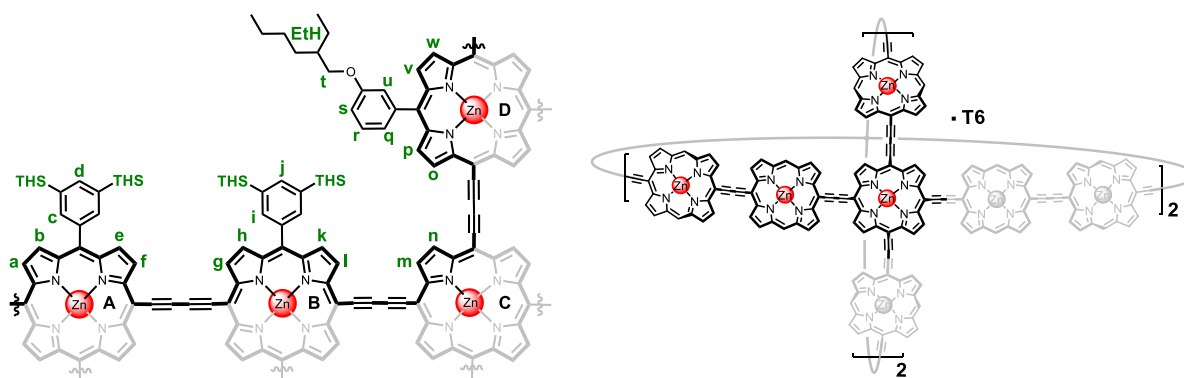λ_{max} **(toluene) / nm log(ε)**: 469 (6.03), 484 (6.02), 726 (5.49), 771 (5.75), 809 (5.89), 852 (5.96).

Figure S3: Symmetric unit of the porphyrins in *b*-P14·T6 with the corresponding proton labeling. Due to the removal of the T4 templates, porphyrins A and B can rotate. As a result, the signals corresponding to c and i are no longer split. Template is not shown for clarity (THS = trihexylsilyl; EtH = ethylhexyl). Right: meso-aryl groups omitted for clarity.

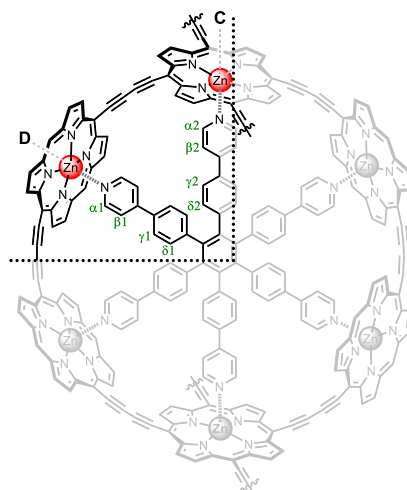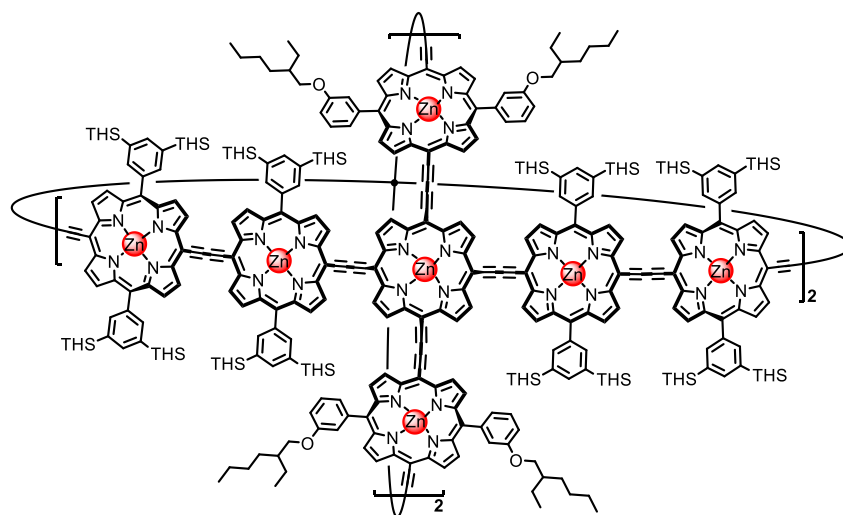**Figure S4: Symmetric unit of the template within _b_-P14·T6 with proton labeling. Only the 6-membered ring of the ball is shown and the aryl groups of the porphyrins have been omitted for clarity.**

Porphyrin ball _b_-P14

A size exclusion column (300 mm length, 10 mm diameter) with Biobeads SX-1 was prepared in toluene. The column was run with a toluene solution saturated with DABCO (~10% of the column length) in order to saturate the top of the column with DABCO. Ball _b_-**P14·T6·(T4)₂** (2.0 mg, 0.10 µmol) was dissolved in the DABCO saturated toluene solution (1 mL) and loaded on the column. The product was eluted with the toluene solution saturated with DABCO (~10% of the column length) followed by eluting with pure toluene. The colored porphyrin band was collected to yield the template-free ball with DABCO coordinating to the zinc centers. The solvent was removed and _b_-**P14·(DABCO)₁₄** was dissolved in toluene (0.4 mL) and pyridine (0.6 mL). The solution was passed over a size exclusion column with

Biobeads SX-1 (toluene 40%, pyridine 60%) in order to remove the DABCO. The colored porphyrin band was collected to yield the title compound as a red solid (1.5 mg, 86%).

^{1}H NMR (700 MHz, CDCl$_3$, 298 K): δ$_H$ (ppm) 9.85 (8H, m, **l**), 9.79-9.71 (16H, m, **f+g**), 9.71-9.60 (16H, m, **a+m**), 9.61 (8H, m, **n**), 9.60 (8H, d, *J* = 4.4 Hz, **o**), 9.56 (8H, d, *J* = 4.4 Hz, **w**), 8.95 (8H, m, **k**), 8.92-8.84 (24H, m, **b+e** and **h**), 8.78 (8H, d, *J* = 4.4 Hz, **p**), 8.76 (8H, d, *J* = 4.4 Hz, **v**), 8.27 (16H, m, **i**), 8.23 (16H, m, **c**), 8.01 (16H, s, **d+j**), 7.58 (8H, m, **q**), 7.52 (8H, s, **u**), 7.46 (8H, m, **r**), 7.15 (8H, d, *J* = 7.7 Hz, **s**), 3.84 (16H, m, **t**), 1.64-0.78 (1,368H, m, **THS+EtH**).

MALDI-TOF: *m/z* = 17893 (C$_{1128}$H$_{1576}$N$_{56}$O$_8$Si$_{32}$Zn$_{14}$, M$^+$ requires 17863).

λ_{max} **(toluene) / nm log(ε):** 466 (6.05), 753 (5.67), 789 (5.77), 831 (5.83), 856 (5.81).
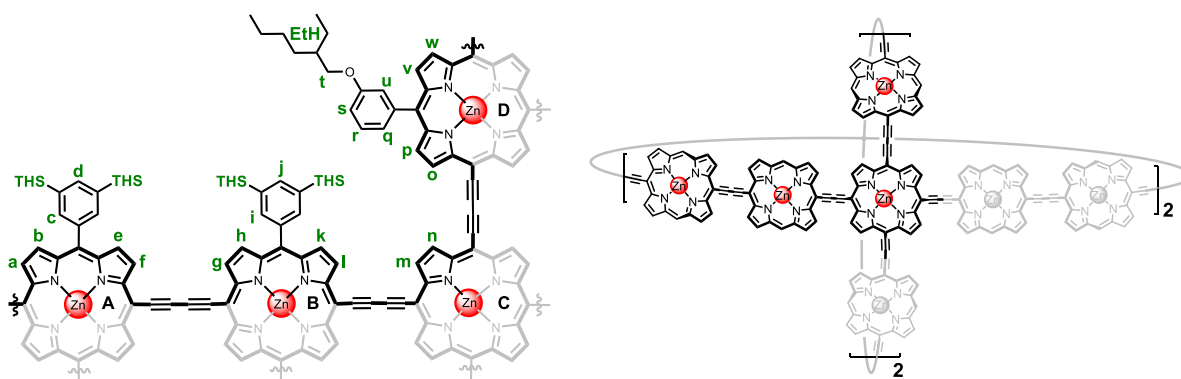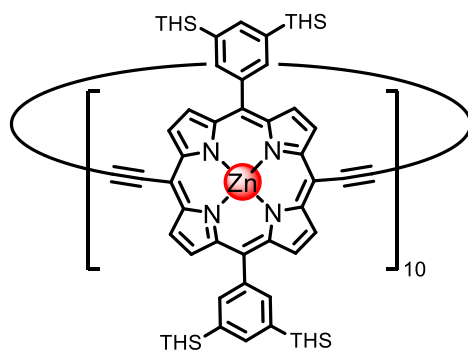

Figure S5: Symmetric unit of the porphyrins in *b*-P14 with the corresponding proton labeling. Template not shown for clarity (THS = trihexylsilyl; EtH = ethylhexyl).

Porphyrin ring *c*-P10

***c*-P10** was isolated as a byproduct in the synthesis of ***c*-P6·T6** from ***l*-P1** (0.8 g scale of monomer).[4] Residual template (**T6**) was removed by passage over a SEC column (20% pyridine in toluene). The product was isolated a brown solid (19.2 mg, 2.3%).

^{1}H NMR (700 MHz, CDCl$_3$, 298 K): δ_H (ppm) 9.80 (40H, d, J = 4.6 Hz), 8.88 (40H, d, J = 4.6 Hz), 8.25 (40H, s), 7.99 (20H, s), 1.60-0.79 (1560H, m).

MALDI-TOF: m/z = 17241 (C$_{1080}$H$_{1700}$N$_{40}$Si$_{40}$Zn$_{10}$, M$^+$ requires 17019).

λ_{max} **(CH$_2$Cl$_2$) / nm log(ε)**: 471 (5.92), 495 (5.89), 598 (4.81), 821 (5.73).

C. ^{1}H-NMR Assignment of *b*-P14·T6·(T4)$_2$, *b*-P14·T6, and *b*-P14

In the following section, the full assignments of the ^{1}H-NMR spectra of the ball *b*-P14, with and without the templates **T6** and **T4**, are described. All ^{1}H-NMR spectra were recorded at 298 K using a Bruker AV700 (700/175 MHz) instrument with CDCl$_3$ as the solvent. The 2D-NMR techniques COSY and NOESY were used to achieve full assignment of the signals. COSY correlations are indicated in blue, both in the molecular structures and in the cross-peaks. NOESY correlations are indicated in red. In addition, 1D-NOESY experiments were carried out with increased mixing times to obtain NOESY correlations between protons across the butadiynes between the porphyrin units. Selective 1D-NOESY experiments were collected using single gradient spin-echoes employing 80 ms 180° selective Gaussian pulses. In situations where closely neighbouring resonances prevented clean selective excitation, 1D-NOESY sequences employing chemical shift selective filters were used. These were performed using 80 ms 180° selective Gaussian pulses with data collected over 16 incremented time steps for suppression of undesired signals and NOE mixing times of 300 or 500 ms.

The assignment of the nanostructure will be discussed systematically. By considering symmetry, the molecule has been split in four parts. First the signals corresponding to the central-porphyrin (C) are assigned, followed by the alkoxy-porphyrin (D) and the THS-porphyrins (A and B). Where relevant, the templates have been assigned last. High complexity is observed in the spectra as a result of the presence of rotamers (diastereomers) in which the **EtH** solubilizing groups can either point towards the center or periphery of the ball. Upon removal of the templates the spectra simplify due to free rotation of the porphyrins. In all three complexes (*b*-P14·T6·(T4)$_2$, *b*-P14·T6, and *b*-P14) the solubilizing groups (**THS** and **EtH**) on the aryls gave rise to an unresolved envelope of 1,368 protons resonating between 2.0 and 0.4 ppm which has not been characterized in detail. Various peaks in the ^{1}H-NMR spectra were found to be too broad to resolve the coupling pattern and are labeled as *multiplets* (m).
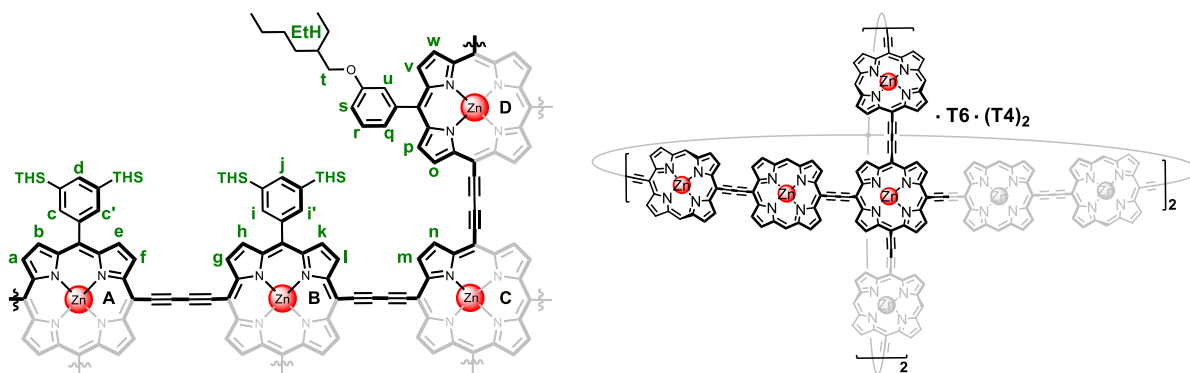
C.1 Assignment of *b*-P14·T6·(T4)₂

Figure S6: Symmetric unit of the porphyrins in *b*-P14·T6·(T4)₂ with proton labeling. Templates are not shown for clarity. Protons c and i point towards the center of the ball whereas c' and i' point outwards. There are two diastereomers of porphyrin D, as drawn the EtH group is pointing towards the center of the ball, the signals with the EtH group pointing outwards will be denoted with a *. (THS = trihexylsilyl; EtH = ethylhexyl).
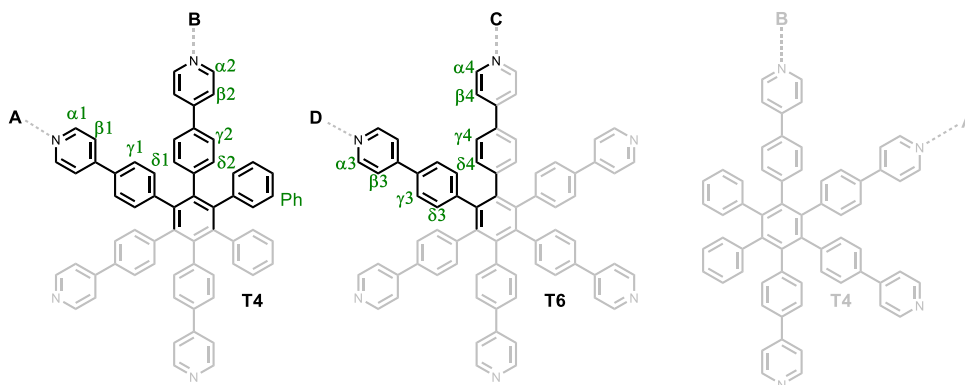

Figure S7: Symmetric unit of the templates within *b*-P14·T6·(T4)₂ with proton labeling.

¹H NMR (700 MHz, CDCl₃, 298 K): δ_H (ppm) 9.79 (8H, s, **l**), 9.66 (8H, m, **g**), 9.65 (16H, m, **f+m**), 9.63 (8H, m, **a**), 9.59 (5H, m, **o***), 9.57 (11H, m, **n+o**) 9.51 (8H, s, **w+w***), 8.95 (8H, s, **k**), 8.86 (8H, m, **h**), 8.83 (16H, m, **b+e**), 8.80 (8H, m, **p+p***), 8.76 (8H, m, **v+v***), 8.47 (8H, s, **c**), 8.43 (8H, m, **i**), 8.20 (8H, m, **i'**), 8.11 (8H, m, **j**), 8.06 (16H, s, **c'+d**), 7.71 (5H, m, **q***), 7.66-7.60 (9H, m, **q+r+u**), 7.55 (5H, m, **u***), 7.51 (5H, m, **r***), 7.29 (8H, m, **s+s***), 5.85 (44H, m, **δ1+δ2+γ2+Ph**), 5.68 (8H, m, **γ1**), 5.30 (32H, m, **β2+γ3+γ4+δ3+δ4**), 5.17 (8H, m, **β1**), 4.93 (4H, m, **β4**), 4.83 (8H, m, **β3**), 4.01 (16H, m, **t**), 2.61 (8H, m, **α2**), 2.45 (12H, m, **α1+α4**), 2.20 (8H, m, **α3**), 1.98-0.38 (1,368H, m, **THS+EtH**).
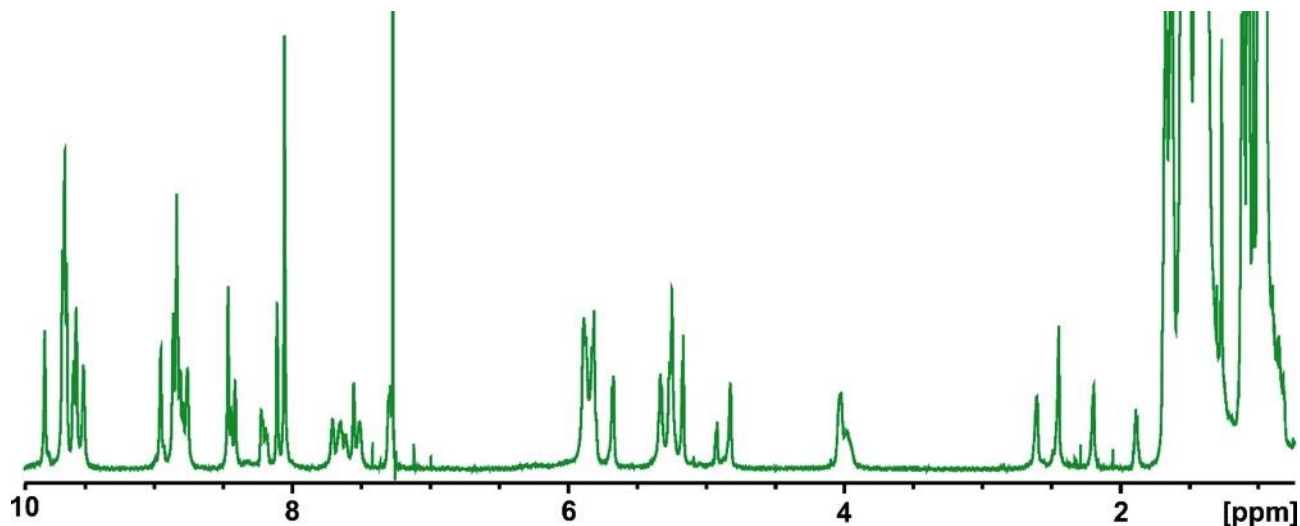
Figure S8: ¹H-NMR spectrum of *b*-P14·T6·(T4)₂.
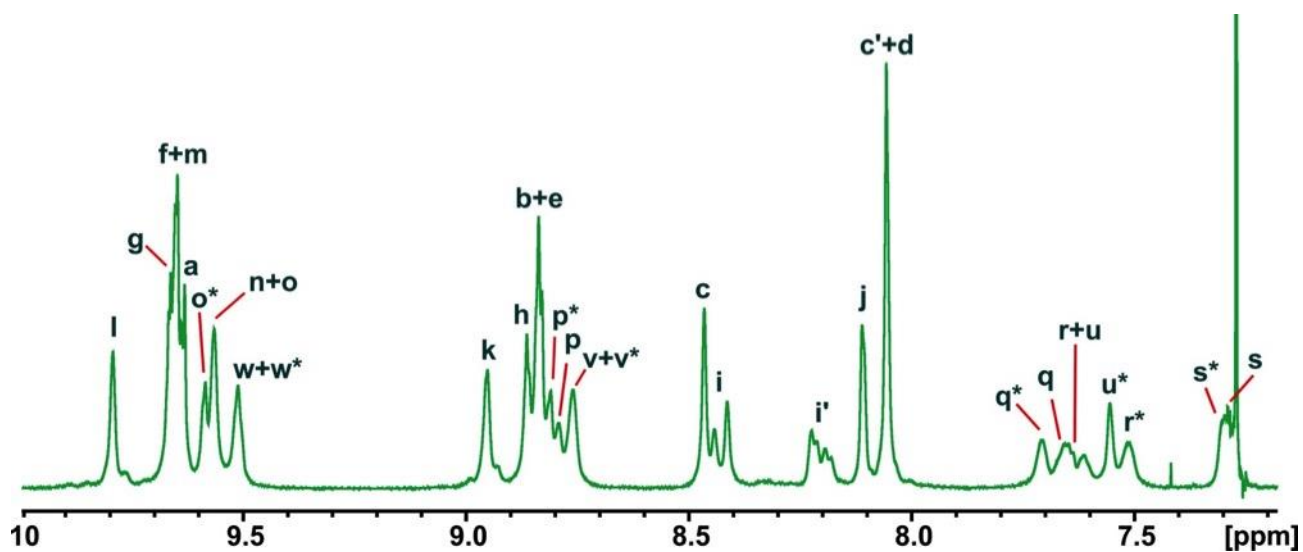
Figure S9: The assigned aromatic region of the ¹H-NMR spectrum of *b*-P14·T6·(T4)₂. The signals corresponding to o-u are split due to the existence of rotamers with the EtH chains pointing inwards or outwards (the signals for the diastereomers in which the EtH group is pointing outwards is denoted with *). The signal at 7.27 ppm corresponds to residual CDCl₃.
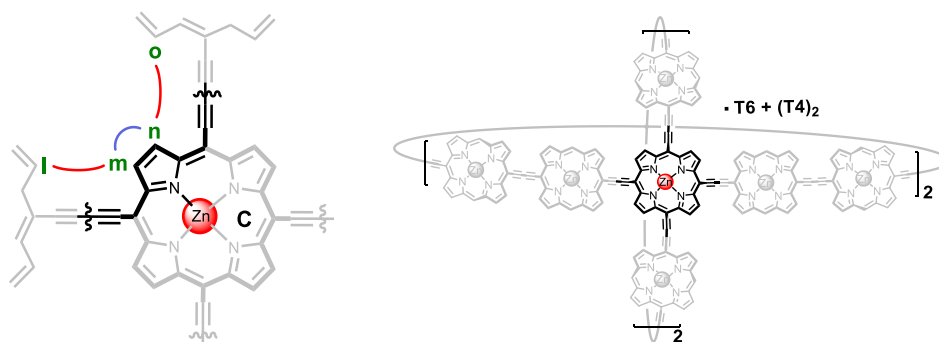
Assignment of the Central-Porphyrin (C)

Figure S10: Proton labeling of the central-porphyrin and its position within the ball. Blue lines denote COSY correlations; red lines denote NOE correlations.

Beta-pyrrole proton signals in close proximity to acetylenes were found between 10.0 and 9.4 ppm (Figure S9). In this region, only the protons corresponding to **m** and **n** are expected to show a COSY correlation which allowed for the identification of the protons **m** and **n** as two multiplets at 9.65 and 9.58 ppm (Figure S11).
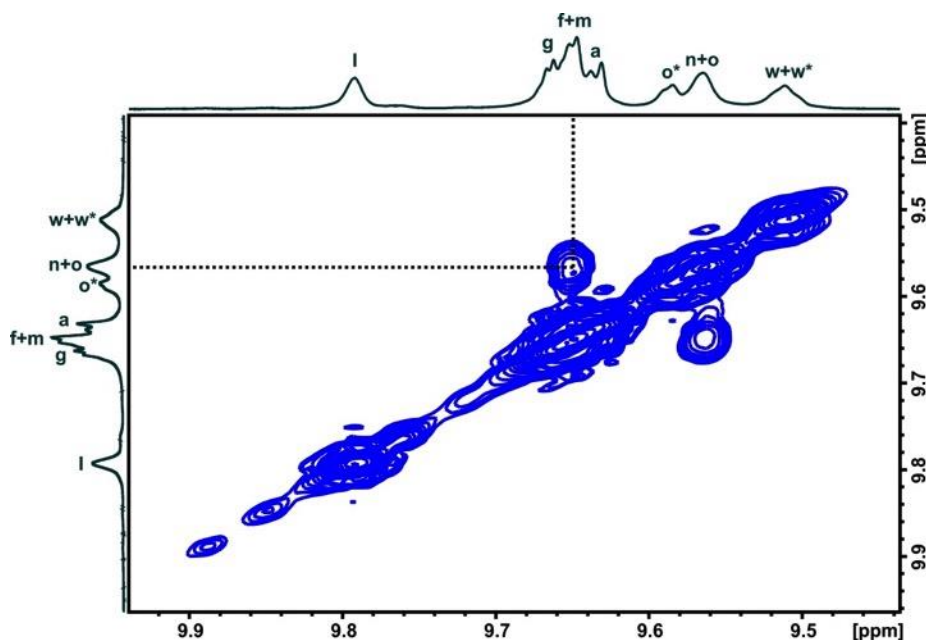

Figure S11: COSY correlation between the protons m and n.

The signals for **m** and **n** were distinguished from each other through 1D-NOESY experiments (Figure S12). By irradiating at 9.806 ppm, the signal corresponding to **l** was selectively excited and revealed a weak NOESY correlation to **m**. Due to signal overlap between **f** and **m** it was not possible to directly irradiate **m**. Irradiation of the signal corresponding to an overlap of **n** and **o** at 9.579 ppm showed no NOESY correlation to **l**, which demonstrates that the signal at 9.579 ppm corresponds to **n** rather than **m**.
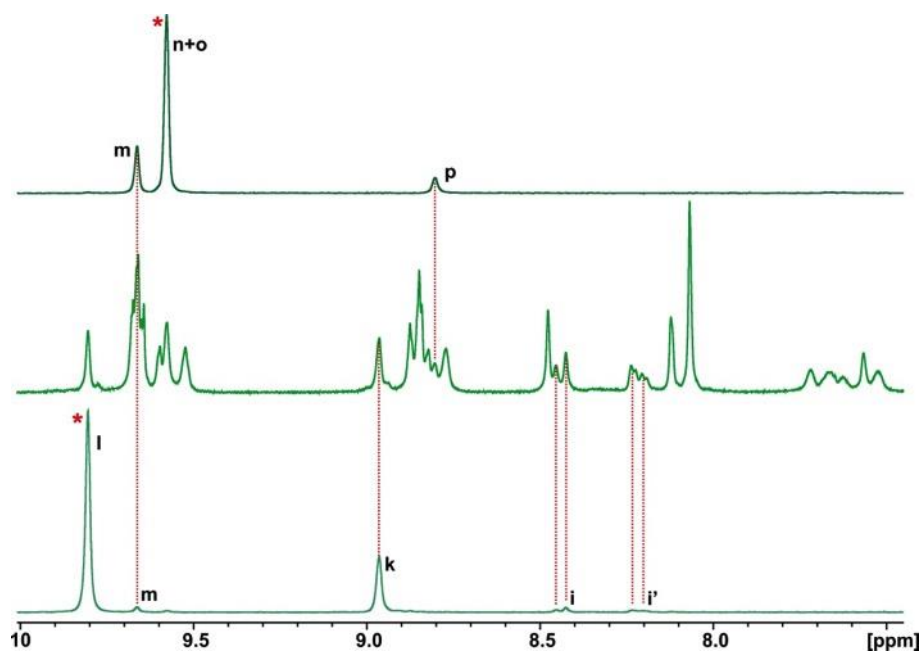
Figure S12: 1D NOESY spectrum irradiating the signals for n+o and l. i and i' enhancements likely arise from relayed NOEs from k rather than direct effects from l. Irradiated signals are denoted by *.

The *alpha*-protons (**α4**) of the template **T6** are in close proximity to the **m** and **n** protons and show an NOE which confirms the assignment (Figure S27).

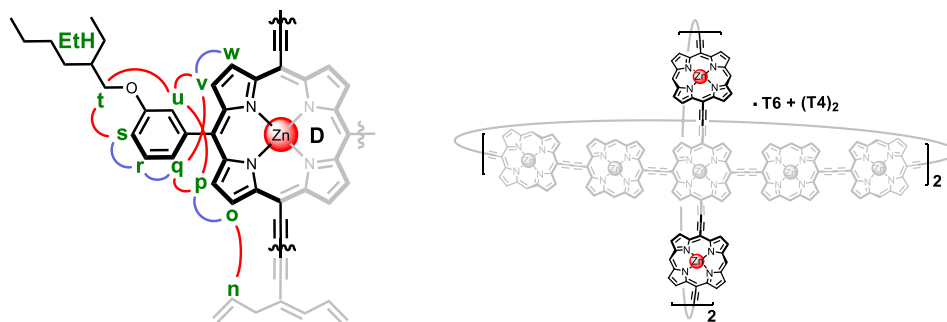## Assignment of the Alkoxy-Porphyrin (D)

Figure S13: Proton labeling of the alkoxy-porphyrin and its position within the ball. Blue lines denote COSY correlations; red lines denote NOE correlations.

The alkoxy-porphyrins (porphyrin D) are located in the 6-porphyrin nanoring of the ball (Figure S13). The aromatic protons of the aryl-groups give rise to a range of multiplets between 7.8 and 7.2 ppm. Due to signal overlap with the residual solvent signal, diffusion editing experiments were performed to suppress the chloroform signal at 7.27 ppm (Figure S14).
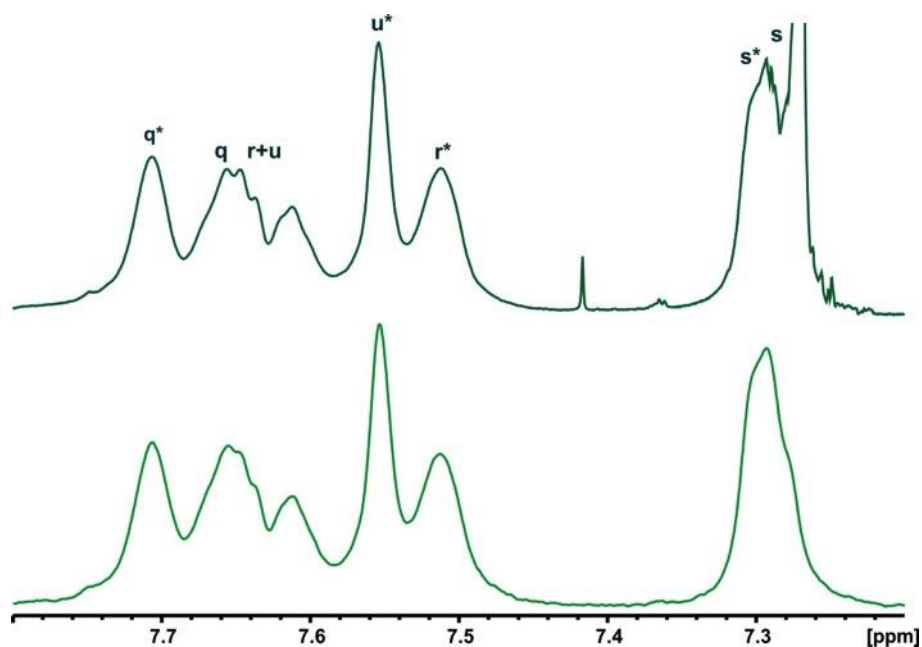
Figure S14: Region of the ¹H-NMR spectrum of *b*-P14·T6·(T4)₂, the residual solvent signal overlaps with the signal for s and is suppressed in the bottom spectrum. (The signal in the top spectrum at 7.42 ppm is the ¹³C satellite of residual CDCl₃).

Splitting in the signals is observed which can be rationalized by the presence of rotamers (splittings might also be expected due to the racemic nature of the **EtH** solubilizing group but this was not observed). The rotation of the aryl-groups is expected to be slow on the NMR timescale (but faster than 1 Hz) with the solubilizing groups either pointing towards the center or towards the periphery of the ball. The signals corresponding to the diastereomer in which the **EtH** group is pointing outwards are denoted with *. The protons for **t** give rise to two multiplets at 3.97 and 4.03 ppm (each corresponding to one rotamer) which were used to identify the protons **s/s*** and **u/u*** through NOESY correlations (Figure S16).

The signal for **u** is split in two multiplets at 7.65 and 7.55 ppm respectively and shows no COSY correlations (Figure S17). The protons pointing towards the center of the ball show NOESY correlations to the α3 protons of the template **T6** (Figure S15).
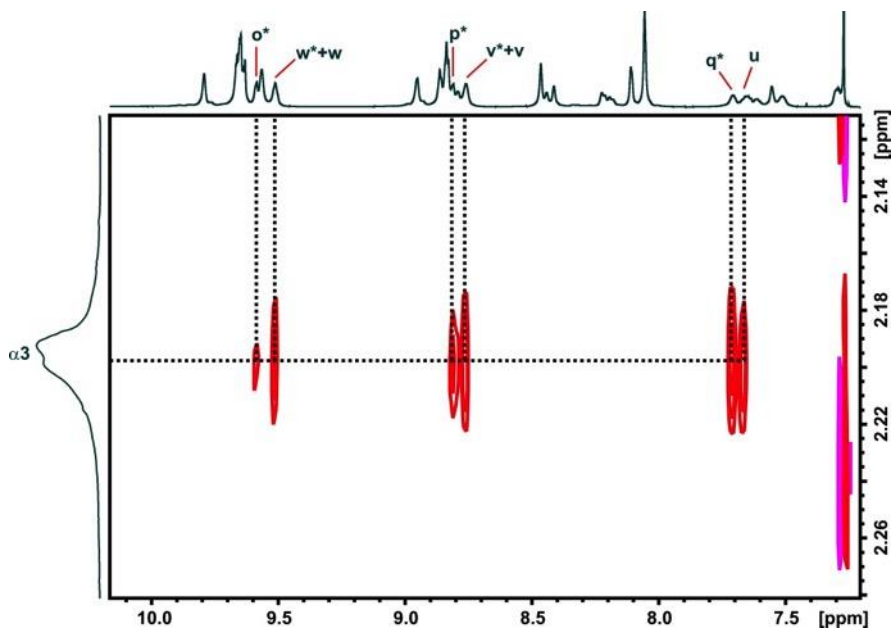
Figure S15: NOESY correlations between the template protons α3 and the protons of Porphyrin D.

No NOE is observed between the signal for **u*** at 7.55 ppm and **α3,** this proton is therefore expected to point towards the periphery of the ball. In agreement with this hypothesis, the signal at 7.65 ppm (**u**) does show an NOE to the template and is expected to point towards the center. COSY and NOESY correlations were used to distinguish between **q/q***, **r/r*** and **s/s***.
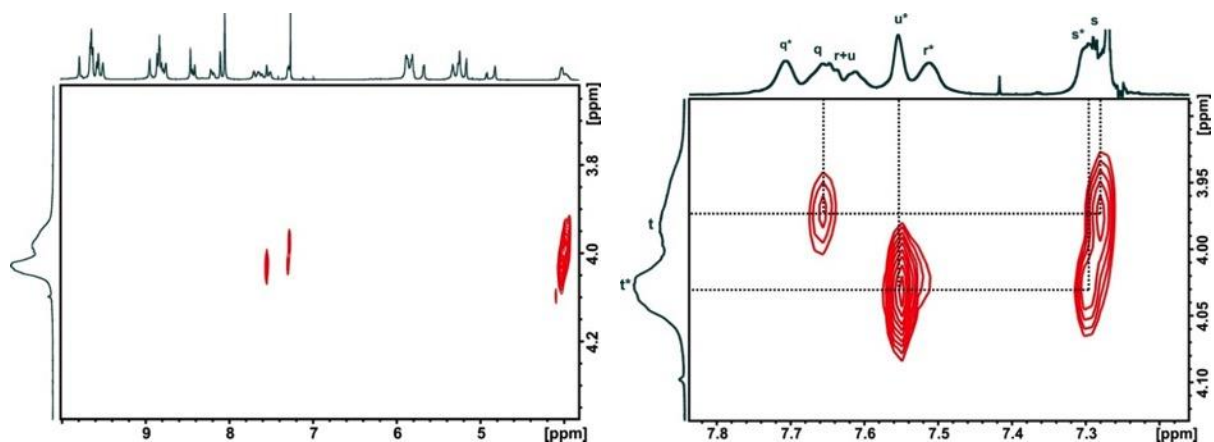

Figure S16: (left) NOESY correlations of t to s and u. (right) Region of the same spectrum.

The 8-proton multiplet at 7.30 ppm was identified as an overlap of **s** and **s***, the NOEs to **t** and **t*** were used to distinguish between the diastereomers (Figure S16). The signal for **s*** shows a COSY correlation to the multiplet at 7.51 ppm identified as **r***. An additional COSY correlation is found between **r*** and **q*** (Figure S17). The signal for **q** is split in two multiplets resonating at 7.71 and 7.65 ppm. The NOESY correlation from **u** to the **α3** protons of the template allow us to the signals corresponding to the

diastereomer with the **EtH** group pointing towards the center of the ball. The signal corresponding to **s** shows a COSY to **r** which overlaps with **u** (the COSY correlation between **t** and **u** discussed above confirms that the signal for **t** at 3.98 ppm belongs to this rotamer, *i.e.* pointing towards the center of the ball). Integration of the signals corresponding to **t** and **t*** indicates that approximately 60% of the **EtH** solubilizing groups are pointing towards the periphery of the ball.
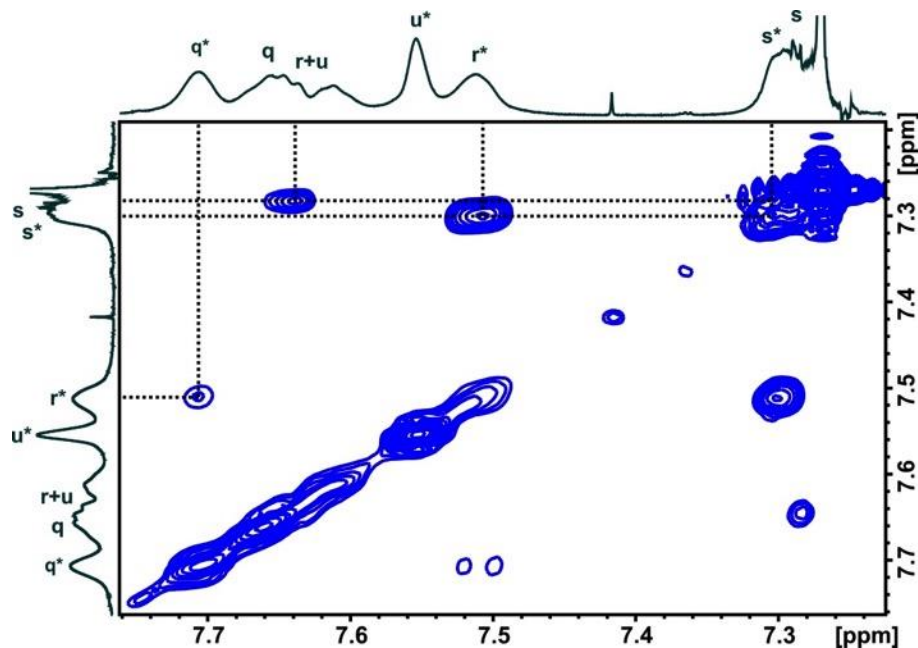

Figure S17: COSY correlations from s to r, s* to r* and r* to q*. The correlation r to q is not seen due to near degeneracy.

The signals for **p/p*** and **v/v*** can be identified through NOESY correlations to both **u/u*** and **q/q*** (Figure S18, left). COSY correlations from **p/p*** and **v/v*** to **o/o*** and **w/w*** respectively were used to identify the last protons on this porphyrin (Figure S18, right).
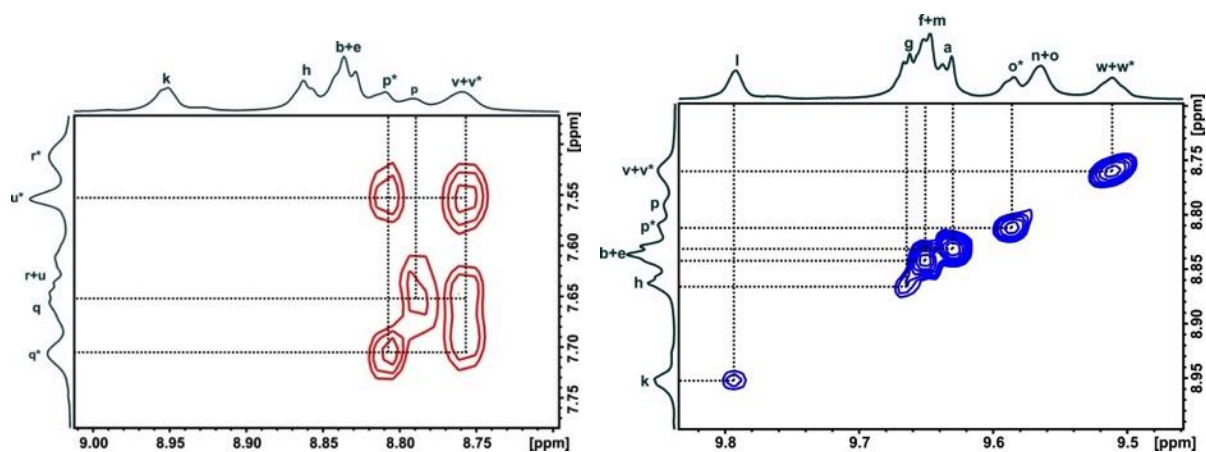

Figure S18: (left) NOESY cross-peaks from p and v to q and u. (right) COSY correlations between the porphyrin *beta*-protons.

To distinguish between the signals for **o**, **p**, **v**, and **w**, we performed 1D-NOESY experiments to see the NOEs across the butadiynes. As shown previously in Figure S12, a weak correlation was observed between **o** and **m** in addition to a stronger correlation to **p**. In Figure S19, selective irradiation of the signals corresponding to **p** and **v** shows the correlations to **o** and **w**. Upon irradiation of **w**, no correlation to **n** was observed, which is in agreement with the assignment. In addition, selectively irradiating **p*** shows NOESY correlations to **q*** and **u***, while selectively irradiating **p** shows NOEs to **q** and **u**, confirming the assignments. As expected, when the overlap of **v** and **v*** is irradiated, **q**, **q***, **u** and **u*** all show NOESY correlations.
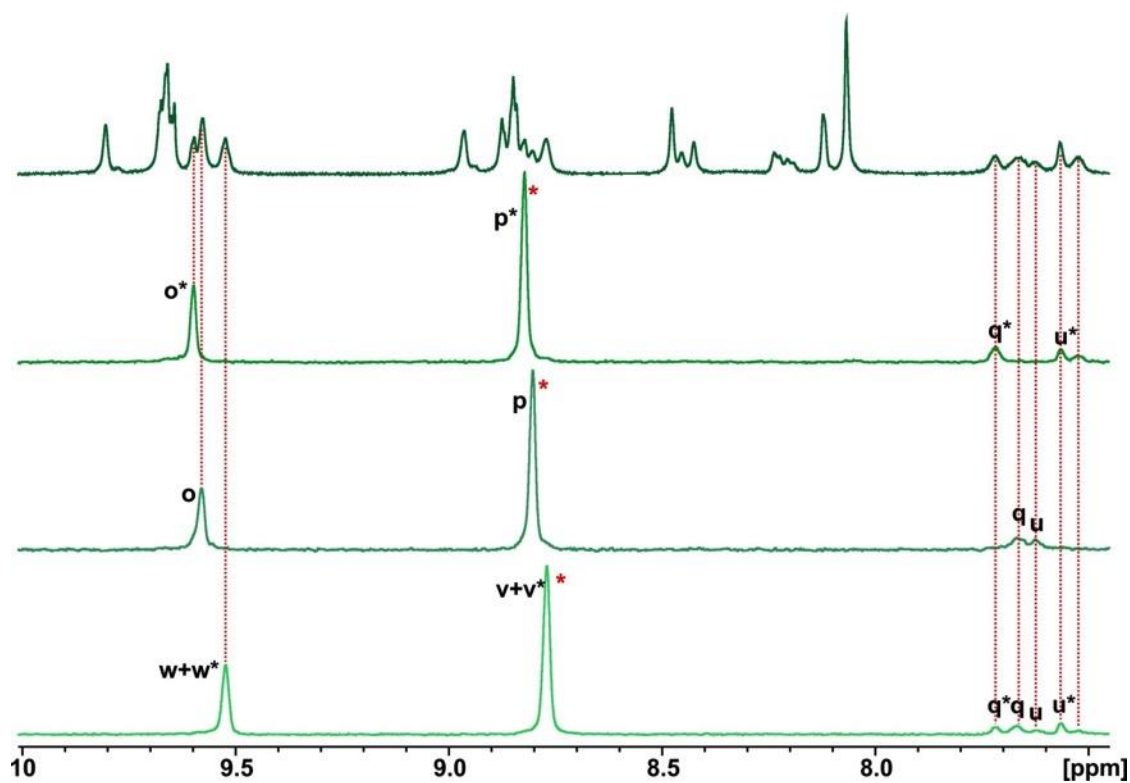

Figure S19: 1D NOESY spectrum irradiating the signals for p and v. Irradiated signal is denoted by *.
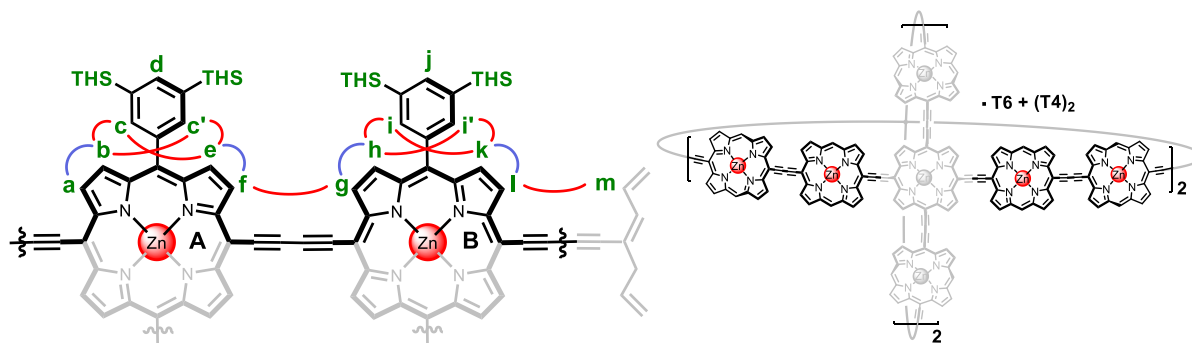
Assignment of the THS-Porphyrins (A and B)

Figure S20: Proton labeling of the THS-porphyrins and an illustration of their position within the nanoball. (THS = trihexylsilyl). Blue lines denote COSY correlations; red lines denote NOE correlations.

There are three distinct regions where the aromatic signals of the THS-porphyrins resonate (Figure S9). Protons **a**, **f**, **g**, and **l** are in close spatial proximity to the acetylenes and are shifted furthest downfield (between 10.0 and 9.4 ppm). The signals for **b**, **e**, **h**, and **k** are found between 9.0 and 8.7 ppm, the aryl protons **c**, **d**, **i**, and **j** resonate between 8.5 and 8.0 ppm. The *ortho*-protons of the aryls give rise to four signals (**c**, **c'**, **i**, and **i'**). The signals for **i** and **i'** are split further as a consequence of the close proximity to the diastereomeric alkoxy-porphyrin.

The protons **c** and **i** point towards the center of the ball causing them to be shifted downfield with respect to **c'** and **i'** which are directed towards the periphery of the ball. This assignment is confirmed by the NOEs of **c** and **i** to the α-protons of the **T4** template (Figure S27). Exchange peaks between **c** and **c'**, and between **i** and **i'** were observed in agreement with the slow rotation of the aryl groups. The *ortho*-protons of the aryl group show NOEs to the porphyrin *beta*-protons (Figure S21), this information was used in combination with the COSY spectrum shown in Figure S18 (right) to identify **a, f**, **b+e**, **g**, **h**, **k**, and **l**. Weak COSY correlation from **c** to **d** and from **i** to **j** were observed which were used to confirm the remaining two signals.
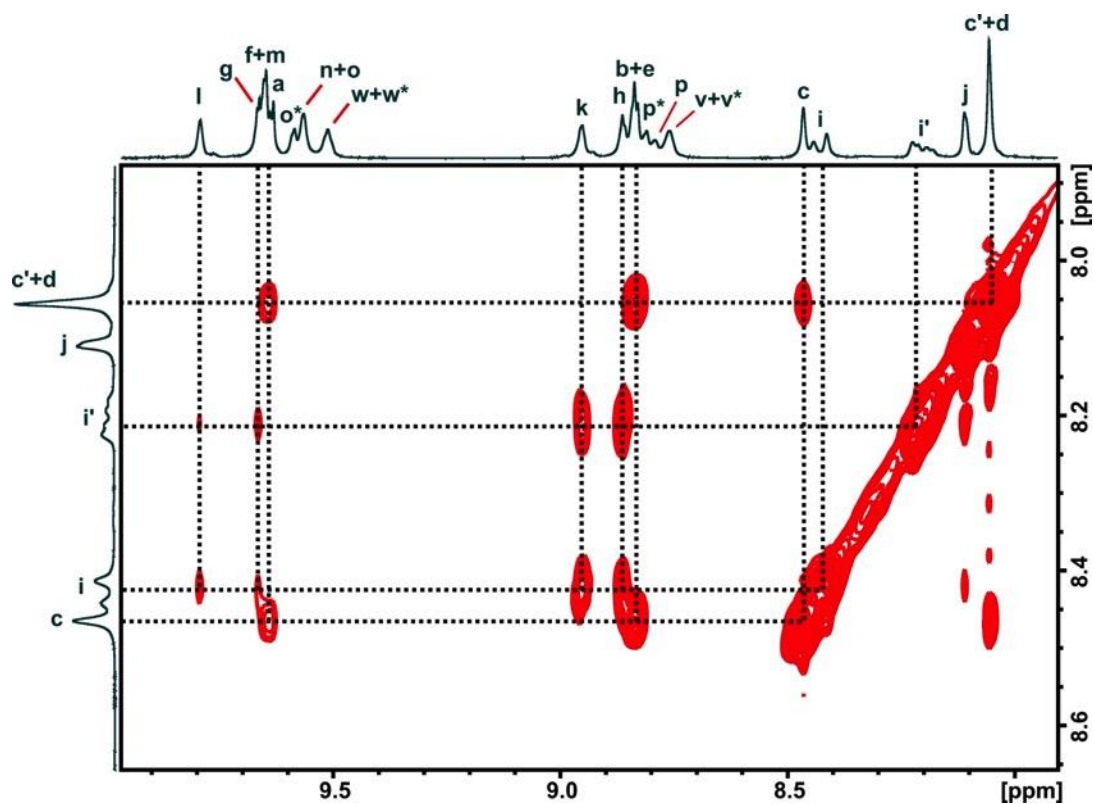
Figure S21: NOESY correlations between the THS-aryl protons to the porphyrin *beta*-protons. Spin diffusion may contribute to long-range effects such as the correlation between i and g.

By performing 1D-NOESY experiments we were able to differentiate between the different *beta*-pyrrole signals (Figure S22). Selective irradiation of **l** revealed the expected correlation with **m** which subsequently showed a relayed NOE to **n**. Upon irradiation of **k**, a direct correlation was observed to **l** which subsequently relays to **m**. In addition, both experiments show NOESY correlations to the aryl group.
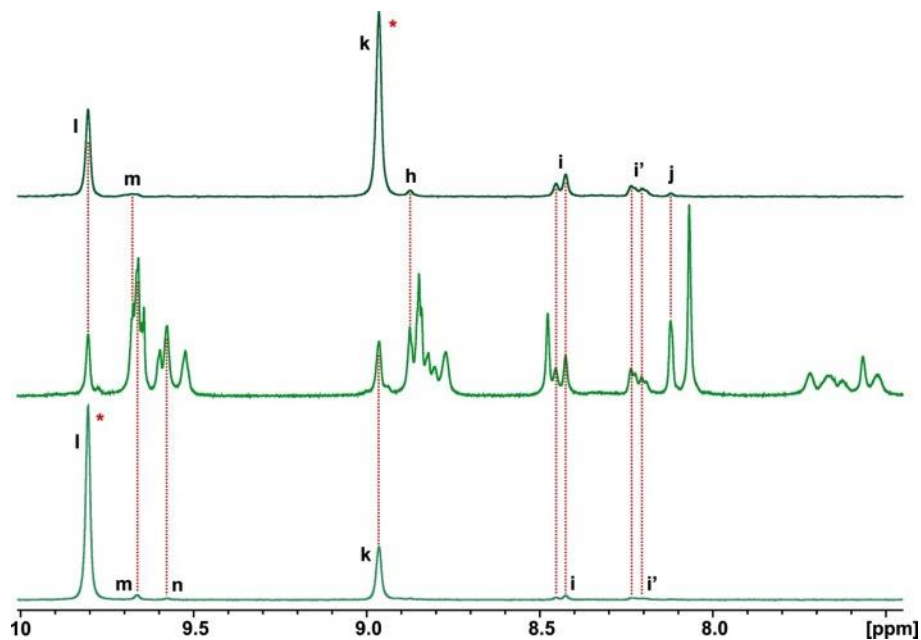
Figure S22: 1D NOESY spectrum irradiating the signals for k and l. Irradiated signal is denoted by *.

Due to signal overlap, it is not possible to selectively irradiate **g** or **f** to see its NOE across the butadiyne. However, by irradiating the more isolated signal corresponding to **h** and increasing the mixing time, a small shoulder appears at 9.64 ppm, through relayed NOE effects from **g**, which allowed for the assignment of **f**. In addition, the absence of a relayed signal for **a** at 9.63 ppm confirms the assignment (Figure S23).
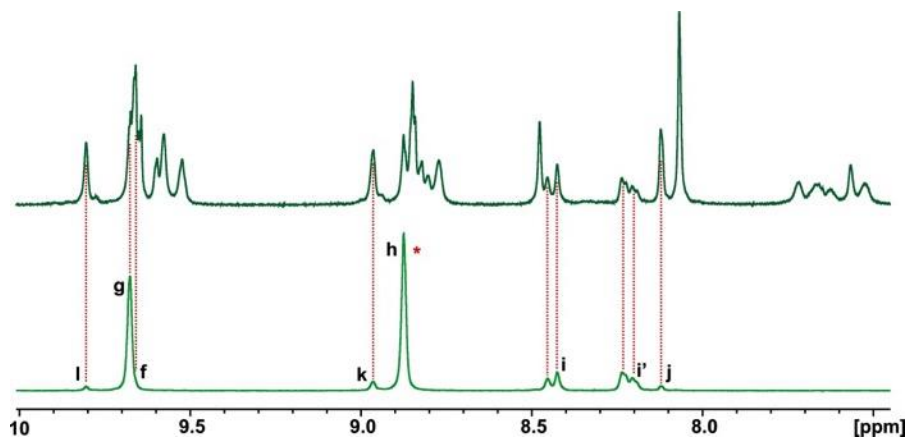

Figure S23: 1D NOESY spectrum irradiating the signal for h. Irradiated signal is denoted by *.
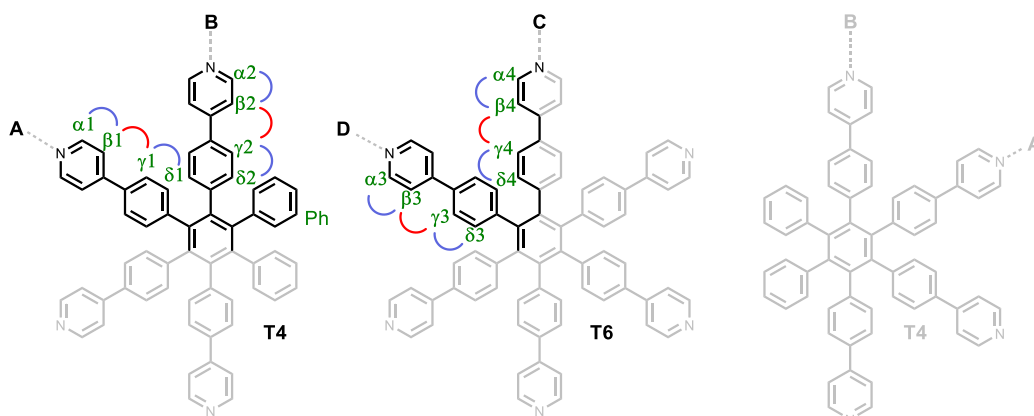
Assignment of the Templates

Figure S24: Symmetric unit of the templates within *b*-P14·T6·(T4)$_2$ with proton labeling. Blue lines denote COSY correlations; red lines denote NOE correlations.

The templates give rise to a number of signals between 6 and 2 ppm (Figure S25). Due to strong shielding by the porphyrin π-system, the *alpha*-protons are found at lower chemical shifts and give rise to three multiplets. By utilizing the NOEs to the porphyrin *beta*-pyrrole protons, the 8-proton multiplet at 2.20 ppm was identified as α**3**, the 12-proton multiplet at 2.45 ppm is an overlap of the signals α**1** and α**4**, and the 8-proton multiplet at 2.61 ppm was identified as α**2** (Figure S27).
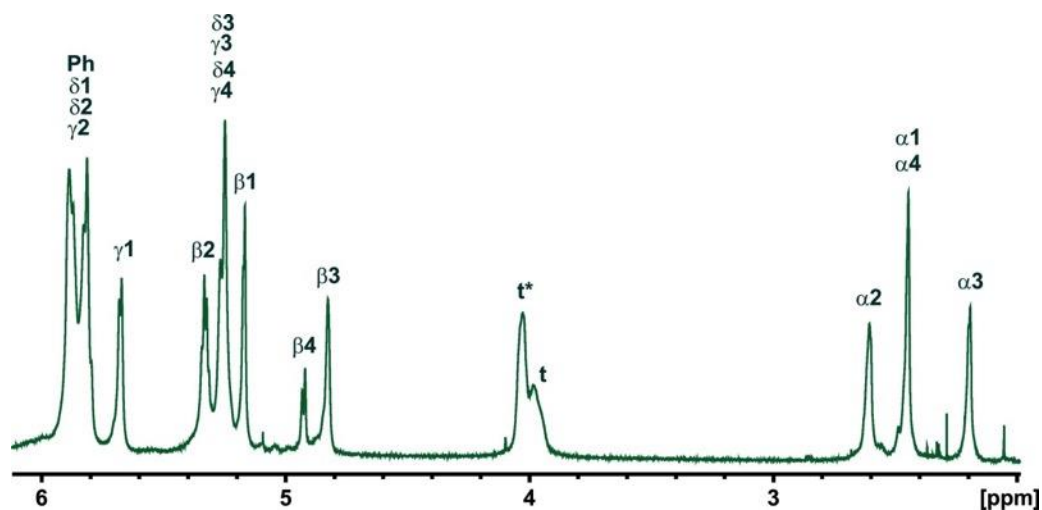

Figure S25: The template region of the ^{1}H-NMR spectrum of *b*-P14·T6·(T4)$_2$.

All four of the protons with the label "β" were identified through COSY correlations to the α-protons (Figure S26, left). Subsequently, NOESY correlations were used to identify the signals for γ**1-4** (Figure S26, right).
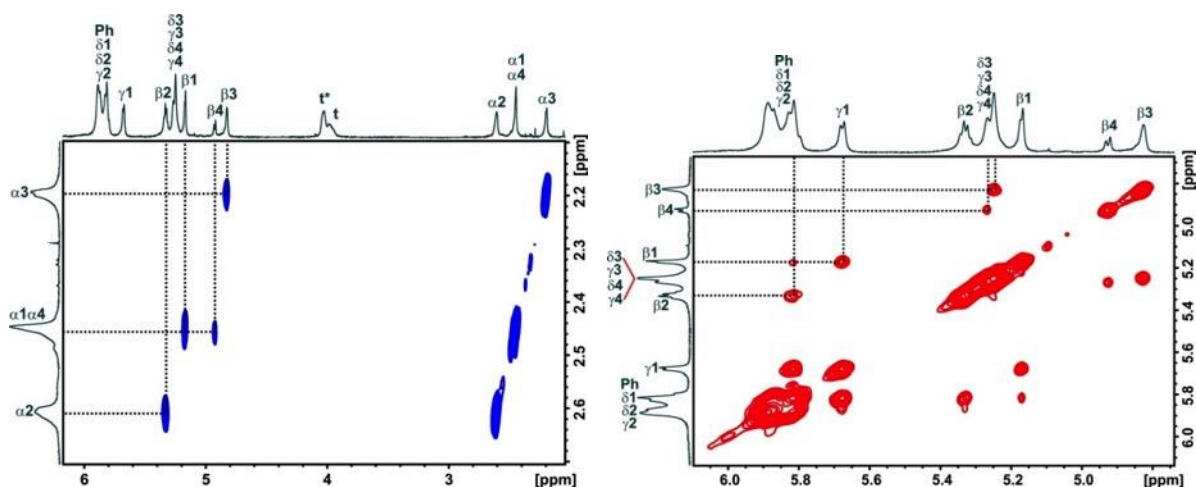
Figure S26: (left) COSY correlations between the templates α and β signals. (right) NOESY correlations between the templates β and γ signals.

The signals for **γ3**, **γ4**, **δ3**, and **δ4** resonate at nearly identical chemical shifts (5.26 ppm) and are not resolved. **γ1** is a multiplet at 5.68 ppm and shows a COSY correlation with **δ1**. The signals for **δ1**, **δ2**, **γ2**, and the ten protons for **Ph** give rise to an overlapping multiplet at 5.85 ppm.

As mentioned before, the α-protons of the templates are in close proximity to the porphyrins and show NOESY correlations (Figure S27). The signal for **α2** shows five NOESY correlations to the THS-porphyrin (B). Intense cross-peaks were observed to **g** and **h** and slightly less intense cross-peaks were found relate to **k** and **l**. In addition, a cross-peak was observed to **i** confirming that **i** is pointing towards the center of the ball (and consequently is in closer proximity to the template than **i'**). The signal for **α3** was confirmed by its NOESY correlations to the alkoxy-porphyrin (D) by showing cross-peaks to **o**, **w**, **p** and **v**. In addition, weak cross-peaks to **q** and **u** were observed. The signals for **α1** and **α4** were found to overlap and show four NOESY correlations. The proton **α4** is in close proximity to the central-porphyrin (C) and shows a cross-peak to **m** and **n**. The signals for **a**, **f**, **b+e** and **c** of the THS-porphyrin (A) show cross-peaks to **α1**. Again, the correlation between **α1** and **c** confirms that **c** is pointing towards the center of the ball.
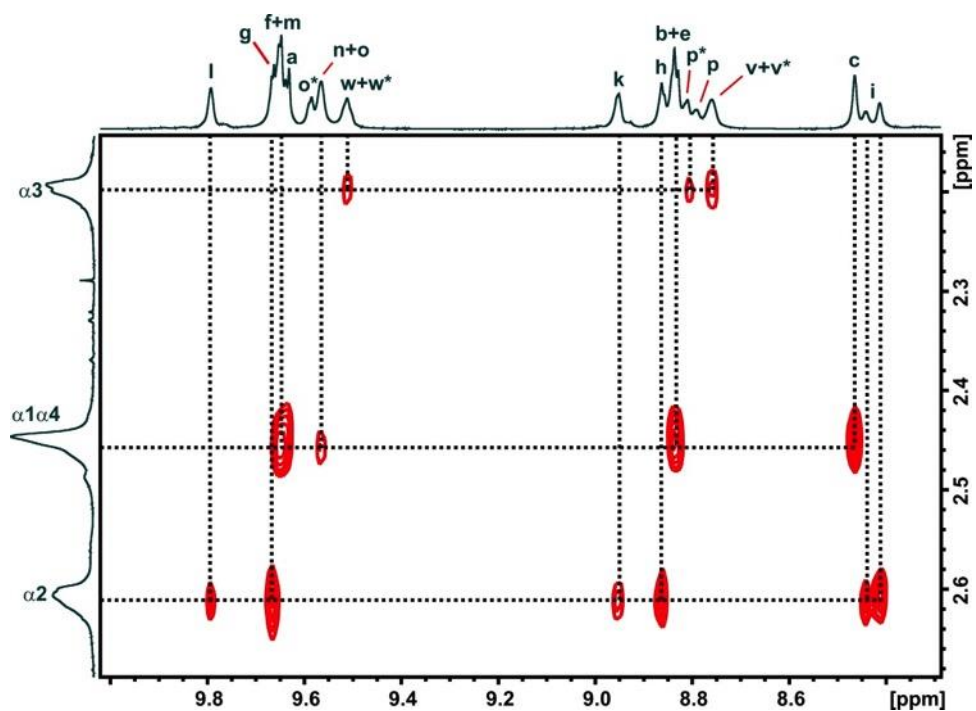
Figure S27: NOESY correlations between the template α-protons and the protons of the porphyrins.
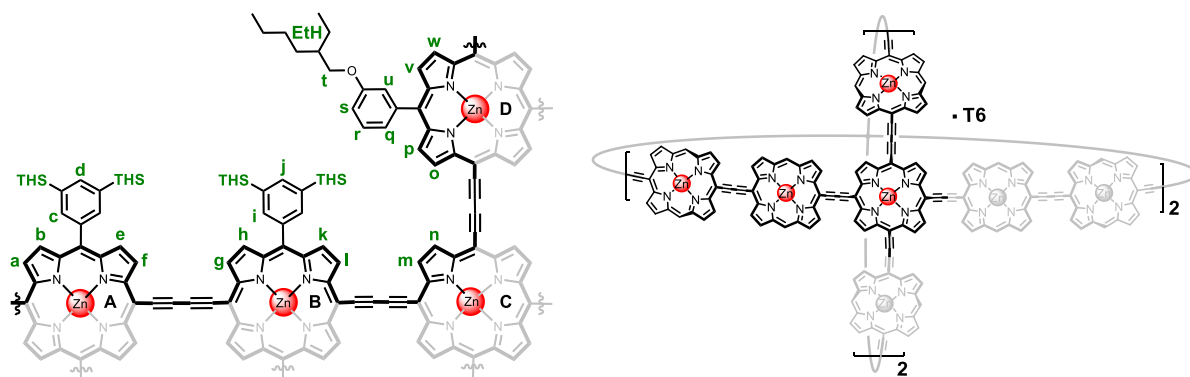
C.2 Assignment of *b*-P14·T6

Figure S28: Symmetric unit of the porphyrins in *b*-P14·T6 with the corresponding proton labeling. Due to the removal of the T4 templates, porphyrins A and B can rotate. As a result, the signals corresponding to c and i are no longer split. Template is not shown for clarity (THS = trihexylsilyl; EtH = ethylhexyl).
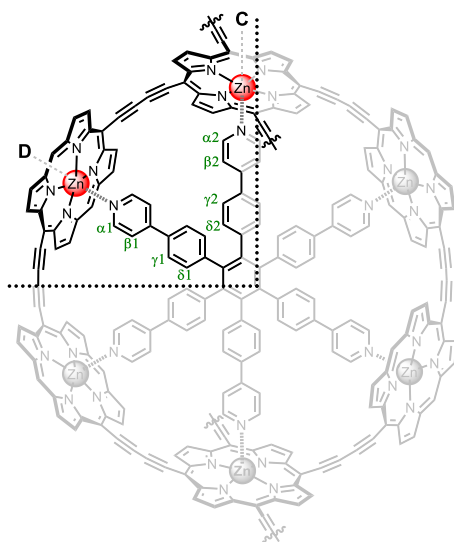
Figure S29: Symmetric unit of the template within *b*-P14·T6 with proton labeling. Only the 6-membered ring of the ball is shown and the aryl groups of the porphyrins have been omitted for clarity.

¹H NMR (700 MHz, CDCl₃, 298 K): δ_H (ppm) 9.84 (8H, m, **l**), 9.76 (8H, m, **g**), 9.75 (8H, m, **f**), 9.70 (8H, m, **a**), 9.66 (8H, m, **m**), 9.55 (16H, m, **n+o**), 9.50 (8H, m, **w**), 8.95 (8H, m, **k**), 8.89 (8H, m, **h**), 8.87 (8H, m, **b+e**), 8.86 (8H, m, **b+e**), 8.76 (16H, m, **p+v**), 8.28 (16H, m, **i**), 8.24 (16H, m, **c**), 8.05 (8H, s, **j**), 8.03 (8H, s, **d**), 7.73-7.61 (8H, m, **q**), 7.61-7.46 (16H, m, **r+u**), 7.32-7.19 (8H, m, **s**), 5.41-5.26 (24H, m, γ1+γ2+δ1+δ2), 4.98 (4H, d, *J* = 7.5Hz, **β2**), 4.87 (8H, m, **β1**), 4.05-3.80 (16H, m, **t**), 2.53 (4H, m, α2), 2.22 (8H, m, α1), 1.88-0.32 (1,368H, m, **THS+EtH**).
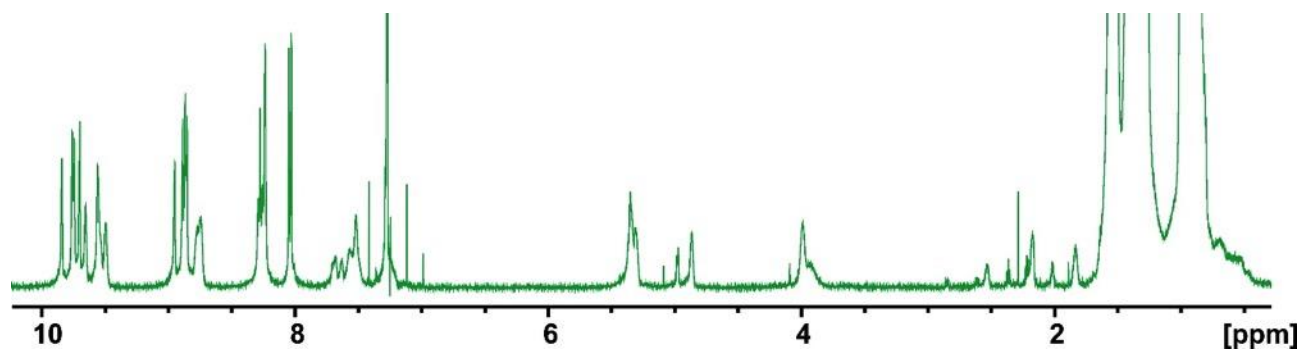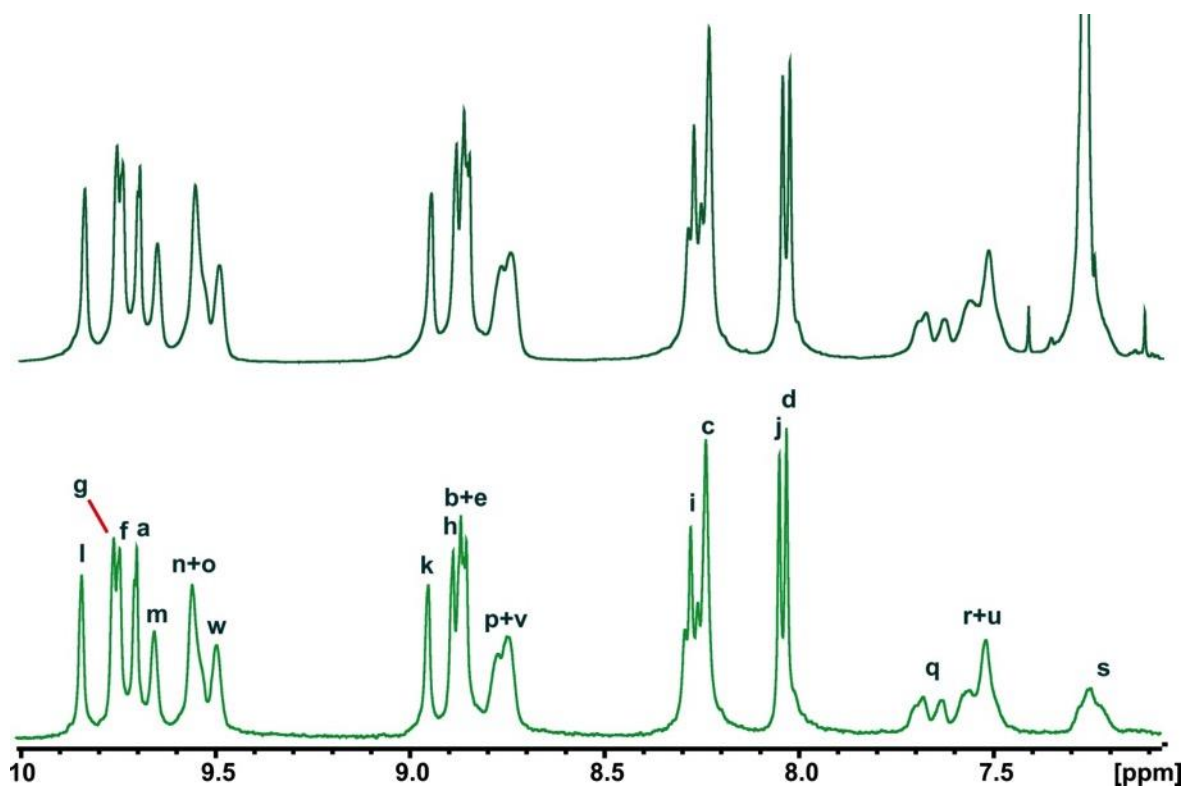

Figure S30: The ¹H-NMR spectrum of *b*-P14·T6.

Figure S31: (top) The aromatic region of the ¹H-NMR spectrum of *b*-P14·T6. (bottom) The diffusion edited ¹H-NMR spectrum.
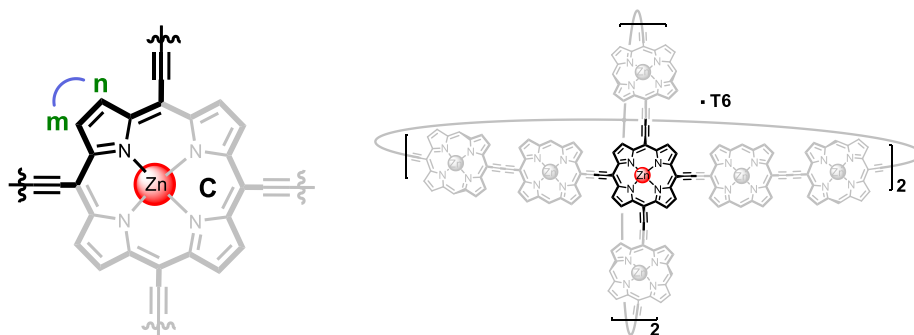
Assignment of the Central-Porphyrin (C)

Figure S32: Proton labeling for the symmetric unit of the central-porphyrin and an illustration of its position within the ball. Blue lines denote COSY correlations.

The central-porphyrin gives rise to two 8-proton multiplets at 9.66 and 9.55 ppm. The signals were distinguished from the other *beta*-signals of the porphyrins through a COSY cross-peak (Figure S33, left). A NOE was observed between the template α2 protons and **m** and **n** as a result of their close spatial proximity (Figure S33, right).
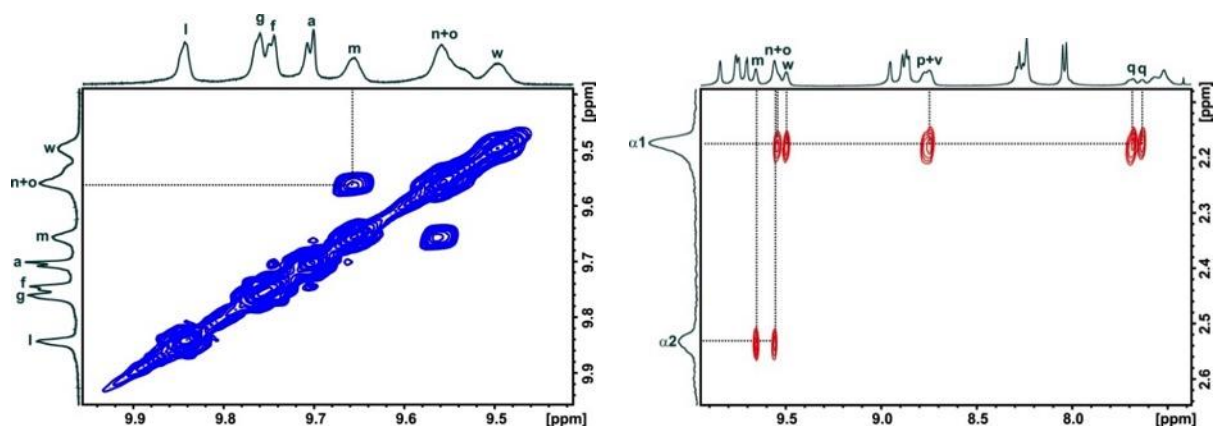
Figure S33: (left) COSY correlations between the **m** and **n** protons. (right) NOESY correlations between the template α-protons and the porphyrin signals.

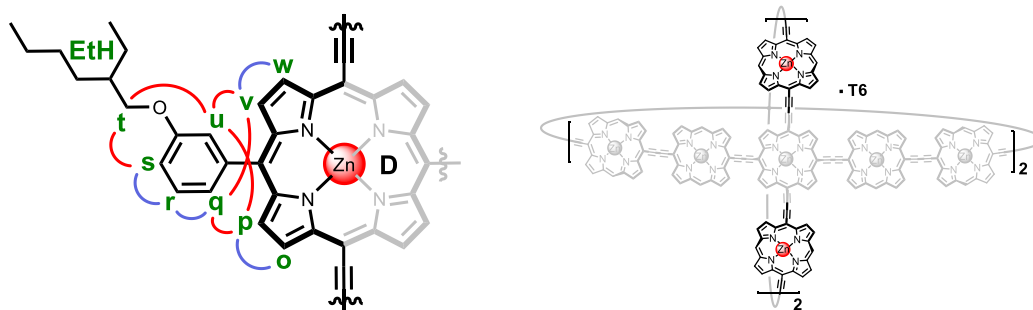## Assignment of the Alkoxy-Porphyrin (D)

Figure S34: Proton labeling for the symmetric unit of the alkoxy-porphyrin and an illustration of its position within the ball. Blue lines denote COSY correlations; red lines denote NOE correlations.

The aromatic region of the ^{1}H-NMR spectrum of **b-P14·T6** shows spectral overlap with the solvent signal. Diffusion editing experiments were performed to suppress the chloroform signal and revealed the proton signals corresponding to **s** (Figure S31). Similar to **b-P14·T6·(T4)$_2$**, the presence of rotamers, in which the **EtH** chain can either point towards the center or the periphery of the ball, gave rise to splitting and broad signals for **q-u**. The ratio between the diastereomers could be obtained by integrating the signals for **t** which revealed a 50-50 split.

The NOESY correlations from **t**, illustrated in Figure S35 (left), were used to identify the signals for **s** and **u**. The COSY spectrum (Figure S35, right) was used to distinguish between **s** and **u**. The protons corresponding to **s** show a COSY cross-peak to **r** which subsequently couples to **q**. No COSY correlations were found for **u**.
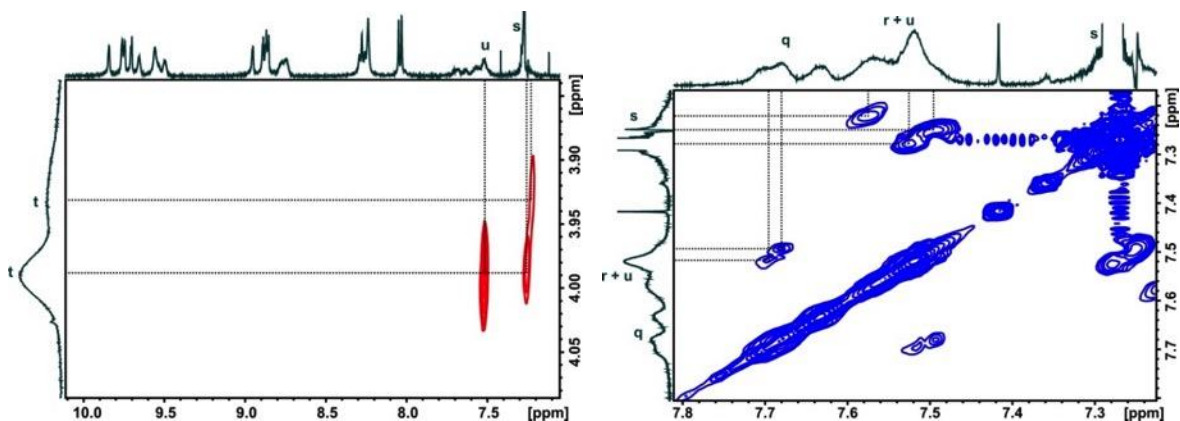
S28

Figure S35: (left) NOESY correlations from t to s and u. (right) COSY correlations between s, r and q.

The aryl protons **q** and **u** are in close proximity to the porphyrin protons **p** and **v** and show NOESY correlations (Figure S36, left). The signals for **o** and **w** were identified through their cross-peak in the COSY spectrum with **p** and **v** (Figure S36, right).
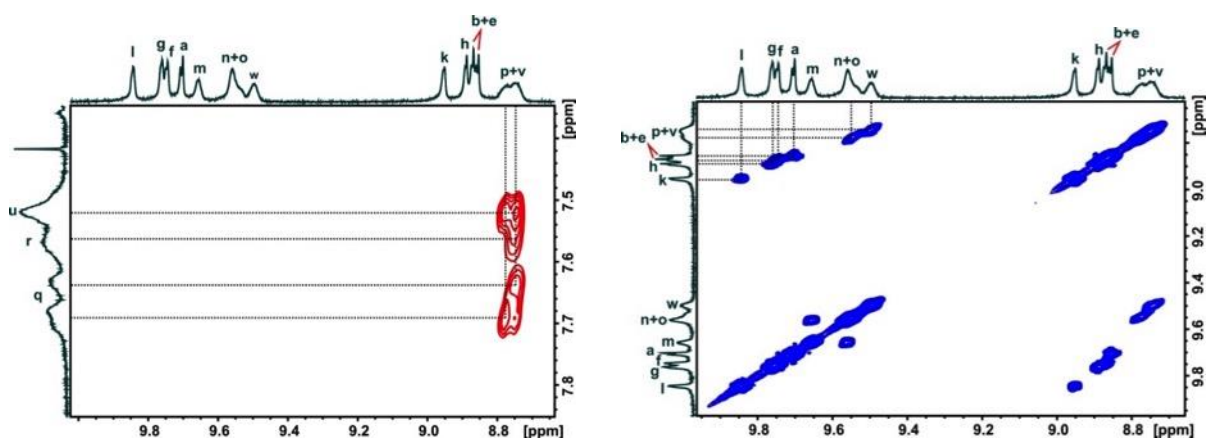

Figure S36: (left) NOESY correlations from p and v to q and u. (right) COSY cross-peaks between the porphyrin's *beta*-protons.

The signals for **o**, **w**, **p** and **v** were confirmed through a NOESY to the template α1 protons depicted in Figure S33 (right).

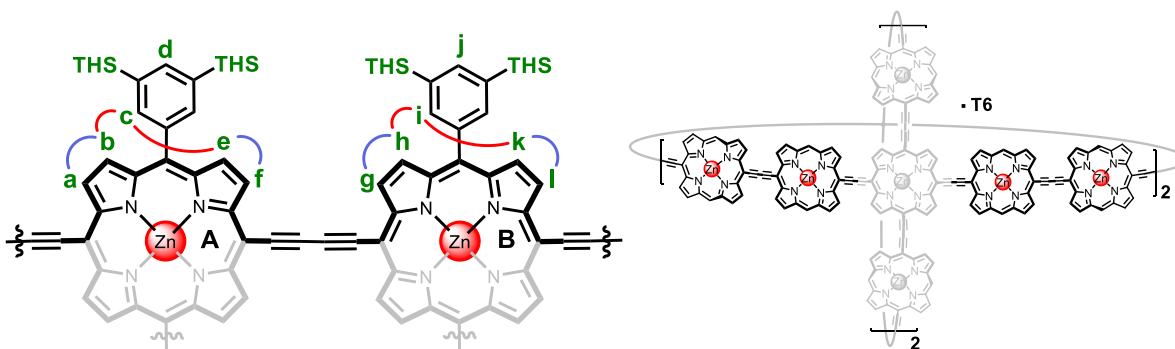## Assignment of the THS-Porphyrins (A and B)

Figure S37: Proton labeling for the symmetric unit of the THS-porphyrins and an illustration of their position within the ball. (THS = trihexylsilyl). Blue lines denote COSY correlations; red lines denote NOE correlations.

By analogy to *b*-**P14·T6·(T4)₂** the *beta*-protons **l** were found furthest downfield as the 8-proton multiplet at 9.84 ppm. A COSY coupling from **l** was observed to the 8-proton multiplet at 9.76 ppm identified as **k** (Figure S36, right). The NOESY spectrum shows a correlation from **k** to the 16-proton multiplet at 8.28 ppm characterized as **i** (Figure S38, left). In the absence of the **T4** templates, the porphyrins A and B are free to rotate. As a result the signals for **c** and **i** are no longer split as was observed in *b*-**P14·T6·(T4)₂**. An additional NOESY coupling from **i** is used to identify **h**, which shows a COSY correlation itself to **g** (Figure S36, right).
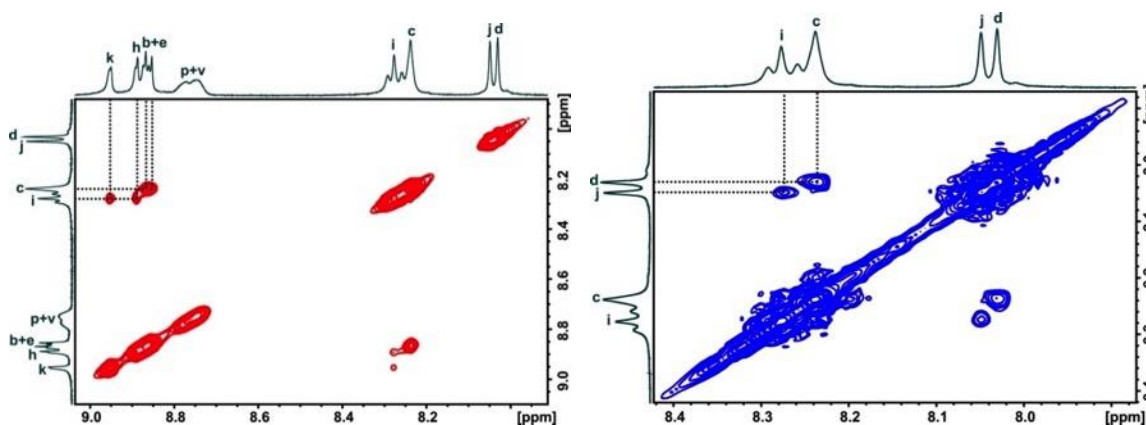

Figure S38: (left) NOESY correlations from c and i to b+e, h and k. (right) COSY cross-peaks from c and i to d and j.

A long range COSY coupling from **i** was used to identify **j** as the 8-proton singlet at 8.05 ppm (Figure S38, right). Similarly, **c** and **d** were identified as the 16-proton multiplet and the 8-proton singlet at 8.24 ppm and 8.03 ppm respectively. An NOE between **c** and **b+e** is depicted in Figure S38 (left) and confirms this assignment. Lastly, COSY correlations from **a** to **b** and from **e** to **f** were found (Figure S36, right).
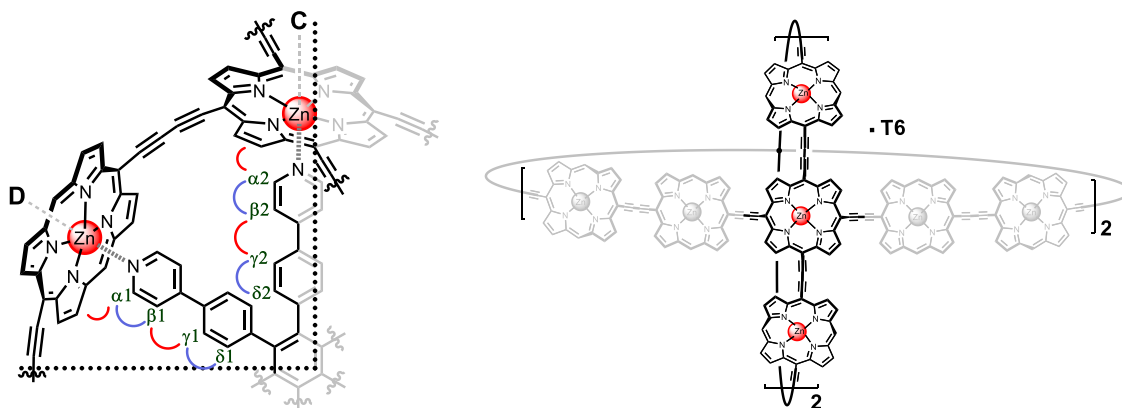
Assignment of the Template

Figure S39: Proton labeling for the symmetric unit of the template T6 and an illustration of its position in *b*-P14·T6.

The proton labeling on the **T6** template is shown in Figure S39 and the template region of the diffusion edited ^{1}H-NMR spectrum in shown in Figure S40. The diffusion edited ^{1}H-NMR allowed us to differentiate between signals from the template and small solvent impurities.

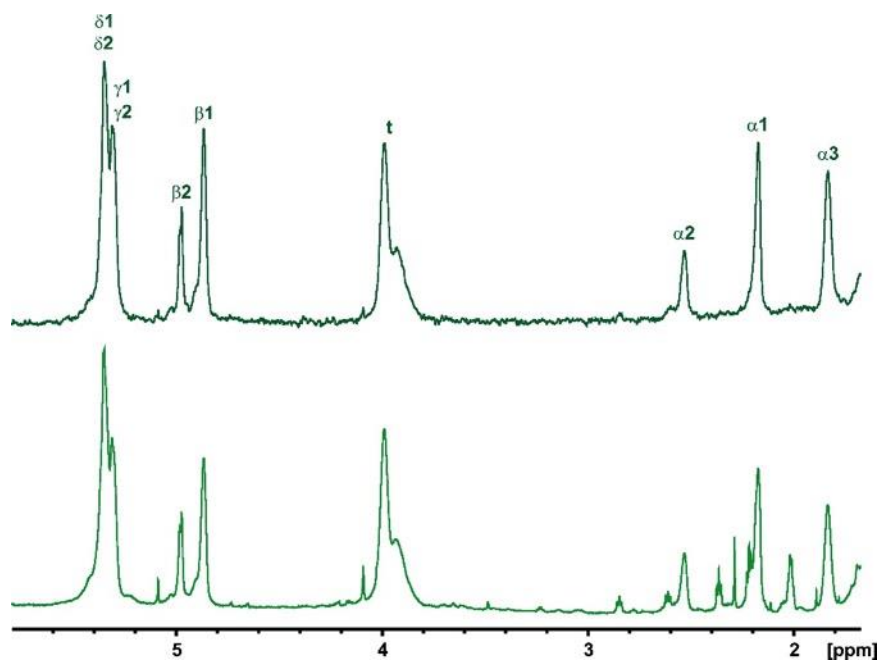**Figure S40: Template region of the diffusion edited ^{1}H-NMR spectrum of *b*-P14·T6.**

The 4-proton and 8-proton multiplets at 2.53 and 2.22 ppm are assigned as α2 and α1 respectively. COSY correlation between these signals and the 4-proton and 8-proton multiplets at 4.98 and 4.87 ppm allows these signals to be identified as β2 and β1 respectively. A subsequent NOESY correlation to the 24-

proton multiplet between 5.41 and 5.26 ppm characterized this signal as an overlap for the protons γ**1**, γ**2**, δ**1**, and δ**2** (Figure S41).
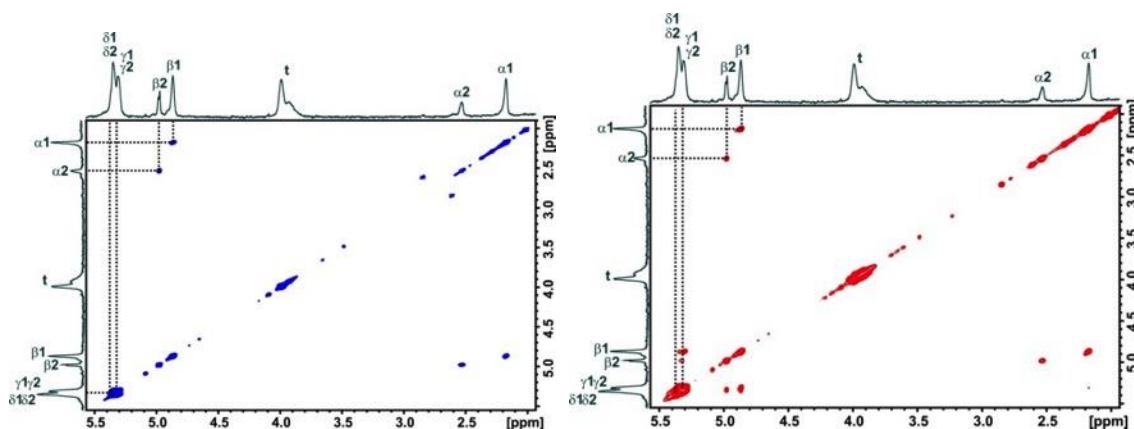
Figure S41: (left) COSY correlations between α2-β2 and α1-β1. (right) NOESY correlation between β2-γ2 and β1-γ1.

C.3 Assignment of template-free ball *b*-P14
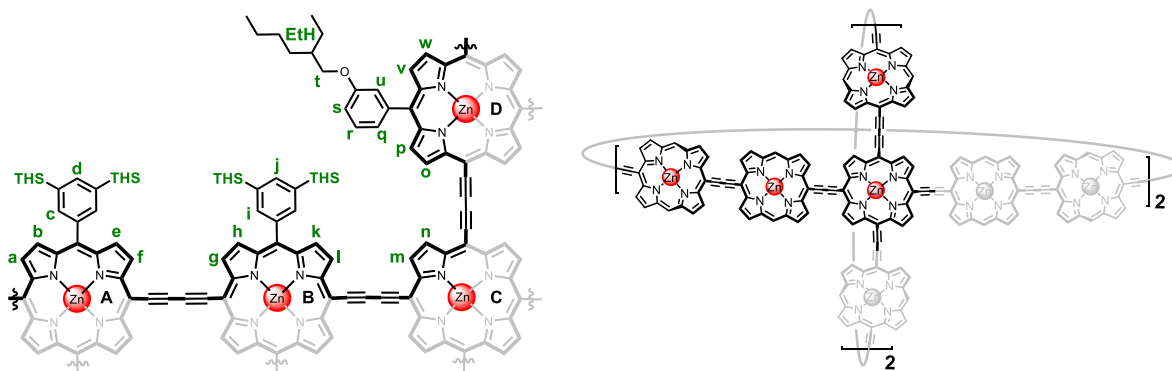
Figure S42: Symmetric unit of the porphyrins in *b*-P14 with the corresponding proton labeling. Template not shown for clarity (THS = trihexylsilyl; EtH = ethylhexyl).

^{1}H NMR (700 MHz, CDCl$_3$, 298 K): δ$_H$ (ppm) 9.85 (8H, m, **l**), 9.79-9.71 (16H, m, **f+g**), 9.71-9.60 (16H, m, **a+m**), 9.61 (8H, m, **n**), 9.60 (8H, d, *J* = 4.4 Hz, **o**), 9.56 (8H, d, *J* = 4.4 Hz, **w**), 8.95 (8H, m, **k**), 8.92-8.84 (24H, m, **b+e** and **h**), 8.78 (8H, d, *J* = 4.4 Hz, **p**), 8.76 (8H, d, *J* = 4.4 Hz, **v**), 8.27 (16H, m, **i**), 8.23 (16H, m, **c**), 8.01 (16H, s, **d+j**), 7.58 (8H, m, **q**), 7.52 (8H, s, **u**), 7.46 (8H, m, **r**), 7.15 (8H, d, *J* = 7.7 Hz, **s**), 3.84 (16H, m, **t**), 1.64-0.78 (1,368H, m, **THS+EtH**).

Figure S43: The ¹H-NMR spectrum of *b*-P14.

Figure S44: The aromatic region of the ¹H-NMR spectrum of *b*-P14.
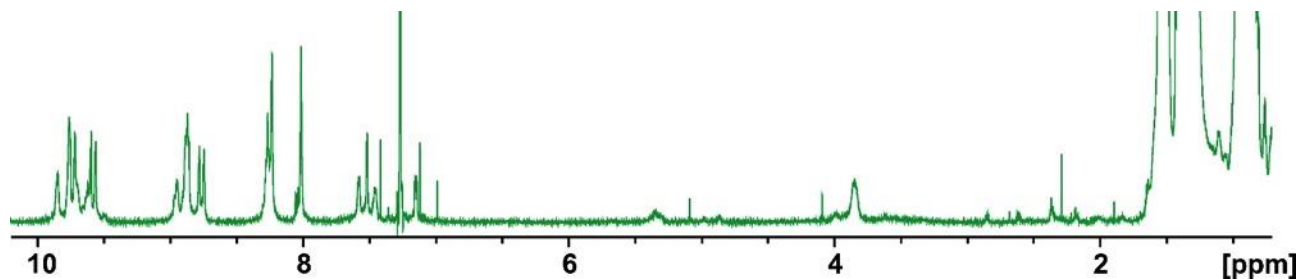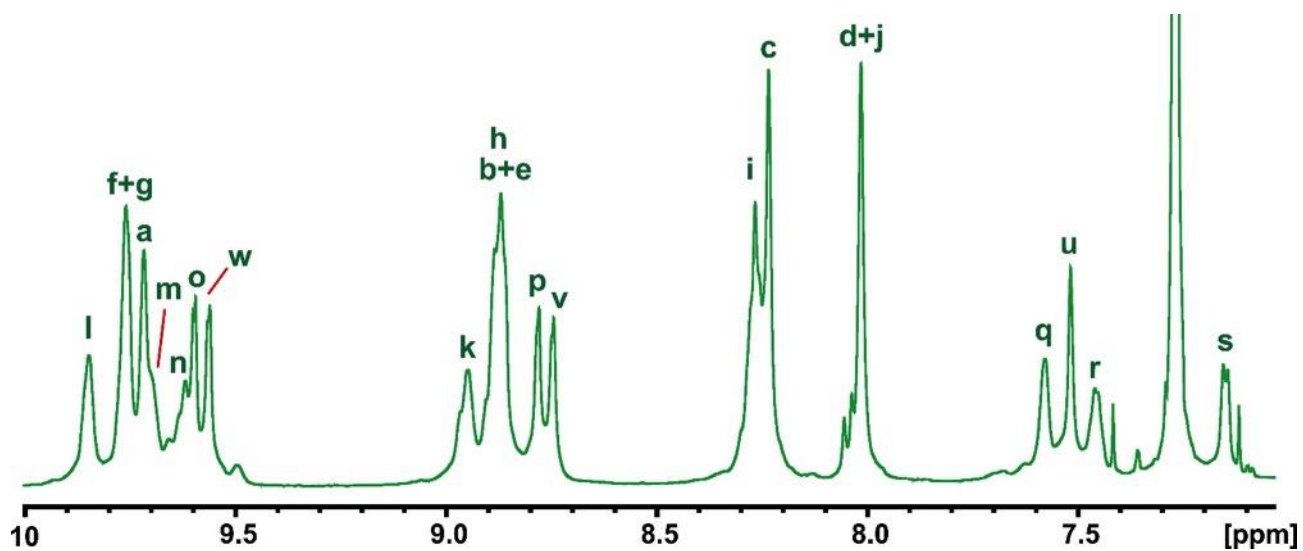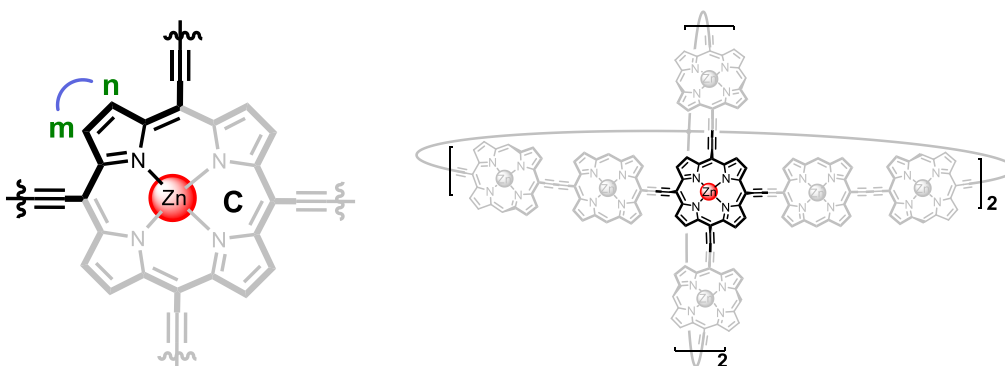
Assignment of the Central-Porphyrin (C)

Figure S45: Proton labeling for the symmetric unit of the central-porphyrin and an illustration of its position within the ball. Blue lines denote COSY correlations.

The signals for **m** and **n** were identified as a 16-proton multiplet resonating between 9.71 and 9.61 ppm (Figure S44). Only the protons **m** and **n** are expected to show a COSY correlation in the region between 10 and 9.5 ppm. This observation was used to confirm the signals for these protons (Figure S46).
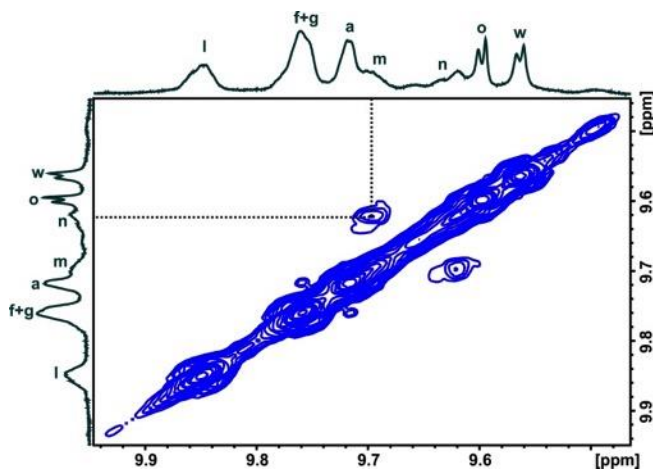
Figure S46: COSY correlation between the m and n protons.

Assignment of the Alkoxy-Porphyrin (D)
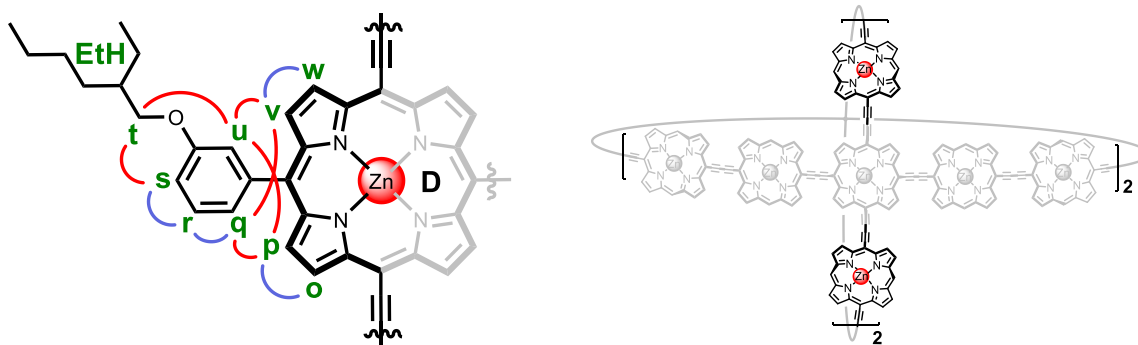
Figure S47: Proton labeling of the symmetric unit of the alkoxy-porphyrin and an illustration of its position within the ball. Blue lines denote COSY correlations; red lines denote NOE correlations.

The signal for proton **t** is found at 3.84 ppm. Due to the removal of the **T6** template, porphyrin D can now freely rotate, as a result there is no longer a splitting for the signals corresponding to the aryl group pointing towards the inside and the periphery of the ball. The signal for **t** is shifted downfield with respect to the other solubilizing protons (**EtH**) due to the deshielding effect of the oxygen. NOESY correlations from **t** were used to identify the signals for **s** and **u** (Figure S48, left)
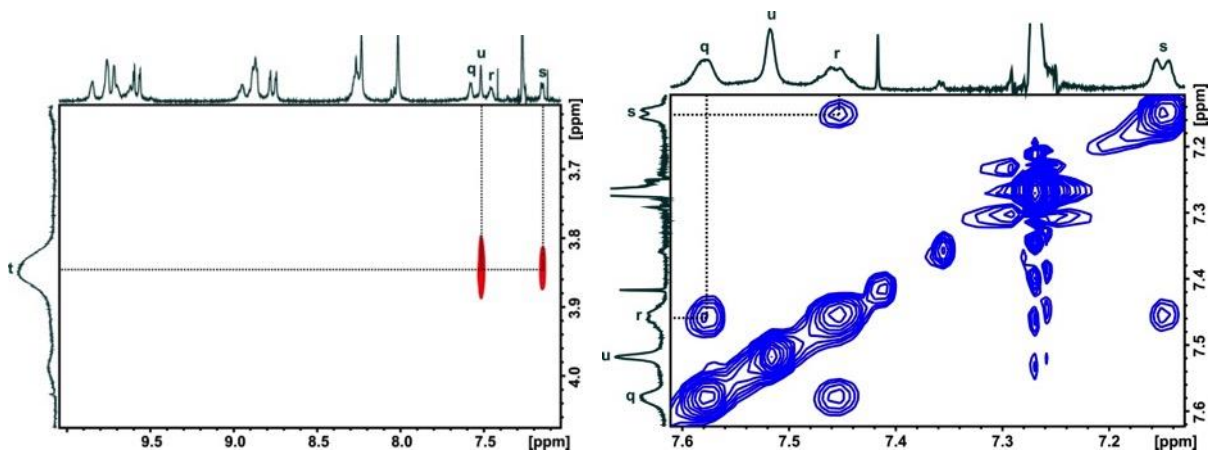
Figure S48: (left) NOESY correlation from t to s and u. (right) COSY correlation from r to s and q, the large signal at 7.27 ppm corresponds to CDCl$_3$.

It was possible to differentiate between **s** and **u** by interpreting the COSY spectrum (Figure S48, right). The protons **u** are identified as the 8-proton singlet at 7.52 ppm and show no COSY correlations, while the 8-proton doublet at 7.15 ppm, identified as **s**, shows a COSY cross-peak with **r** (8-proton multiplet at 7.46 ppm). In addition, **r** is coupled to the 8-proton doublet at 7.58 ppm labelled as **q**. The *beta*-protons from the alkoxy-porphyrin can be identified through NOESY correlations from **u** and **q** to the two 8-proton doublets (**p** and **v**) at 8.78 and 8.76 ppm, which subsequently show COSY cross-peaks to the two 8-proton doublets at 9.60 and 9.56 ppm corresponding to **o** and **w** respectively (Figure S49).

Figure S49: (left) NOESY correlations from q and u to p and v. (right) COSY correlations between the porphyrin's *beta*-protons (for the COSY cross-peak between the m and n protons please refer to Figure S46).

Assignment of the THS-Porphyrins
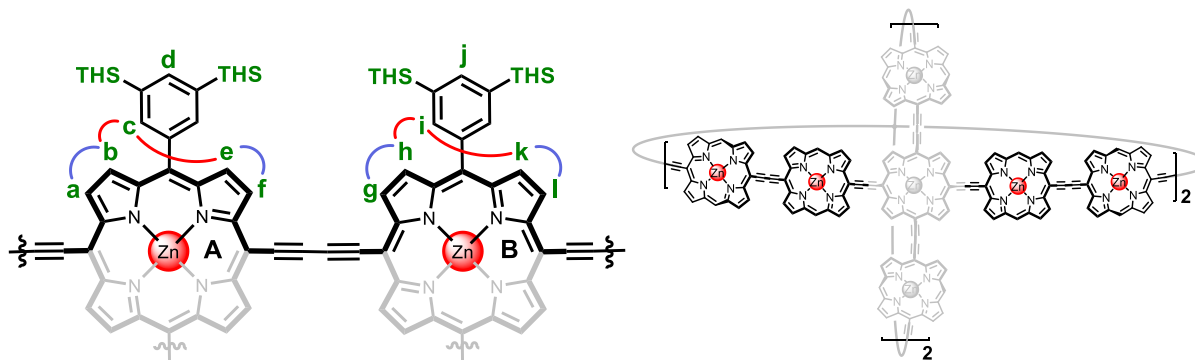
Figure S50: Proton labeling for the symmetric unit of the THS-porphyrins and an illustration of their position within the ball (THS = trihexylsilyl). Blue lines denote COSY correlations; red lines denote NOE correlations.
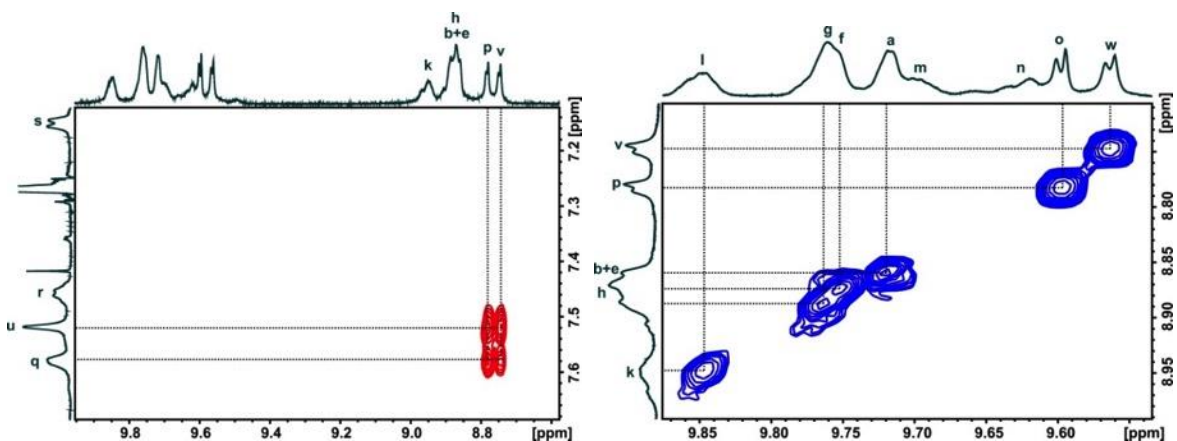
By analogy to the templated structures, the proton **l** is identified as an 8-proton multiplet at 9.85 ppm. The COSY cross-peak in Figure S49 (right) from **l** was used to characterize **k**. The NOESY correlation between the aryl protons and the porphyrins *beta*-protons are illustrated in Figure S51. The NOESY spectrum shows that **g**, **h**, **k** and **l** are coupled to **i**. Similar NOESY correlations were found for **a**, **f** and **b+e** to **c**. Both **c** and **i** were found to couple to the 16-proton singlet at 8.01 ppm which was assigned to an overlap of **d** and **j**. The correlations between **a-b**, **e-f**, **g-h**, and **k-l** were confirmed through their COSY correlations (Figure S49, right).
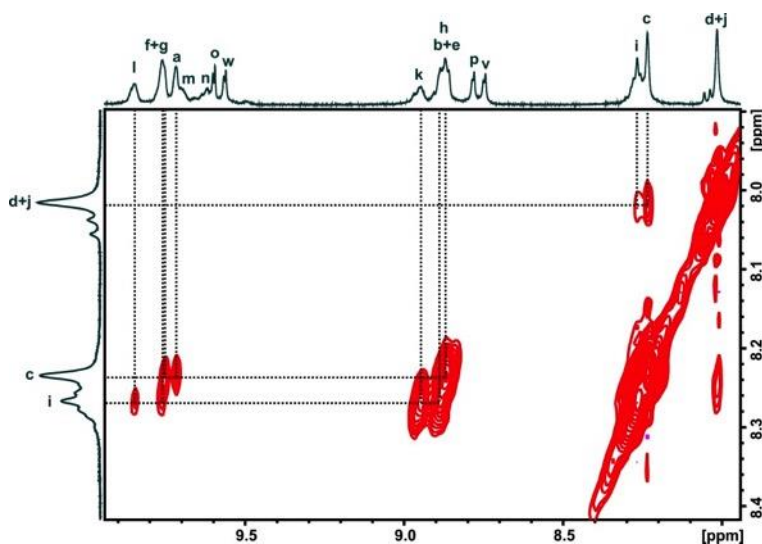
Figure S51: Direct and relayed NOESY correlations between the aryl protons to the porphyrin *beta*-protons.

D. Spectra Confirming Identity of New Compounds

Porphyrin ring (2)
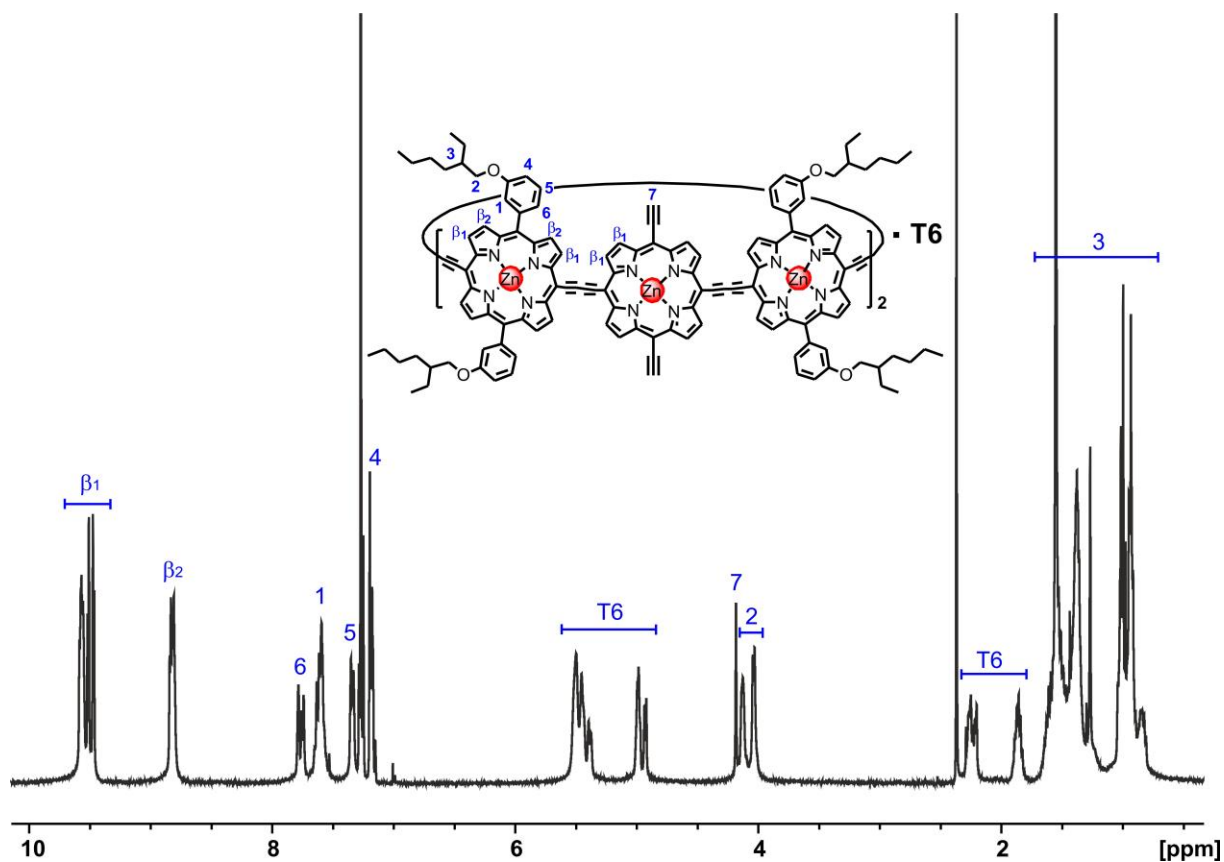
Figure S52: The ^1H NMR spectrum of 2 (400 MHz, CDCl$_3$).
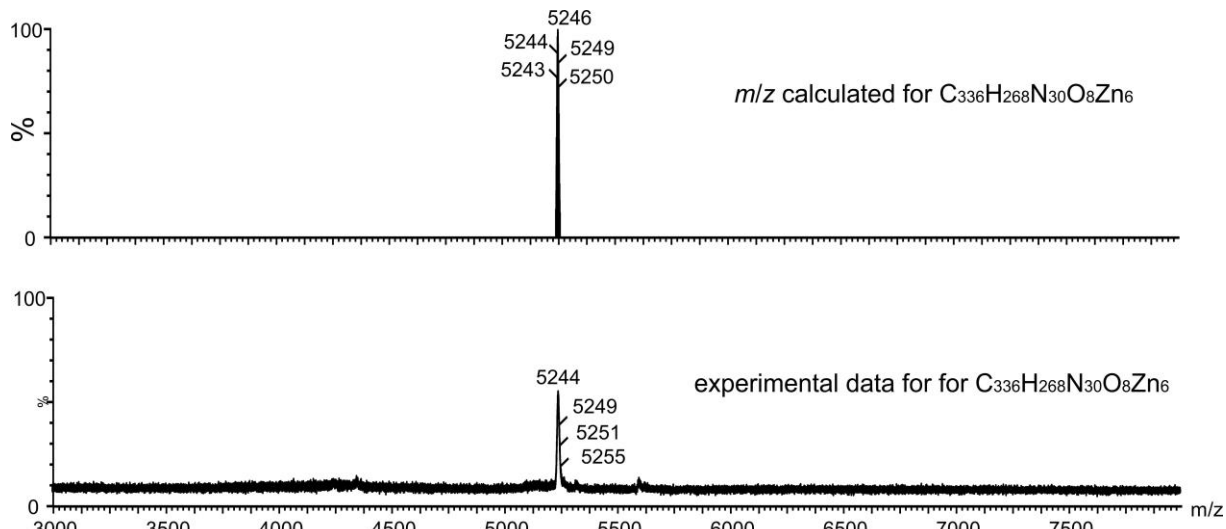
Figure S53: The MALDI-MS spectrum of 2 (m/z = 5244 (C$_{336}$H$_{268}$N$_{30}$O$_8$Zn$_6$, M$^+$ requires 5246), matrix: dithranol).
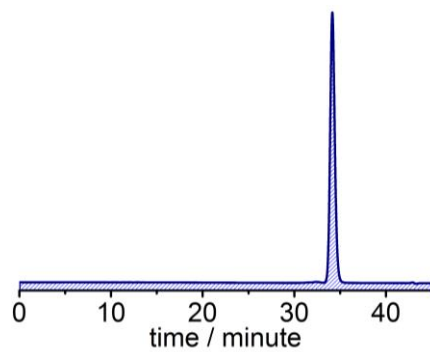
Figure S54: Analytical GPC traces (PLGel columns, THF, detection at 800 nm) of the pure 2.

Ball Precursor (4)

Figure S55: The ^{1}H NMR spectrum of 4 (400 MHz, CDCl$_3$). * indicates signals corresponding to pyridine.
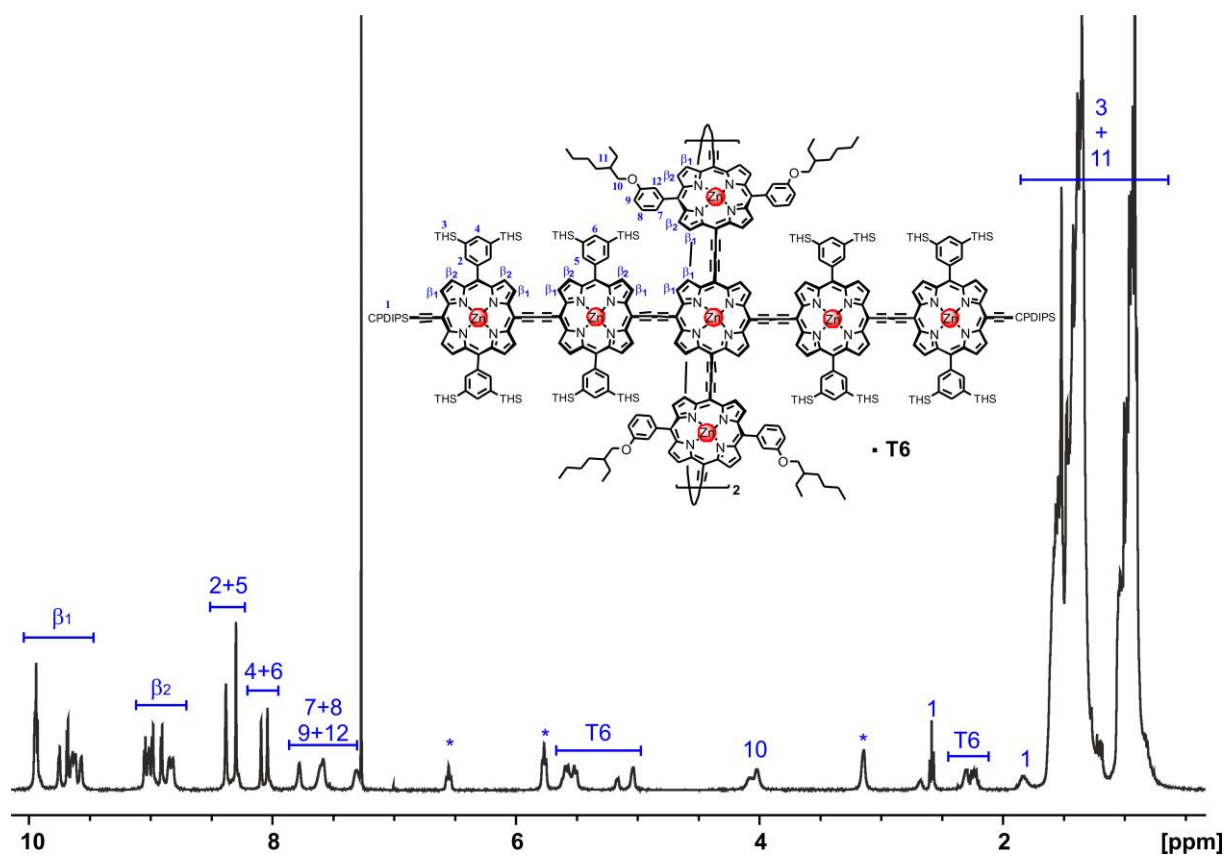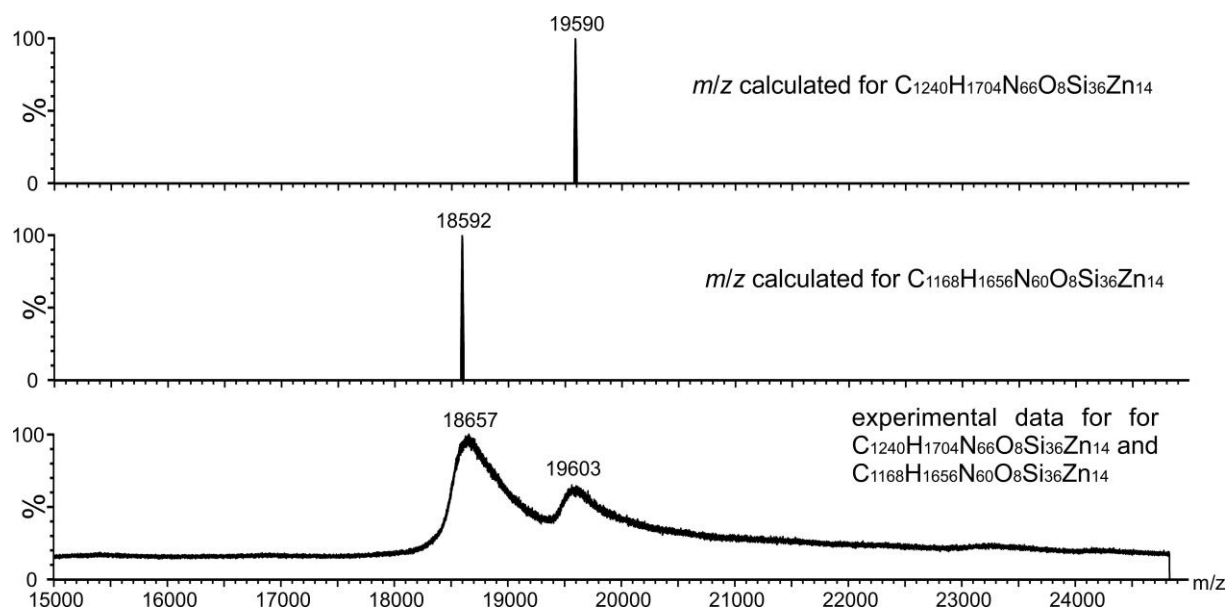
Figure S56: The MALDI-MS spectrum of 4 (*m/z* = 19590 (C$_{1240}$H$_{1704}$N$_{66}$O$_8$Si$_{36}$Zn$_{14}$, M$^+$ requires 19590), displacement of T6: 18592 (C$_{1168}$H$_{1656}$N$_{60}$O$_8$Si$_{36}$Zn$_{14}$, M$^+$ requires 18657), matrix: dithranol).

Ball Precursor (5)
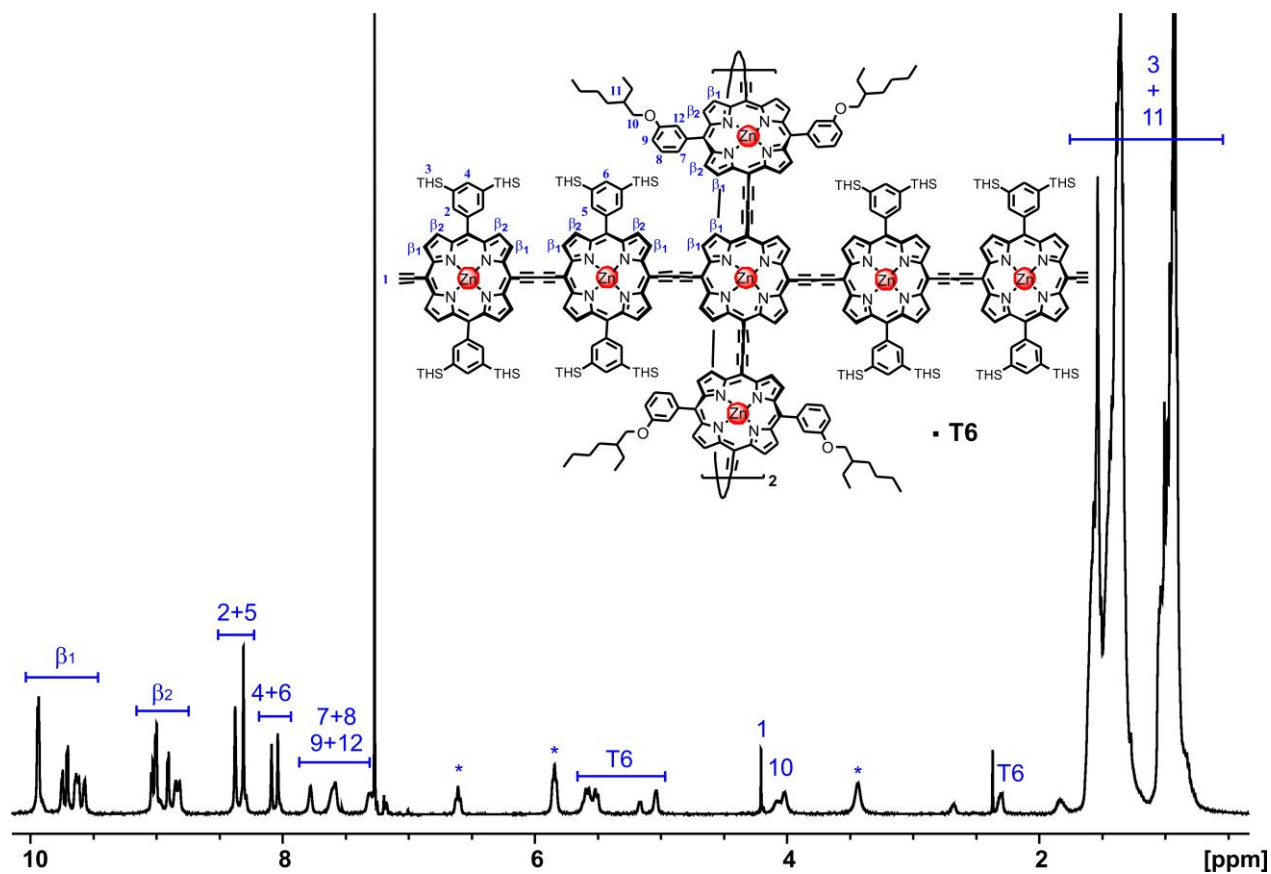
Figure S57: The ^{1}H NMR spectrum of 5 (400 MHz, CDCl$_3$). * indicates signals corresponding to pyridine.
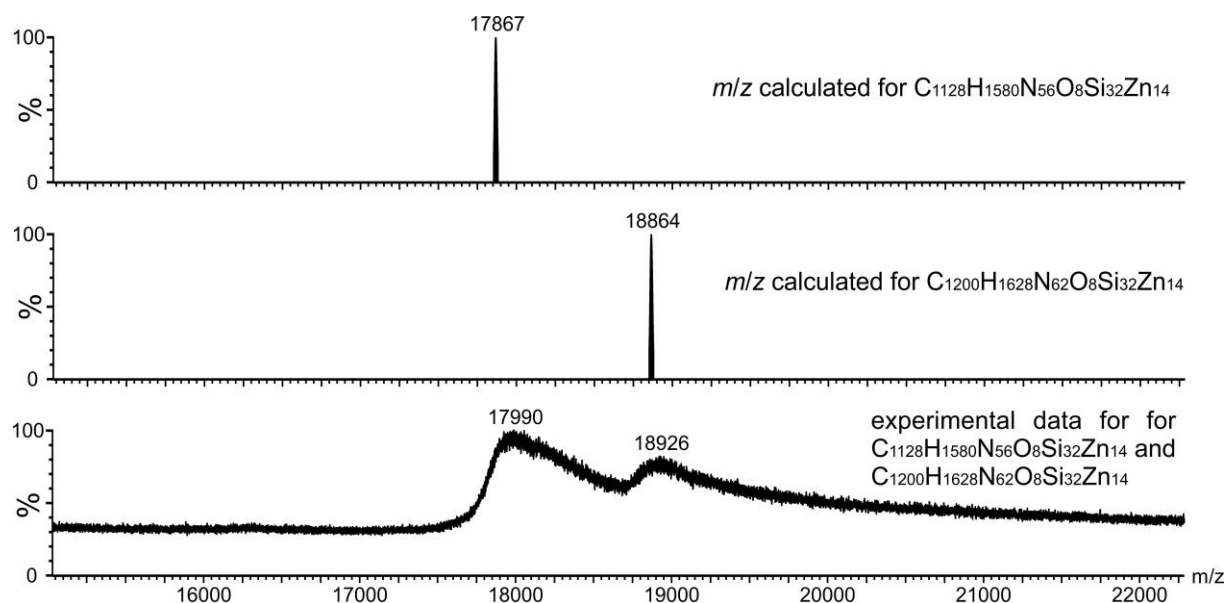
Figure S58: The MALDI-MS spectrum of 5 (m/z = 18926 ($C_{1200}H_{1628}N_{62}O_8Si_{32}Zn_{14}$, M^+ requires 18864), displacement of T6: 17990 ($C_{1128}H_{1580}N_{56}O_8Si_{32}Zn_{14}$, M^+ requires 17867), matrix: dithranol).
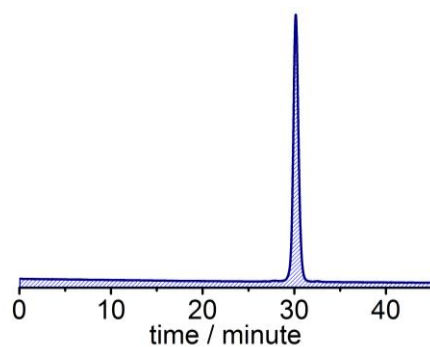
Figure S59: Analytical GPC traces (PLGel columns, THF, detection at 800 nm) of the pure 5.

b-P14·T6·(T4)₂
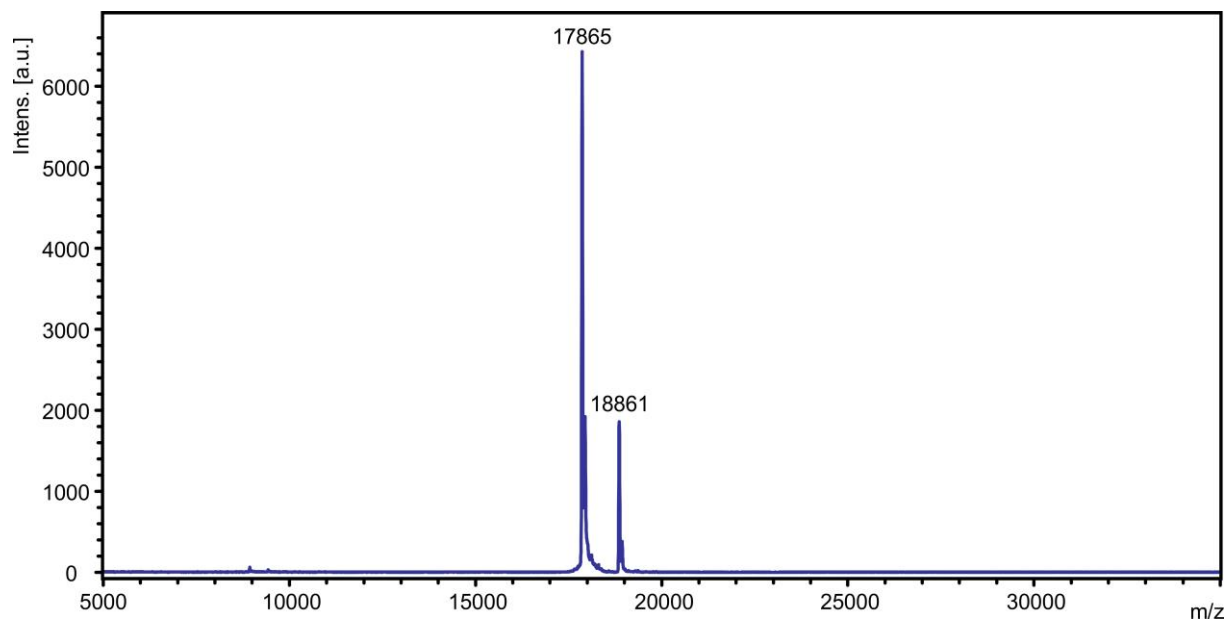
Figure S60: MALDI-ToF analysis of *b*-P14·T6·(T4)₂ acquired by the EPSRC Mass Spectrometry Center at Swansea University. DCTB was used as a matrix and samples were dissolved in CH_2Cl_2 / 5% pyridine before mixing with the matrix. Templates are fully/partially displaces upon recording of the spectrum. *b*-P14 (m/z = 17865 ($C_{1128}H_{1576}N_{56}O_8Si_{32}Zn_{14}$, M⁺ requires 17863), *b*-P14·T6 (m/z = 18861 ($C_{1200}H_{1624}N_{62}O_8Si_{32}Zn_{14}$, M⁺ requires 18861).
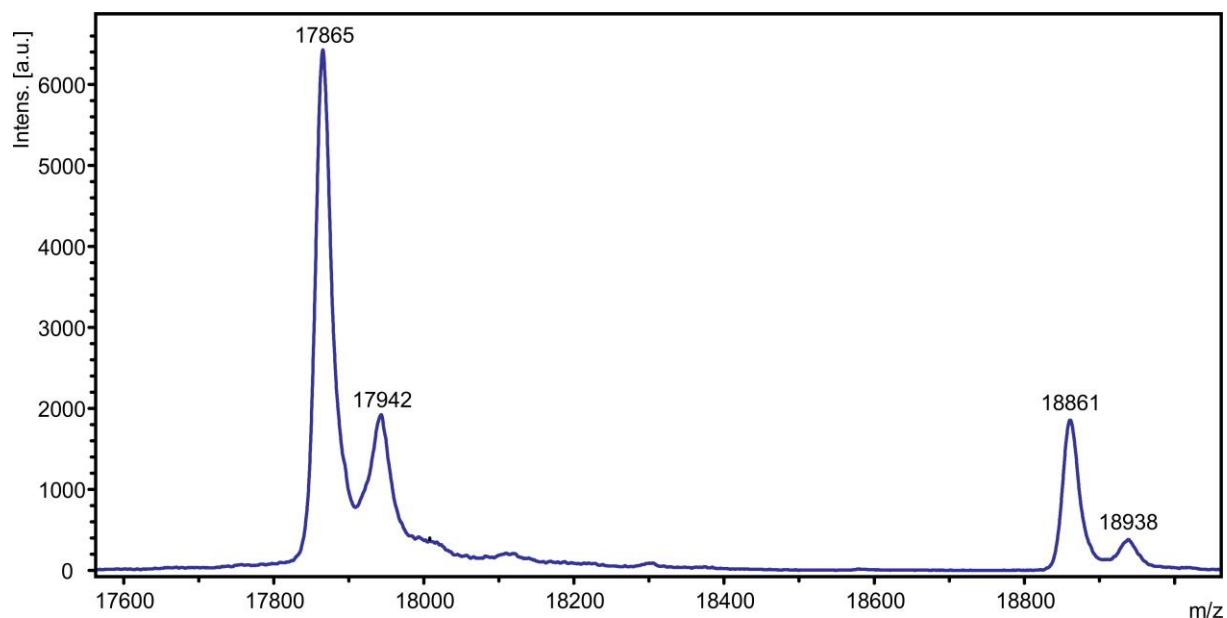
Figure S61: A zoom-in of Figure S60 reveals shoulders corresponding to complexation with pyridine. *b*-P14·pyridine (m/z = 17942 ($C_{113}H_{1581}N_{57}O_8Si_{32}Zn_{14}$, M⁺ requires 17943), *b*-P14·T6·pyridine (m/z = 18938 ($C_{1205}H_{1629}N_{63}O_8Si_{32}Zn_{14}$, M⁺ requires 18940).
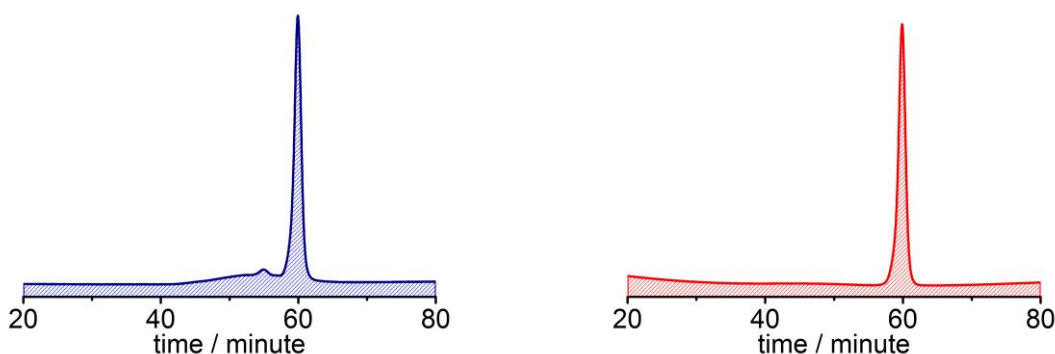
Figure S62: Recycling GPC traces (JAIGEL columns, 1st cycle shown, toluene / 1% pyridine, detection at 800 nm) of the crude reaction mixture (left) and the purified *b*-P14·T6·(T4)₂ (right).

E. UV-Vis-NIR Titrations

E.1 Reference titrations with porphyrin monomers and quinuclidine
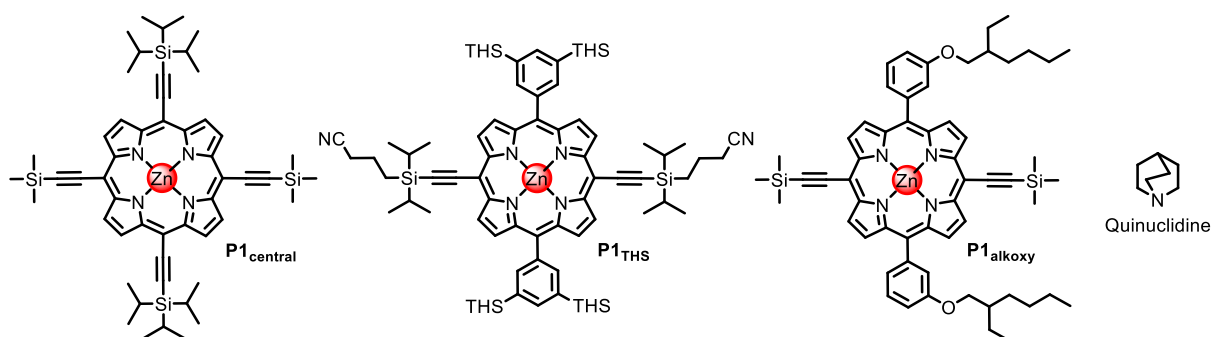
Figure S63: Structures of reference porphyrin monomers and the monodentate ligand quinuclidine.

Titrations with porphyrin monomers **P1$_{central}$**, **P1$_{THS}$** and **P1$_{alkoxy}$** with quinuclidine were performed in order to determine reference binding constants ($K_{central}$, K_{THS}, and K_{alkoxy}).

All titrations were performed in toluene at 298 K. Care was taking to keep the porphyrin concentration constant throughout the entire titration by adding porphyrin to the ligand solution before titrations were started. The binding curves were fitted using a 1:1 binding isotherm using the equation:

$$\frac{A - A_{initial}}{A_\infty - A_{initial}} = \left(\frac{(K_a([L] + [P]_0) + 1) - \sqrt{(K_a([L] + [P]_0) + 1)^2 - 4K_a^2[P]_0[L]}}{2K_a[P]_0} \right)$$

where A is the observed absorption at a specific wavelength or the difference of absorbance between two wavelengths; $A_{initial}$ is the starting absorption at this wavelength; A_∞ is the asymptotic final absorption at this wavelength; K_a is the association constant between ligand and porphyrin host; [L] is

the concentration of ligand; $[P]_0$ is the concentration of porphyrin host. The free variables which were adjusted to optimize the fit to the experimental data during the fitting procedure are $A_{initial}$, A_∞, and K_a. Fitting analysis was carried out using the Origin software (Figures S64–S69) giving K_{central} = (6.45 ± 0.42) × 10^6 M^{-1}, K_{THS} = (1.30 ± 0.04) × 10^6 M^{-1}, and K_{alkoxy} = (2.04 ± 0.09) × 10^6 M^{-1}.
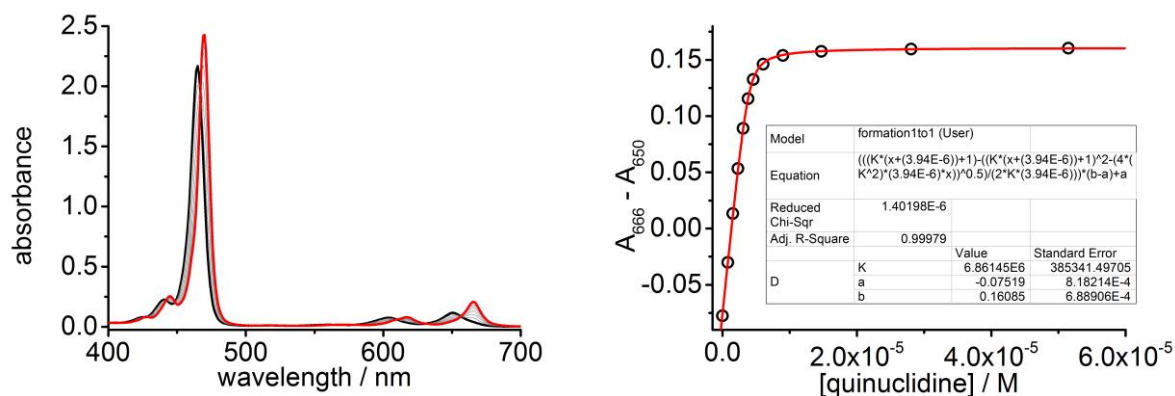
Figure S64: UV-vis titration of P1$_{central}$ and quinuclidine, R^2 = 0.9998. (Run 1, toluene, 298 K, [P1$_{central}$] = 3.94 µM, K = 6.86 × 10^6 M^{-1}).
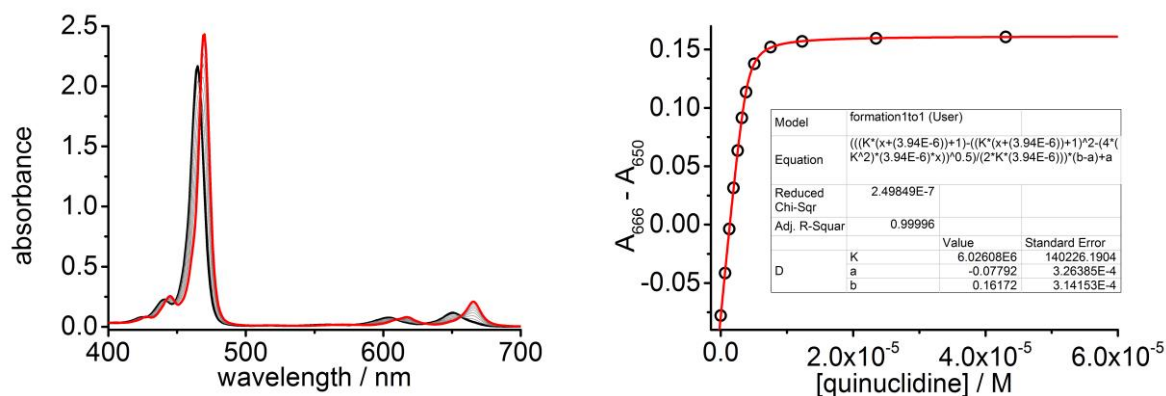
Figure S65: UV-vis titration of P1$_{central}$ and quinuclidine, R^2 = 1.0000. (Run 2, toluene, 298 K, [P1$_{central}$] = 3.94 µM, K = 6.03 × 10^6 M^{-1}).
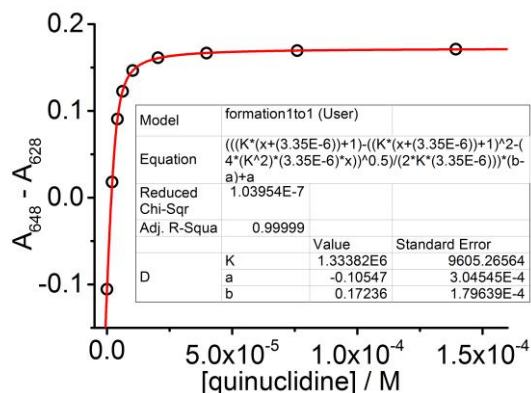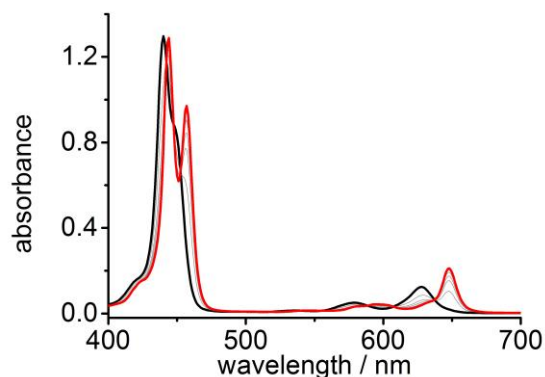
Figure S66: UV-vis titration of P1$_{THS}$ and quinuclidine, R^2 = 1.0000. (Run 1, toluene, 298 K, [P1$_{THS}$] = 3.35 µM, K = 1.33 × 10^6 M^{-1}).

Model	formation1to1 (User)	
Equation	(((K*(x+(3.35E-6))+1)-((K*(x+(3.35E-6))+1)^2-(4*(K^2)*(3.35E-6)*x))^0.5)/(2*K*(3.35E-6)))*(b-a)+a	
Reduced Chi-Sqr	1.03954E-7	
Adj. R-Squa	0.99999	
	Value	Standard Error
D K	1.33382E6	9605.26564
a	-0.10547	3.04545E-4
b	0.17236	1.79639E-4
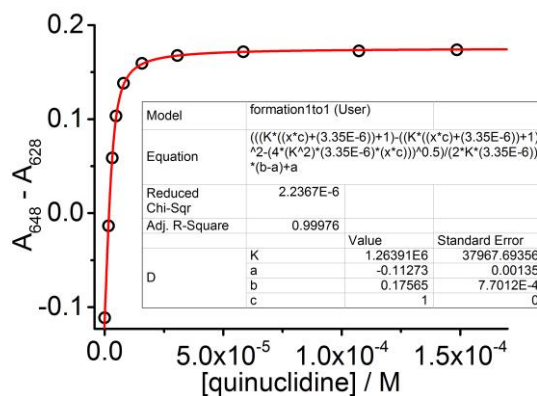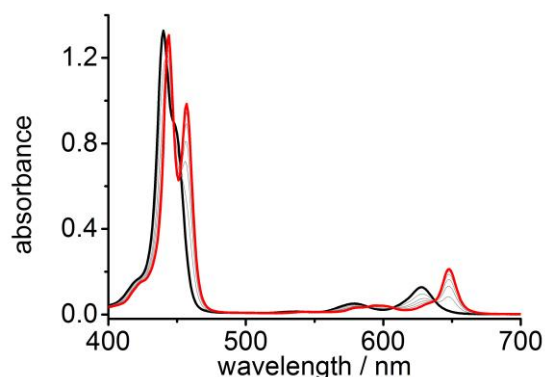
Figure S67: UV-vis titration of P1$_{THS}$ and quinuclidine, R^2 = 0.9998. (Run 2, toluene, 298 K, [P1$_{THS}$] = 3.35 µM, K = 1.26 × 10^6 M^{-1}).

Model	formation1to1 (User)	
Equation	(((K*((x*c)+(3.35E-6))+1)-((K*((x*c)+(3.35E-6))+1)^2-(4*(K^2)*(3.35E-6)*(x*c)))^0.5)/(2*K*(3.35E-6)))*(b-a)+a	
Reduced Chi-Sqr	2.2367E-6	
Adj. R-Square	0.99976	
	Value	Standard Error
D K	1.26391E6	37967.69356
a	-0.11273	0.00135
b	0.17565	7.7012E-4
c	1	0
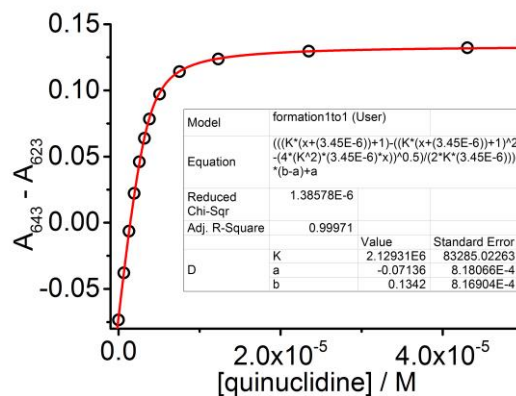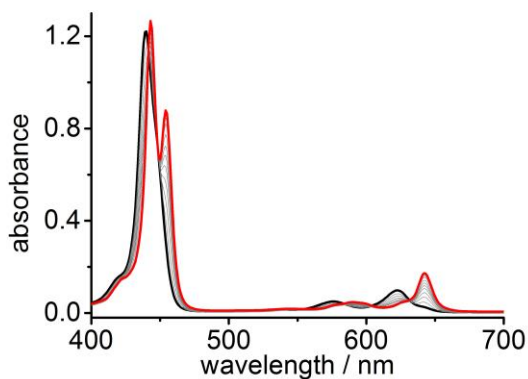
Figure S68: UV-vis titration of P1$_{alkoxy}$ and quinuclidine, R^2 = 0.9997. (Run 1, toluene, 298 K, [P1$_{alkoxy}$] = 3.45 µM, K = 2.13 × 10^6 M^{-1}).

Model	formation1to1 (User)	
Equation	(((K*(x+(3.45E-6))+1)-((K*(x+(3.45E-6))+1)^2-(4*(K^2)*(3.45E-6)*x))^0.5)/(2*K*(3.45E-6)))*(b-a)+a	
Reduced Chi-Sqr	1.38578E-6	
Adj. R-Square	0.99971	
	Value	Standard Error
D K	2.12931E6	83285.02263
a	-0.07136	8.18066E-4
b	0.1342	8.16904E-4
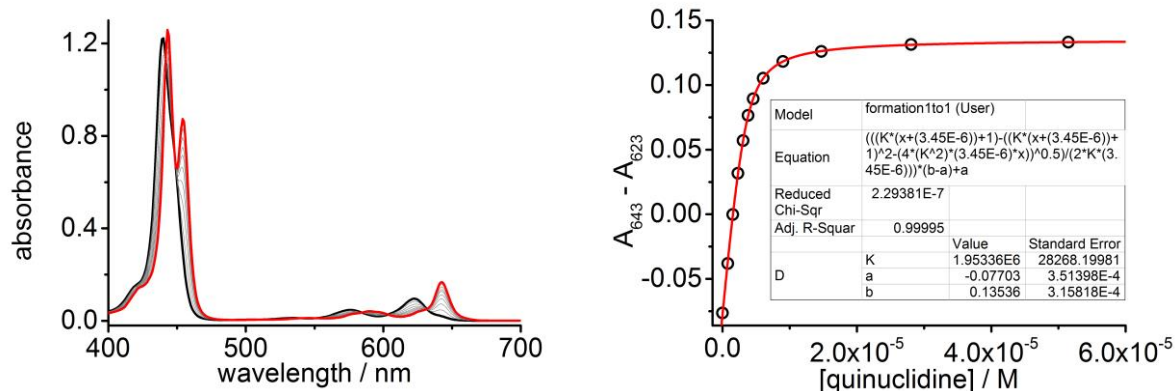
Figure S69: UV-vis titration of P1$_{alkoxy}$ and quinuclidine, R^2 = 1.0000. (Run 2, toluene, 298 K, [P1$_{alkoxy}$] = 3.45 µM, K = 1.95 × 10^6 M^{-1}).

E.2 Denaturation titrations with quinuclidine on *b*-P14·T6·(T4)$_2$

The ball *b*-P14·T6·(T4)$_2$ was isolated containing the three templates bound strongly within its cavity. In order to derive binding constant for the templates **T6** and **T4** within the ball, denaturation titrations (break-up titration) were performed with the competing ligand quinuclidine. Using the data from these break-up titrations (K_{dn} = denaturation constant) and the formation constant of the single site binding event of the competing ligand with a zinc-porphyrin monomer ($K_{central}$, K_{THS}, K_{alkoxy} = association constant for quinuclidine to its respective porphyrin monomer (K_Q)) allows us to derive the formation binding constant (K_f) between the ball and the templates using the following equation:

$$K_f = \frac{K_Q^N}{K_{dn}}$$

in which N = number of zinc porphyrin binding sites, via the thermodynamic cycle shown in Figure S70. The displacement of the templates **T4** and **T6** occurs at distinctly different quinuclidine concentrations, which makes it valid to split the thermodynamic cycle in two separate parts.

b-P14·T6·(T4)₂ ⇌ b-P14·T6 (+ 2·T4 / $K_{f(T4)}{}^2$)

$K_{dn(T4)}{}^2$ — T4 / + quinuclidine (8 equivalents)

$K_Q{}^8$ + quinuclidine (8 equivalents)

b-P14·T6·(Q)₈

+ T6 / $K_{f(T6)}$ — T6 / + quinuclidine (6 equivalents) / $K_{dn(T6)}$

b-P14·(Q)₈ ⇌ b-P14·(Q)₁₄ $K_Q{}^6$ / + quinuclidine (6 equivalents)

Figure S70: Individual thermodynamic cycles relating the formation constant of the template complex (K_f) to the denaturation constant (K_{dn}) and binding constant of each porphyrin unit for quinuclidine (K_Q).

As a result, the association constants for **T4** and **T6** within the **b-P14** can be calculated using the following equations:

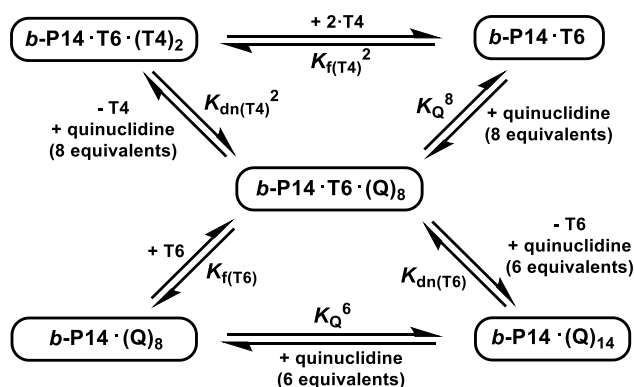$$K_{f(T4)} = \sqrt{\frac{K_Q^8}{K_{dn(T4)}^2}} \qquad \text{and} \qquad K_{f(T6)} = \frac{K_Q^6}{K_{dn(T6)}}$$

Denaturation titrations were performed in toluene at 298 K. All denaturation titrations were carried out at constant **b-P14·T6·(T4)₂** concentration by adding complex to the ligand (quinuclidine) stock solution before titrations started.

Data were fitted to the *N*-dentate denaturation binding isotherm described in the following equation:

$$\frac{A - A_{initial}}{A_\infty - A_{initial}} = \left(\frac{-K_{dn}[L]^N + \sqrt{K_{dn}^2[L]^{2N} + 4K_{dn}[L]^N[P]_0}}{2[P]_0} \right)$$

where *A* is the observed absorption at a specific wavelength or difference of absorption between two wavelengths; $A_{initial}$ is the starting absorption at a specific wavelength or difference between absorption in two wavelengths; A_∞ is the asymptotic absorption at a specific wavelength or difference of absorption in two wavelengths; K_{dn} is the denaturation constant between ligand and porphyrin oligomer complex on titrating with quinuclidine, [L] is the concentration of quinuclidine; $[P]_0$ is the concentration of porphyrin oligomer complex, *N* is the number of binding sites in the complex. The titration curves and fittings are shown below.

Table S1: Results from UV-vis-NIR titrations in Figures S71-S76

complex	K_{dn}	K_f (M^{-1})	K_σ	K_{chem} (M^{-1})	log K_{chem} (M^{-1})
b-P14·T6·(T4)$_2$ ↔ *b*-P14·T6	(1.57 ± 0.07) $\times 10^2$ M^{-3}	(1.82 ± 0.24) $\times 10^{22}$	32	(5.68 ± 0.74) $\times 10^{20}$	20.8 ± 0.1
b-P14·T6 ↔ *b*-P14	(6.84 ± 0.20) $\times 10^{-2}$ M^{-5}	(1.05 ± 0.23) $\times 10^{40}$	192	(5.47 ± 1.21) $\times 10^{37}$	37.7 ± 0.1

Figure S71: UV-vis-NIR titration of quinuclidine and *b*-P14·T6·(T4)$_2$. (Run 1, toluene, 298K, [*b*-P14·T6·(T4)$_2$] = 0.583 µM). Two stages of the titration can be observed: black to green shows the removal of the T4 templates; green to red shows the removal of T6. On the right the experimental data (black circles) and a plotted line (blue line) are shown.

Figure S72: First part of the UV-vis-NIR titration of quinuclidine and *b*-P14·T6·(T4)$_2$ illustrating the selective removal of the T4 templates. $R^2 = 0.9986$. (Run 1, toluene, 298K, [*b*-P14·T6·(T4)$_2$] = 0.583 µM, $K_{dn} = 1.51 \times 10^2$ M^{-3}). The effective concentration of the host is doubled in the calculation of the binding isotherm due to the presence of two T4 templates per ball molecule.

Figure S73: Second part of the UV-vis-NIR titration of quinuclidine and *b*-P14·T6·(T4)$_2$ illustrating the removal of the T6 template. R^2 = 0.9972. (Run 1, toluene, 298K, [*b*-P14·T6·(T4)$_2$] = 0.583 μM, K_{dn} = 6.64 × 10^{-2} M^{-3}).
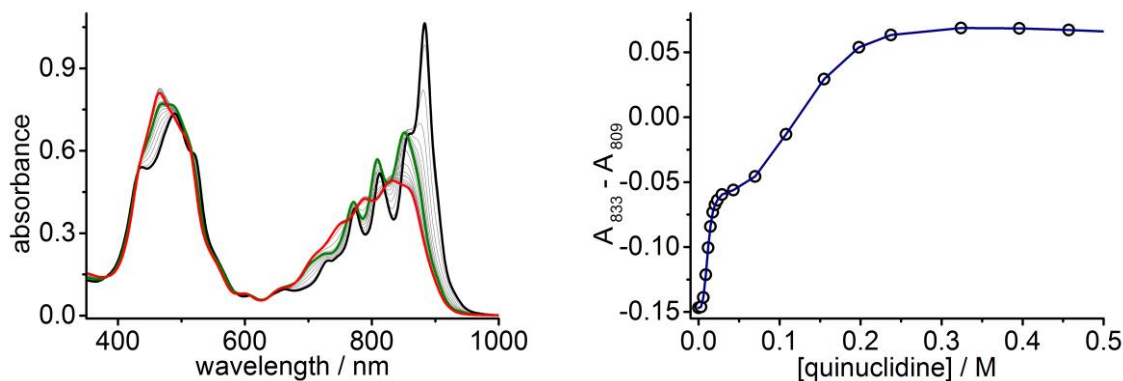
Figure S74: UV-vis-NIR titration of quinuclidine and *b*-P14·T6·(T4)$_2$. (Run 2, toluene, 298K, [*b*-P14·T6·(T4)$_2$] = 0.728 μM). Two stages of the titration can be observed: black to green shows the removal of the T4 templates; green to red shows the removal of T6. On the right the experimental data (black circles) and a plotted line (blue line) are shown.
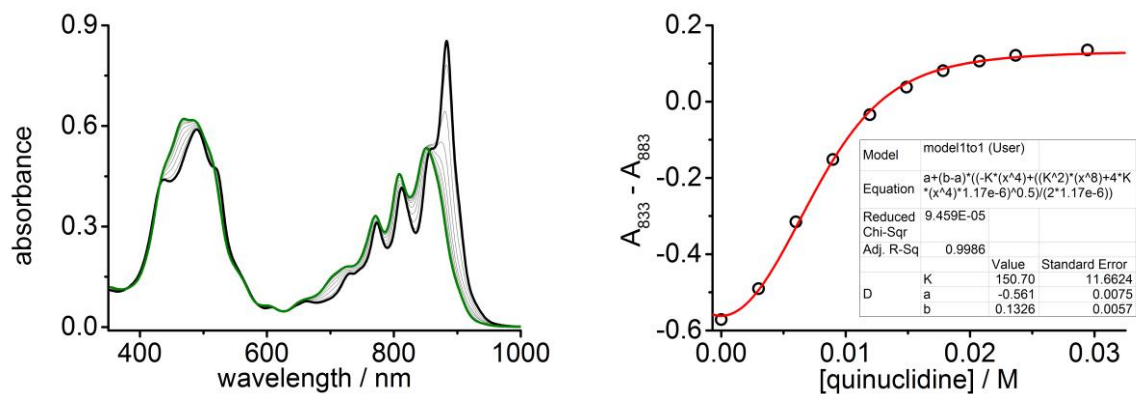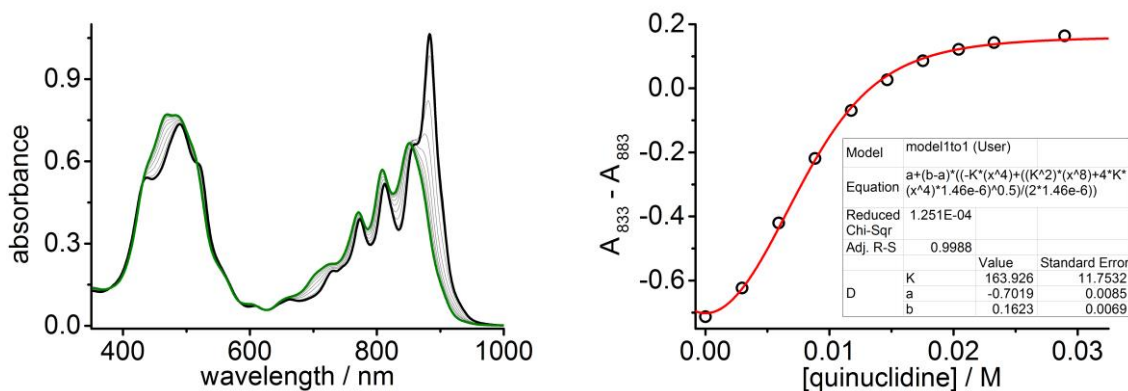

Figure S75: First part of the UV-vis-NIR titration of quinuclidine and *b*-P14·T6·(T4)$_2$ illustrating the selective removal of the T4 templates. R^2 = 0.9988. (Run 2, toluene, 298K, [*b*-P14·T6·(T4)$_2$] = 0.728 μM, K_{dn} = 1.64 × 10^2 M^{-3}). The effective concentration of the host is doubled in the calculation of the binding isotherm due to the presence of two T4 templates per ball molecule.
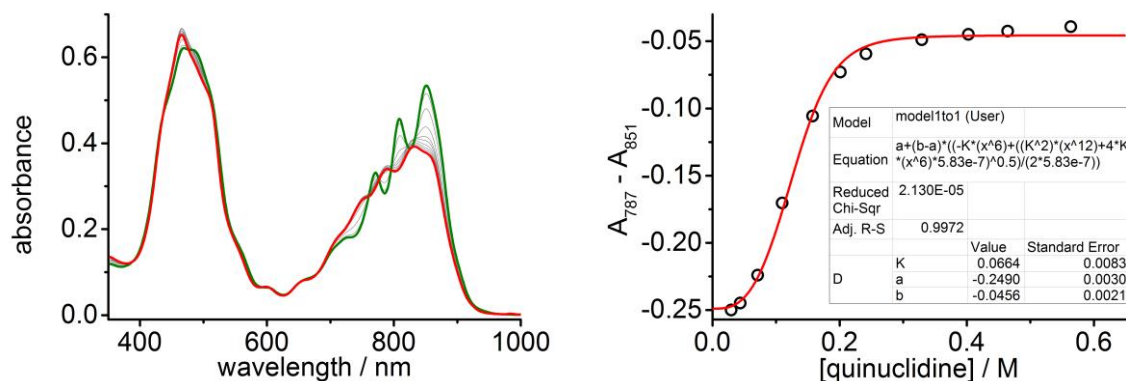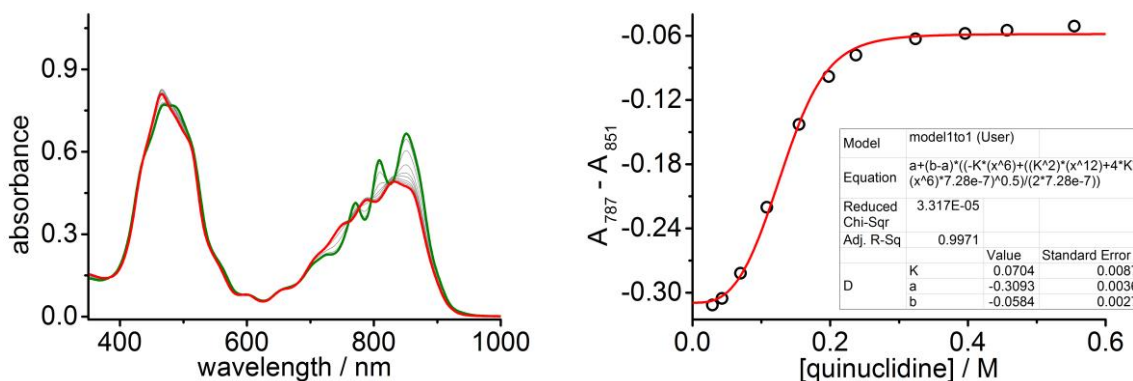
Figure S76: Second part of the UV-vis-NIR titration of quinuclidine and *b*-P14·T6·(T4)$_2$ illustrating the removal of the T6 template. R^2 = 0.9971. (Run 2, toluene, 298K, [*b*-P14·T6·(T4)$_2$] = 0.728 µM, K_{dn} = 7.04 × 10^{-2} M^{-3}).

F. Calculation of Statistical Factors

To understand the stability constants of different complexes, it is useful to factor out statistical contributions. A measured equilibrium constant K_{eq} can be factorized into its statistical component K_σ and its statistically corrected value K_{chem} according to the following equation:

$$wA + xB \rightleftharpoons yC + zD$$

$$K_{eq} = \frac{Q_C^y Q_D^z}{Q_A^w Q_C^x} = \frac{Q_A^w Q_B^x}{Q_C^y Q_D^z} \frac{Q'^y_C Q'^z_D}{Q'^w_A Q'^x_C} = K_\sigma K_{chem}$$

where for each species *i*, Q_i is the partition coefficient, Q'_i is the statistically corrected partition coefficient, and σ_i is the symmetry number.[5-7]

Values of K_σ were calculated using Benson's symmetry number method.[8,9] The symmetry number (σ) of each species is the product of its external symmetry number, σ_{ext}, (calculated from the point group of the molecule) and its internal symmetry number, σ_{int}, (calculated from the number of degenerate internal rotors). The values of σ for all the complexes involved are shown in Table S2. The external symmetry number is defined as the number of different but indistinguishable atomic arrangements that can be obtained by rotating a given molecule as a whole as a rigid object. The internal symmetry number is defined as the number of different but indistinguishable atomic arrangements that can be obtained by internal rotations around single bonds.

Table S2: Internal, external and total symmetry numbers for each component.*

component	point group	σ_{int}	σ_{ext}	σ
quinuclidine	C$_{3v}$	1	3	3
T4	C$_{2v}$	1	2	2
T6	D$_{6h}$	1	12	12
P1$_{central}$	D$_{2h}$	1	4	4
P1$_{THS}$	D$_{2h}$	1	4	4
P1$_{alkoxy}$	D$_{2h}$	1	4	4
b-P14·T6·(T4)$_2$	D$_{2h}$	1	4	4
b-P14·T6	D$_{2h}$	256	4	1024
b-P14	D$_{2h}$	16	4	64

[* Note that when counting internal rotations and calculating σ_{int}, we do not include rotors which are unaffected by the binding process, such as the para-phenylene links in **T5,** because if a rotor is unaffected by the binding process it has no influence on K_σ.]

The binding isotherm used to calculate the denaturation constants for **T4** and **T6** described in Section E.2, assume the break-up of a 1:1 porphyrin oligomer template complexes. Since the displacement of the ligands **T4** and **T6** occurs at vastly different quinuclidine concentrations, we can fit the data for both processes independently to obtain both $K_{dn(\mathbf{T4})}$ and $K_{dn(\mathbf{T6})}$. In order to factor out statistical contributions we have calculated the statistical factors for all the species involved in the process (Figure S77).
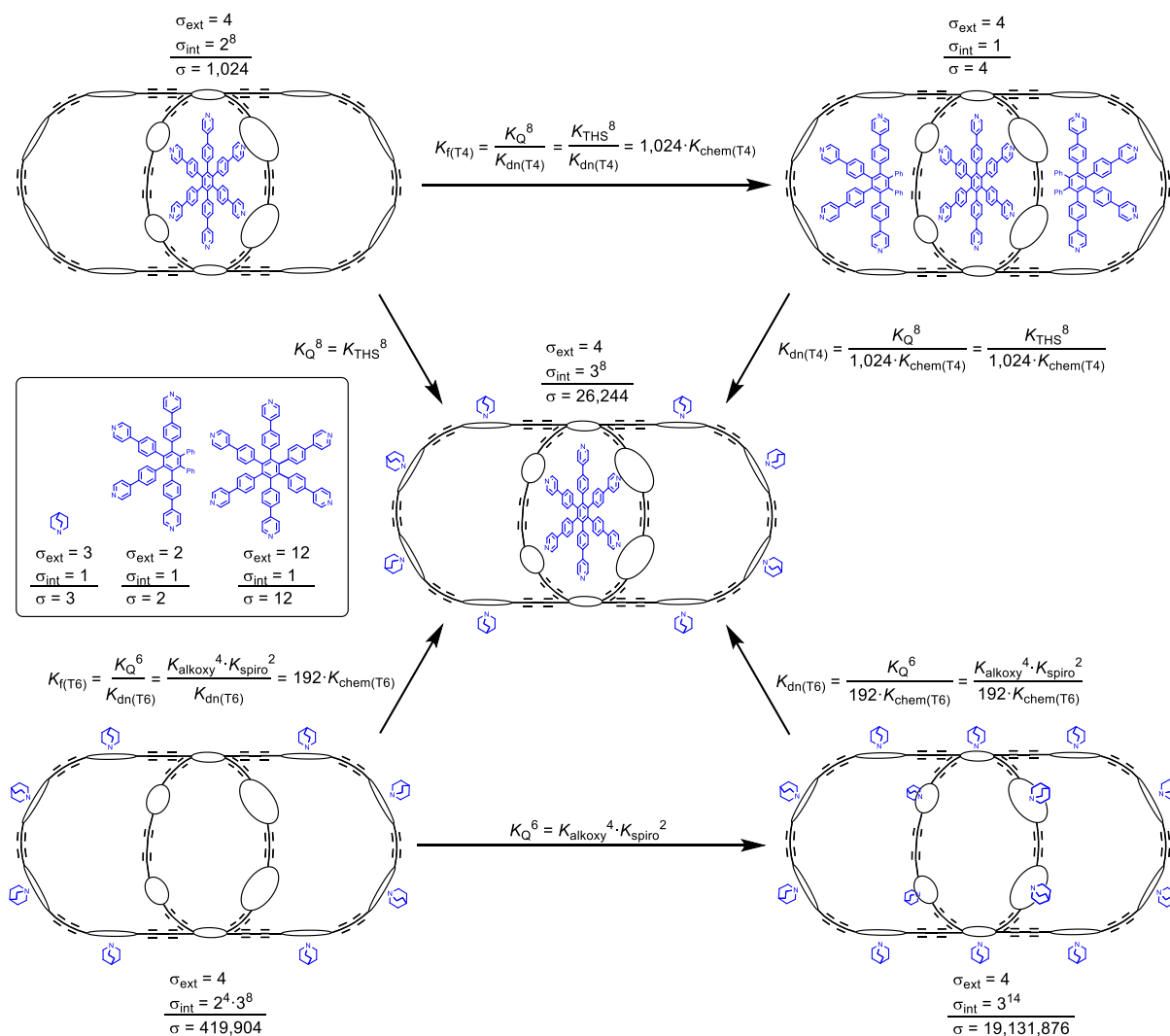
$\sigma_{ext} = 4$
$\dfrac{\sigma_{int} = 2^8}{\sigma = 1{,}024}$

$\sigma_{ext} = 4$
$\dfrac{\sigma_{int} = 1}{\sigma = 4}$

$K_{f(T4)} = \dfrac{K_Q{}^8}{K_{dn(T4)}} = \dfrac{K_{THS}{}^8}{K_{dn(T4)}} = 1{,}024 \cdot K_{chem(T4)}$

$K_Q{}^8 = K_{THS}{}^8$

$K_{dn(T4)} = \dfrac{K_Q{}^8}{1{,}024 \cdot K_{chem(T4)}} = \dfrac{K_{THS}{}^8}{1{,}024 \cdot K_{chem(T4)}}$

$\sigma_{ext} = 4$
$\dfrac{\sigma_{int} = 3^8}{\sigma = 26{,}244}$

$\sigma_{ext} = 3$ $\quad$ $\sigma_{ext} = 2$ $\quad$ $\sigma_{ext} = 12$
$\dfrac{\sigma_{int} = 1}{\sigma = 3}$ $\quad$ $\dfrac{\sigma_{int} = 1}{\sigma = 2}$ $\quad$ $\dfrac{\sigma_{int} = 1}{\sigma = 12}$

$K_{f(T6)} = \dfrac{K_Q{}^6}{K_{dn(T6)}} = \dfrac{K_{alkoxy}{}^4 \cdot K_{spiro}{}^2}{K_{dn(T6)}} = 192 \cdot K_{chem(T6)}$

$K_{dn(T6)} = \dfrac{K_Q{}^6}{192 \cdot K_{chem(T6)}} = \dfrac{K_{alkoxy}{}^4 \cdot K_{spiro}{}^2}{192 \cdot K_{chem(T6)}}$

$K_Q{}^6 = K_{alkoxy}{}^4 \cdot K_{spiro}{}^2$

$\sigma_{ext} = 4$
$\dfrac{\sigma_{int} = 2^4 \cdot 3^8}{\sigma = 419{,}904}$

$\sigma_{ext} = 4$
$\dfrac{\sigma_{int} = 3^{14}}{\sigma = 19{,}131{,}876}$

Figure S77: Statistical factors involved in the formation and denaturation (quinuclidine) of the *b*-P14·T6·(T4)$_2$ complex.

Since we assume the denaturation of a 1:1 porphyrin oligomer template complex, we need to assume that both halves of the 10-porphyrin nanoring containing the **T4** templates act independently. This observation drastically changes the statistical factors involved in the process and subsequently changes the equations used to determine the formation constant for the **T4** template (Figure S78).
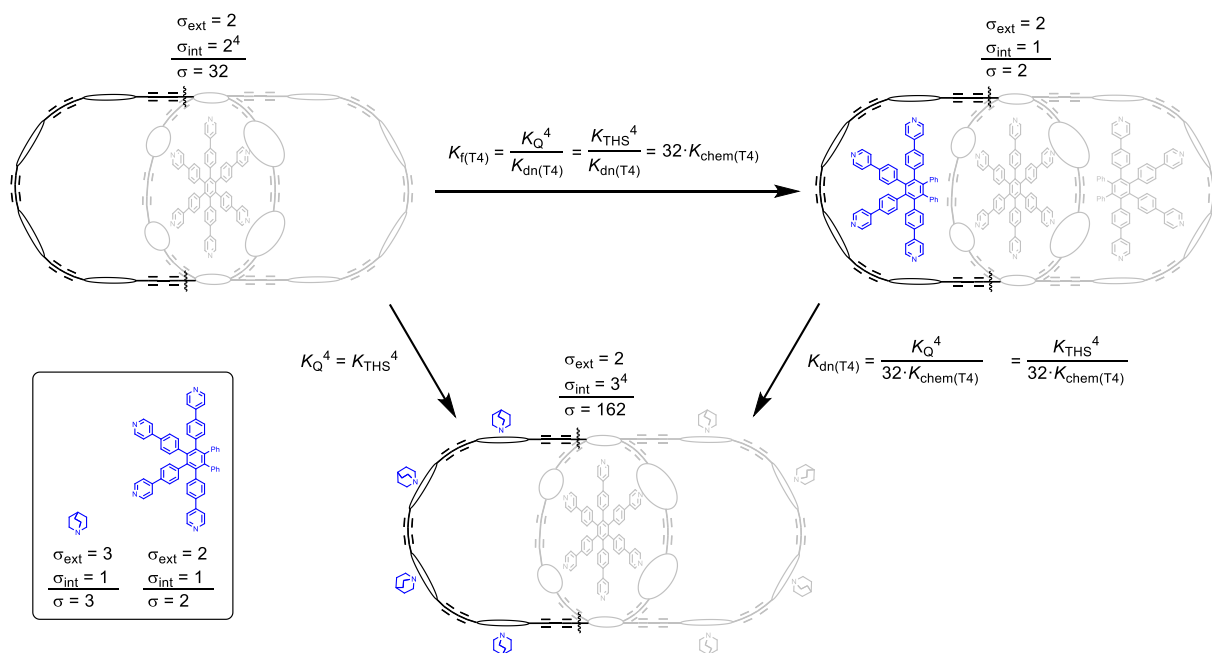
$\sigma_{ext} = 2$
$\dfrac{\sigma_{int} = 2^4}{\sigma = 32}$

$\sigma_{ext} = 2$
$\dfrac{\sigma_{int} = 1}{\sigma = 2}$

$$K_{f(T4)} = \frac{K_Q^4}{K_{dn(T4)}} = \frac{K_{THS}^4}{K_{dn(T4)}} = 32 \cdot K_{chem(T4)}$$

$$K_Q^4 = K_{THS}^4$$

$\sigma_{ext} = 2$
$\dfrac{\sigma_{int} = 3^4}{\sigma = 162}$

$$K_{dn(T4)} = \frac{K_Q^4}{32 \cdot K_{chem(T4)}} = \frac{K_{THS}^4}{32 \cdot K_{chem(T4)}}$$

$\sigma_{ext} = 3$
$\dfrac{\sigma_{int} = 1}{\sigma = 3}$

$\sigma_{ext} = 2$
$\dfrac{\sigma_{int} = 1}{\sigma = 2}$

Figure S78: Statistical factors involved in the removal of the T4 templates from the *b*-P14·T6·(T4)₂ complex with quinuclidine.

When calculating the statistical factors involved with the removal of the **T6** template, σ_{int} is drastically reduced in size by not including the rotors which are unaffected by the binding process, such as the rotations of the eight quinuclidine units bound to the 10-porphyrin nanoring (Figure S79). Since these rotors are identical in all three complexes, they have no influence on K_σ.
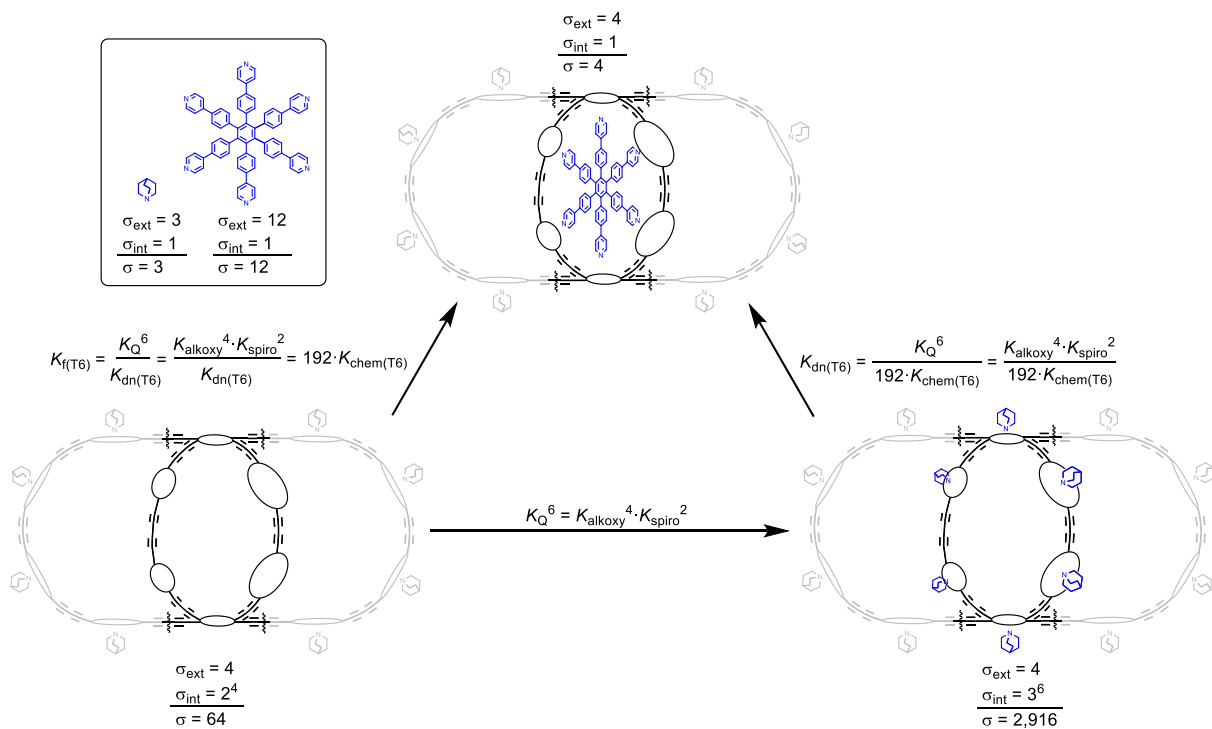
$\sigma_{ext} = 4$
$\dfrac{\sigma_{int} = 1}{\sigma = 4}$

$\sigma_{ext} = 3$
$\dfrac{\sigma_{int} = 1}{\sigma = 3}$

$\sigma_{ext} = 12$
$\dfrac{\sigma_{int} = 1}{\sigma = 12}$

$$K_{f(T6)} = \frac{K_Q^6}{K_{dn(T6)}} = \frac{K_{alkoxy}^4 \cdot K_{spiro}^2}{K_{dn(T6)}} = 192 \cdot K_{chem(T6)}$$

$$K_{dn(T6)} = \frac{K_Q^6}{192 \cdot K_{chem(T6)}} = \frac{K_{alkoxy}^4 \cdot K_{spiro}^2}{192 \cdot K_{chem(T6)}}$$

$$K_Q^6 = K_{alkoxy}^4 \cdot K_{spiro}^2$$

$\sigma_{ext} = 4$
$\dfrac{\sigma_{int} = 2^4}{\sigma = 64}$

$\sigma_{ext} = 4$
$\dfrac{\sigma_{int} = 3^6}{\sigma = 2{,}916}$

Figure S79: Statistical factors involved in the removal of the T6 template from the *b*-P14·T6 complex with quinuclidine.

G. Computational Chemistry

G.1 Geometry Optimization

Starting coordinates for **b-P14** were derived by combining fragments from the previously optimized **c-P6** porphyrin nanoring.[10] The computational model of **b-P14** does not include template molecules, and the aryl side-groups are truncated to –H.

An initial Molecular Mechanics geometry optimization of **b-P14** was performed using HyperChem 8, using a modified form of HyperChem's MM+ forcefield, incorporating literature parameters for porphyrins and butadiynes.[11-14] Minimizations were performed using the steepest descent and Polak-Ribiere algorithms. The coordinates of the Molecular Mechanics optimized geometry were used as starting point for the subsequent DFT calculations.

All DFT calculations were carried out using Gaussian 09/D.01.[15] The optimized geometry of **b-P14** was calculated at the B3LYP[16] level of theory employing the 6-31G* basis set,[17-20] with the addition of Grimme's empirical dispersion correction (GD3).[21] First, a geometry optimization was performed using loose convergence criteria. For the ultimate geometry optimization, tight convergence criteria were used and D_{2h} symmetry was followed during the optimization. The minimum nature of the optimized geometry was confirmed by the absence of imaginary vibrational frequencies. The computed energy of **b-P14** is −41164.80707 a.u. (B3LYP/6-31G* GD3).

When the optimization was performed without symmetry constraints, the resulting optimized geometry has essentially D_{2h} symmetry (the root-mean-squared deviation in the position of atoms between the final geometry (C_1) and a resymmetrized (D_{2h}) form is only about 0.001 Å). Furthermore, the computed energy, orbital energies, excited state energies with corresponding oscillator strengths and NTO eigenvalues are near identical for the geometries computed with and without symmetry constraints. The values depicted below are those obtained following D_{2h} symmetry.

Table S3: Energies of the Molecular Orbitals as shown in Figure 5 of the main text (calculated at the B3LYP/6-31G* level of theory).

Orbital	Energy (eV)
LUMO+7	-2.9197
LUMO+6	-2.9339
LUMO+5	-3.0035
LUMO+4	-3.0114

LUMO+3	-3.1388
LUMO+2	-3.1426
LUMO+1	-3.2245
LUMO	-3.2310
HOMO	-4.6556
HOMO-1	-4.7832
HOMO-2	-4.8381
HOMO-3	-4.8673
HOMO-4	-4.9834
HOMO-5	-5.0732
HOMO-6	-5.1799
HOMO-7	-5.1821

The calculated Cartesian coordinates can be found in the separately provided .xyz file.

G.2 Time-Dependent Density Functional Theory (TD-DFT)

TD-DFT calculations (B3LYP/6-31G*) were conducted for the first 32 excited states.

Natural transition orbitals (NTOs) were calculated for the excited states marked in red in Table S4: The first three excited states and the subsequent six states with the highest oscillation strengths (f).

Table S4: TD-DFT Excitation energies and oscillator strengths calculated at the B3LYP/6-31G* level of energy. NTOs were calculated for the excited states marked in red.

excited state	eV	nm	f
1	1.163	1066.0	0
2	1.203	1030.4	0
3	1.295	957.3	0.129
4	1.335	928.8	5.119
5	1.401	884.7	0.829
6	1.427	868.7	0
7	1.437	863.0	0.438
8	1.451	854.4	0.295
9	1.478	839.1	0
10	1.489	832.6	0
11	1.497	828.2	0.606
12	1.504	824.4	0
13	1.510	821.4	1.611

14	1.524	813.7	0
15	1.571	789.5	0
16	1.579	785.3	2.817
17	1.589	780.2	0.989
18	1.594	778.0	0
19	1.594	778.0	0
20	1.600	774.8	0
21	1.609	770.8	0
22	1.609	770.8	1.516
23	1.619	766.0	0
24	1.631	760.2	0
25	1.677	739.6	0
26	1.688	734.6	0
27	1.696	730.9	0.064
28	1.710	724.9	0
29	1.716	722.5	0.398
30	1.717	722.0	0
31	1.719	721.4	0
32	1.722	720.2	0.428
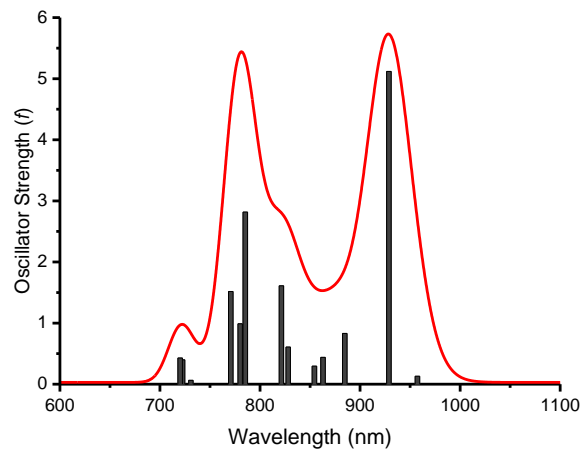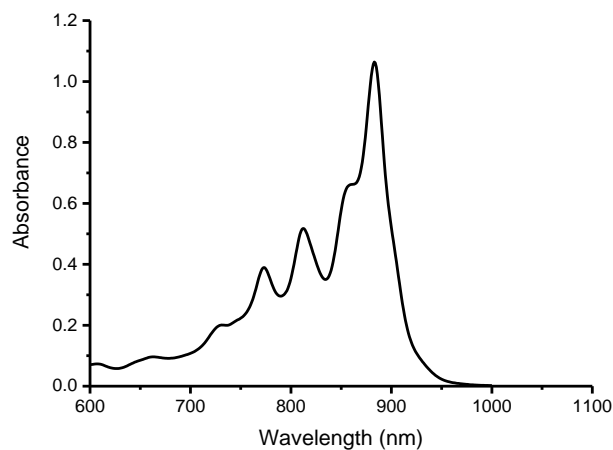
Figure S80: (Left) Region of the UV-vis-NIR absorption of the b-P14·T6·(T4)$_2$ complex ([0.7 µM], measured in toluene at 298 K). (Right) (grey bars) Calculated wavelength vs. oscillator strength of the 14-porphyrin nanoball. (red) simulated absorption spectrum assuming a Gaussian line-shape for each transition, with width 575 cm^{-1}. Calculated at the B3LYP/6-31G* level of energy.

Table S5: Natural Transition Orbitals (NTOs) calculated at the B3LYP/6-31G* level of theory of the 1st excited state (f = 0.0). The eigenvalue associated with the NTO hole/electron pair is shown as λ.
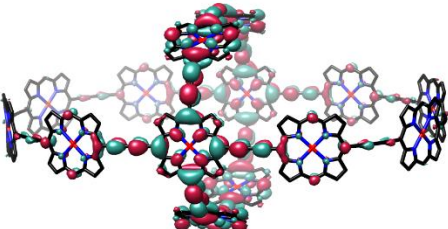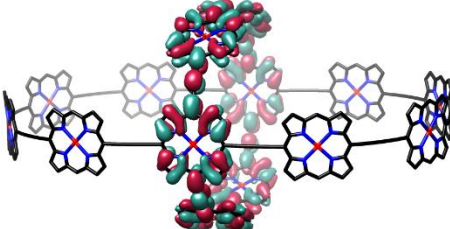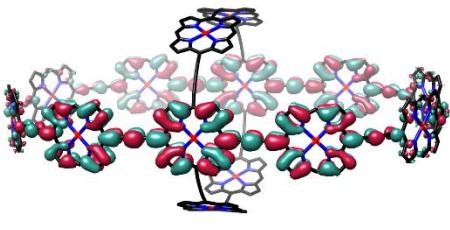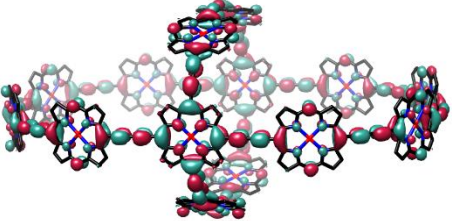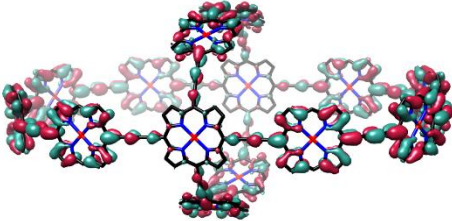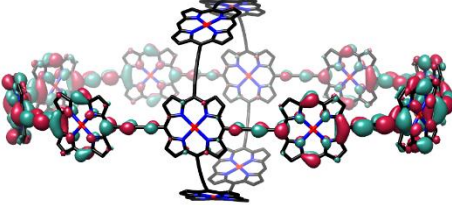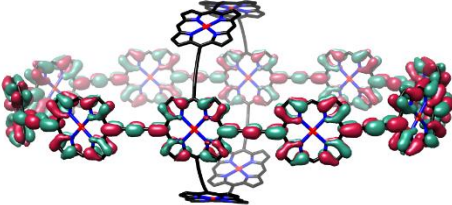
Hole	Electron	λ
S$_0$-S$_1$ (1066.0 nm; *f* = 0.0)		

0.912

Table S6: Natural Transition Orbitals (NTOs) calculated at the B3LYP/6-31G* level of theory of the 2nd excited state (f = 0.0). The eigenvalue associated with the NTO hole/electron pair is shown as λ.
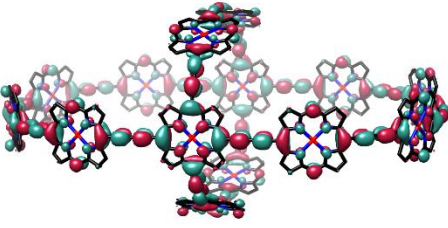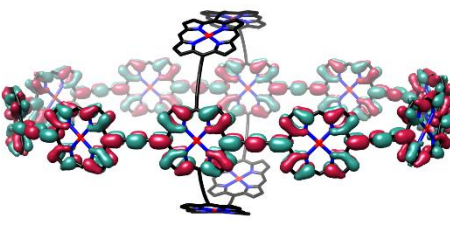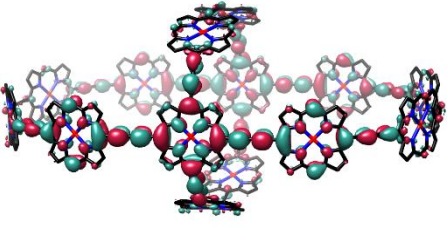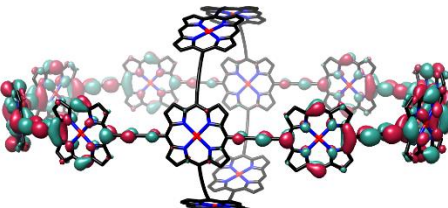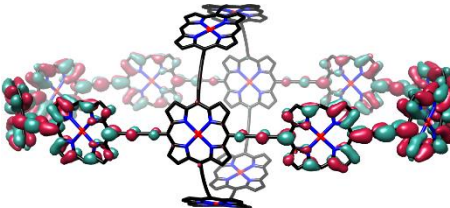
Hole	Electron	λ
S$_0$-S$_2$ (1030.4 nm; *f* = 0.0)		

0.756

0.111

0.096

Table S7: Natural Transition Orbitals (NTOs) calculated at the B3LYP/6-31G* level of theory of the 3rd excited state (f = 0.129). The eigenvalue associated with the NTO hole/electron pair is shown as λ.
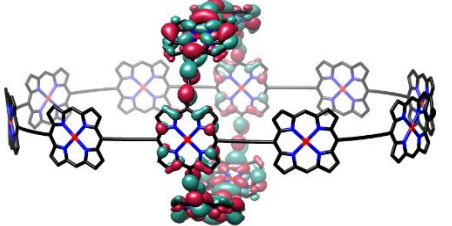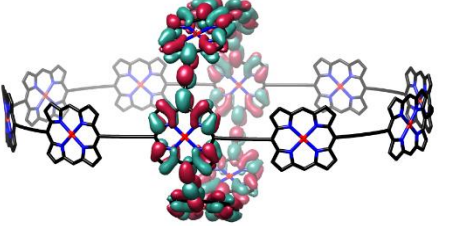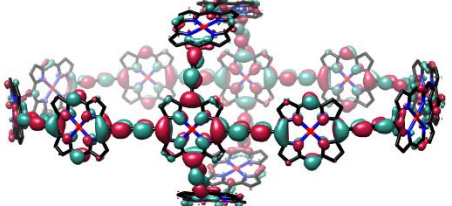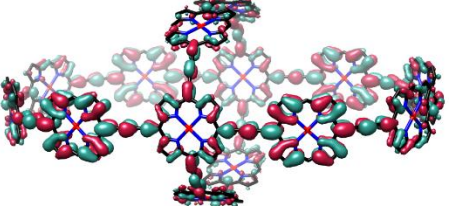
Hole	Electron	λ

S$_0$-S$_3$ (957.3 nm; *f* = 0.129)

		0.660
		0.190
		0.048
		0.037

Table S8: Natural Transition Orbitals (NTOs) calculated at the B3LYP/6-31G* level of theory of the 4th excited state (f = 5.119). The eigenvalue associated with each NTO hole/electron pair is shown as λ.
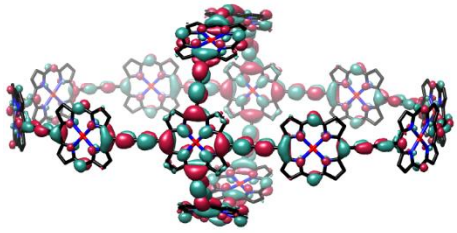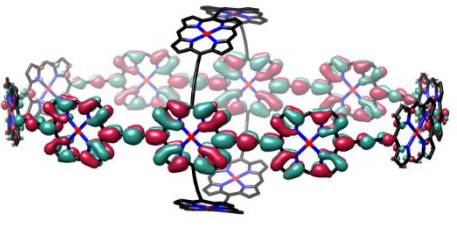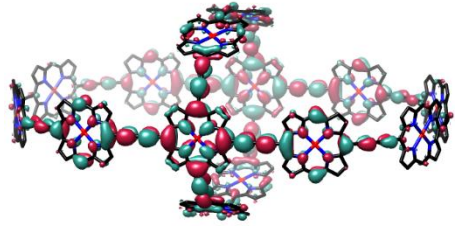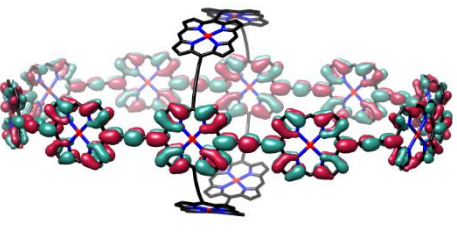
Hole	Electron	λ

S_0-S_4 (928.8 nm; f = 5.119)

0.703

0.260

Table S9: Natural Transition Orbitals (NTOs) calculated at the B3LYP/6-31G* level of theory of the 5th excited state (f = 0.829). The eigenvalue associated with each NTO hole/electron pair is shown as λ.

Hole	Electron	λ

S_0-S_5 (884.7 nm; f = 0.829)

0.953

Table S10: Natural Transition Orbitals (NTOs) calculated at the B3LYP/6-31G* level of theory of the 13th excited state (f = 1.611). The eigenvalue associated with each NTO hole/electron pair is shown as λ.
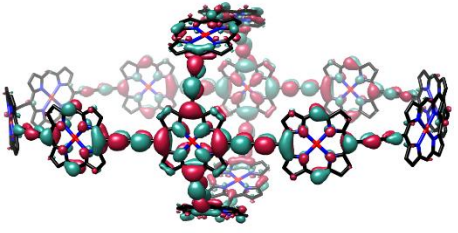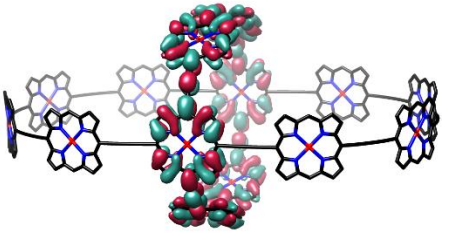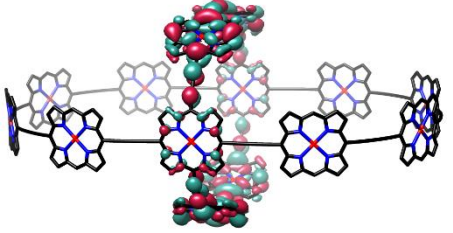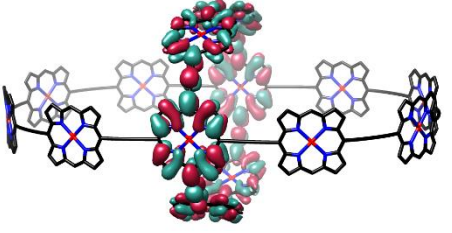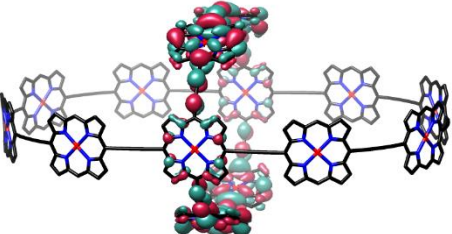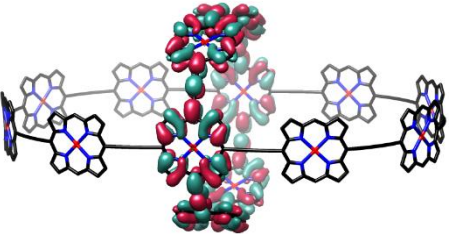
Hole	Electron	λ

S₀-S₁₃ (821.4 nm; _f_ = 1.611)

		0.891
		0.057
		0.035

Table S11: Natural Transition Orbitals (NTOs) calculated at the B3LYP/6-31G* level of theory of the 16th excited state (f = 2.817). The eigenvalue associated with each NTO hole/electron pair is shown as λ.
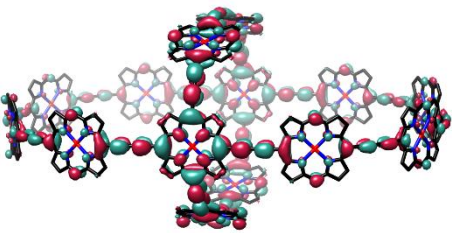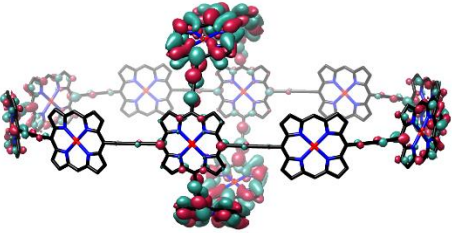
Hole	Electron	λ

S₀-S₁₆ (785.3 nm; _f_ = 2.817)

		0.746

0.145

0.046

0.030

Table S12: Natural Transition Orbitals (NTOs) calculated at the B3LYP/6-31G* level of theory of the 17th excited state (f = 0.989). The eigenvalue associated with each NTO hole/electron pair is shown as λ.
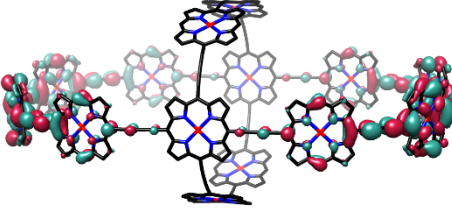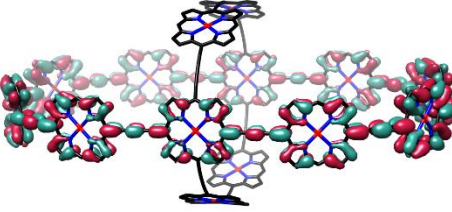
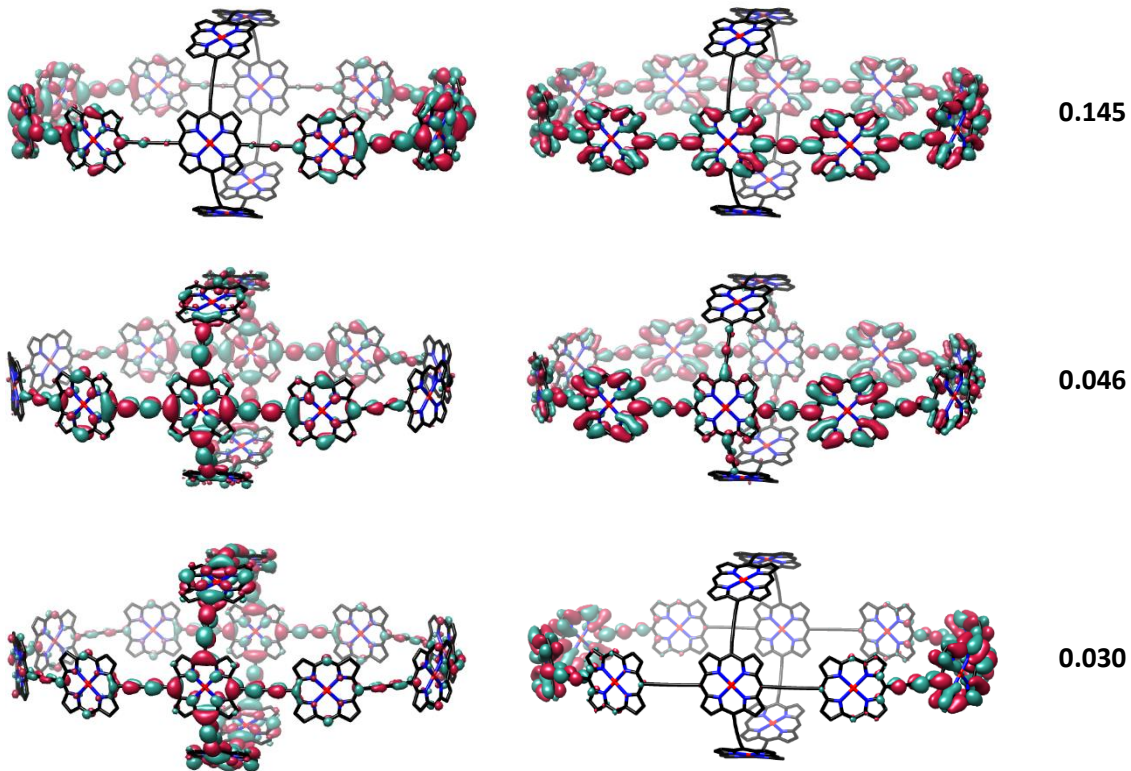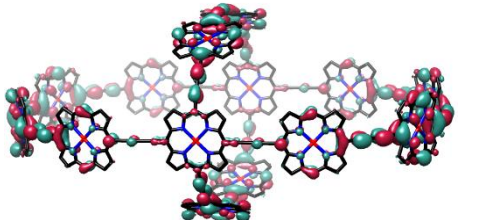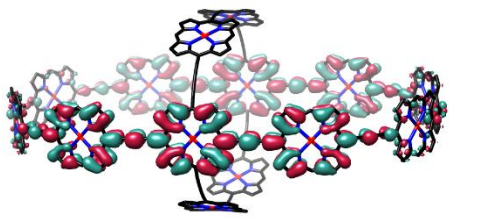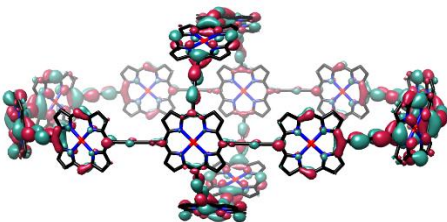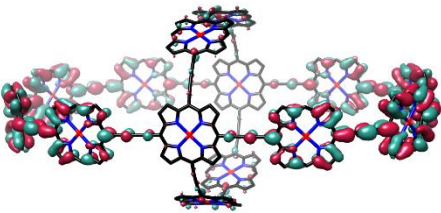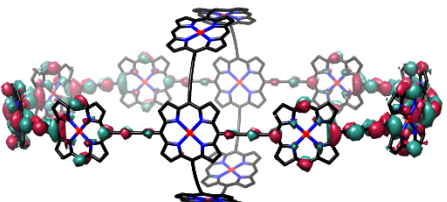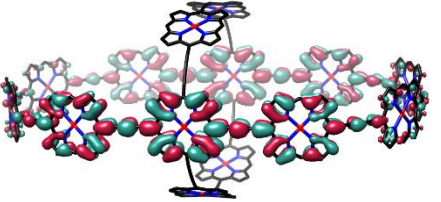| Hole	Electron	λ
S_0-S_{17} (780.2 nm; *f* = 0.989)		
		0.924

Table S13: Natural Transition Orbitals (NTOs) calculated at the B3LYP/6-31G* level of theory of the 22nd excited state (f = 1.516). The eigenvalue associated with each NTO hole/electron pair is shown as λ.

Hole	Electron	λ

S$_0$-S$_{22}$ (770.8 nm; *f* = 1.516)

0.819

0.134

H. Photophysical Measurements

H.1 Absorption and emission spectra

Initially investigations were carried out on the rigid *b*-P14·T6·(T4)$_2$ with three templates and *b*-P14 without any template. By referencing to three control samples for each of the porphyrin ball samples, we can compare photophysical properties of the ball complexes with those of their constituent 6 and 10 porphyrin rings (Figure S81). Reference samples for *b*-P14 are *c*-P6 and *c*-P10 and a mixture of both rings in 1:1 ratio; analogously *b*-P14·T6·(T4)$_2$ compared with *c*-P6·T6, *c*-P10·(T5)$_2$ and their mixture. However, because the geometric structure of *c*-P10·(T5)$_2$ demonstrates extensive out-of-plane bending and twisting which is not present in *b*-P14·T6·(T4)$_2$, *c*-P10·(T5)$_2$ is a poor reference sample for *b*-P14·T6·(T4)$_2$ especially with respect to investigations of polarization memory loss.
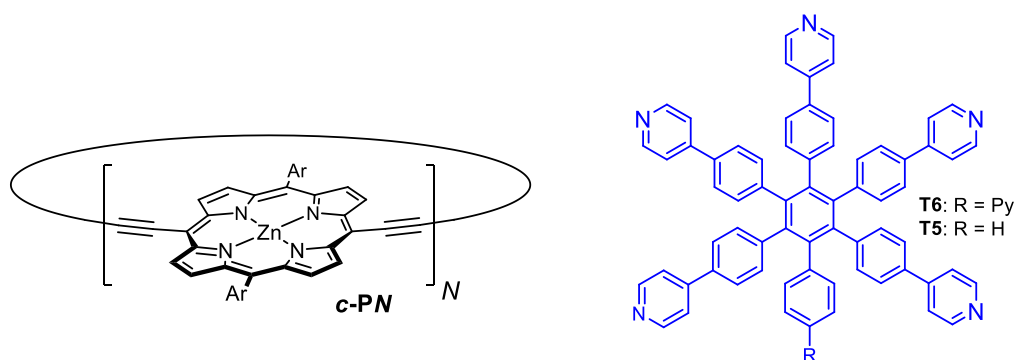
Figure S82 shows normalized absorption and emission spectra at room temperature for **b-P14·T6·(T4)₂** and **b-P14** together with those for their reference samples. The absorption spectra of porphyrin nanorings consist of a strong Soret band (400 - 550 nm) and a split Q band. The Q bands of both porphyrin ball structures are red-shifted with respect to those for their 6-ring and 10-ring reference samples, indicating a more rigid and conjugated conformation of the ball.[23] Further redshifts in the Q band maxima and a sharpening of both absorption and emission features are found in the molecules upon binding to templates as a result of a more rigid structure that is then adopted.[24] Analysis of the peak ratios of the three prominent features in the Q band in Figure S82(a) shows that the mixture **c-P6·T6** + **c-P10·(T5)₂** has a narrow and intense peak at the long-wavelength end due to contribution of **c-P10·(T5)₂**, whereas features attributed to **c-P6·T6** dominate at the short-wavelength end. In comparison, porphyrin ball **b-P14·T6·(T4)₂** demonstrates a sharpening and red shift in the Q band features, but still adopts a similar peak ratio as the mixture **c-P6·T6** + **c-P10·(T5)₂**. This observation suggests that with longer excitation wavelength in the Q band region, absorption into a **c-P10·(T5)₂**-like state increasingly dominates over absorption into the **c-P6·T6**-like state. For **b-P14** on the other hand, because the Q band of its reference samples are broadly overlapping and lack distinct features, a clear separation of contributions is difficult. By examining the emission spectra in Figure S82, it becomes apparent that emission features from both reference mixtures are largely dominated by **c-P10/c-P10·(T5)₂** components, most likely because the fluorescence quantum yield of those components is almost an order of magnitude larger than those of **c-P6/c-P6·T6**.[25]
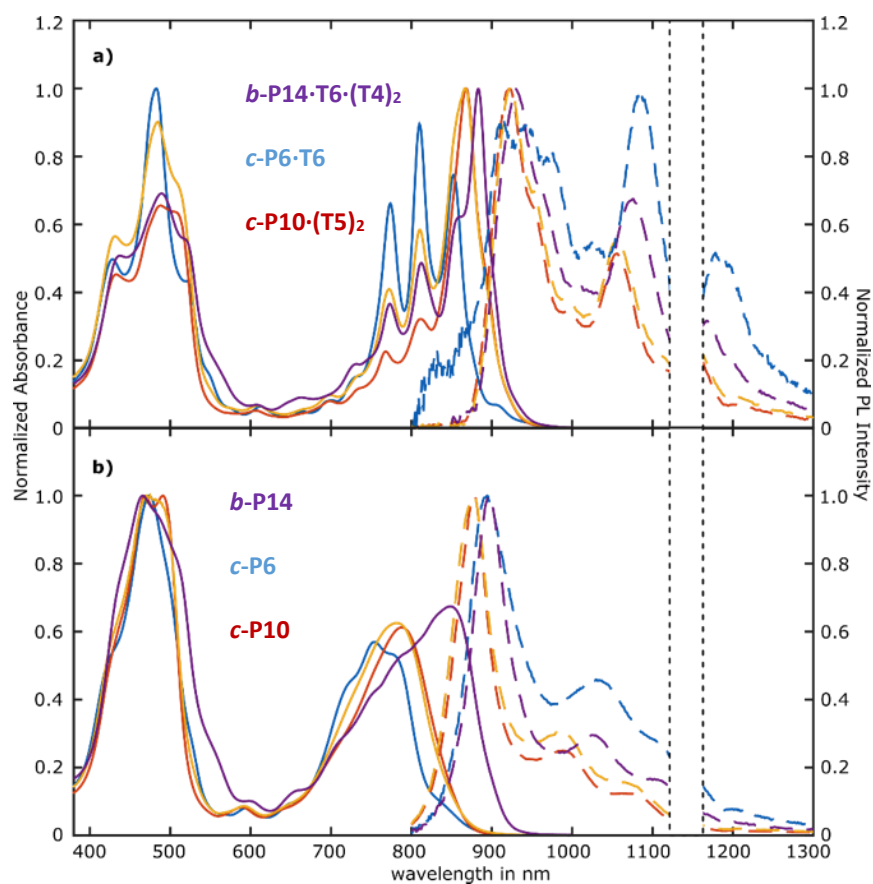
Figure S82 (a) Normalized absorbance (solid line) and PL intensity (dashed line) of *b*-P14·T6·(T4)₂ (purple), *c*-P6·T6 (blue), *c*-P10·(T5)₂ (red) and control mixture *c*-P6·T6 + *c*-P10·(T5)₂ (yellow); **(b)** normalized absorbance (solid line) and PL intensity (dashed line) of *b*-P14 (purple), *c*-P6 (blue), *c*-P10 (red) and control mixture *c*-P6 + *c*-P10 (yellow). Data points between dotted vertical lines at 1120-1160 nm in the PL intensity spectrum are excluded because of solvent absorption effects.

H.2 Photoluminescence anisotropy

The photoluminescence (PL) upconversion technique was engaged to investigate the PL and anisotropy dynamics of sample solutions held in quartz cuvettes. An excitation pulse was generated by a mode-locked Ti:Sapphire laser with pulse duration of 100 fs and a repetition rate of 80 MHz. PL is collected and optically gated in a beta-barium-borate (BBO) crystal by a vertically polarized time-delayed gate beam. The upconverted signal, which consists of sum-frequency photons from the gate pulse and the vertical component of the PL, was collected, dispersed in a monochromator and detected using a nitrogen-cooled CCD. Using a combination of a half-wave plate and a Glan-Thompson polarizer, the polarization of the excitation pulse was varied and the PL intensity dynamics were recorded separately for components polarized parallel ($I_{||}$) and perpendicular ($I_{\perp}$) to the excitation pulse polarization as shown in Figure S83 (a)-(c). The PL anisotropy is defined using

$$\gamma = (I_{||} - I_{\perp})/(I_{||} + 2I_{\perp})$$

and calculated from the measured components. The full-width-half-maximum of the instrumental response function was measured to be 270 fs, which gives the time-resolution limit of the system. The concentration of the sample solutions was on the order of 10^{-4} M. To achieve a good signal-to-noise ratio and comparability, the detection wavelength was chosen to be 900 nm for all the samples and kept constant for all excitation wavelengths.

For *b*-P14·T6·(T4)₂, the PL anisotropy is found to be constant at $\gamma = 0.02 \pm 0.01$ within at least the first 20 ps after excitation as shown in Figure S83 (d). *b*-P14·T6 and *b*-P14, however, exhibit a fast initial drop in anisotropy within the first 4 ps from $\gamma = 0.1$ to near zero which remains constant thereafter within the observation window of the first 20 ps after excitation (Figure S83 e, f). In a solution of randomly oriented molecules, an anisotropy value of $\gamma = 0.1$ is expected for complete depolarization of an excited state transition dipole moment within a 2D plane, e.g. for a cyclic porphyrin ring structure with an exciton delocalized over the entire ring.[26,27] If, on the other hand, the emission transition dipole moment is always oriented perpendicular to polarization direction of the absorbing state, $\gamma = -0.2$ is expected.[26,28] Because the porphyrin ball possesses two ring planes with perpendicular orientations, contributions from these two effects may yield an anisotropy value close to zero. The almost complete polarization memory loss therefore suggests that an excitation can access any segment on the ball complex.

The fast initial drop resembles the anisotropy decay dynamics of large porphyrin nanorings with n>24 porphyrin units that has previously been observed.[27] The initial anisotropy of 0.1 suggests that upon excitation, an exciton is delocalized over a full ring and both absorption and emission transition dipoles are polarized in this ring plane. After ultrafast relaxation, the exciton localizes and migrates rapidly around the entire porphyrin ball complex. Contributions from emission components polarized in both planes thus result in the low anisotropy value close to zero. Due to the lack of templates, an exciton may be initially more localized in *b*-P14 and *b*-P14·T6, resulting in the initial observed anisotropy drop, whereas *b*-P14·T6·(T4)₂ reaches the low anisotropy within the time resolution of the system.

To obtain a representative value for the PL anisotropy, ten PL intensity values were independently recorded at 5 ps delay after excitation for each polarization direction, averaged and the equation above was applied. This process was repeated several times for a range of excitation wavelengths between 760 nm and 880 nm. The anisotropy values were averaged and presented in Table S14. The reference sample *c*-P6·T6 and the mixture *c*-P6 + *c*-P10 exhibit anisotropy values of about 0.1, as expected for a ring system sustaining delocalized excitations.[27] *c*-P10·(T5)₂ demonstrates a somewhat lower anisotropy, because it adopts a twisted geometry with out-of-plane bending which is not present in the rigid

b-P14·T6·(T4)$_2$; this anisotropy-lowering effect has been extensively investigated, as reported in the literature.[24]

Table S14: PL anisotropy of porphyrin balls and reference samples 5 ps after excitation.

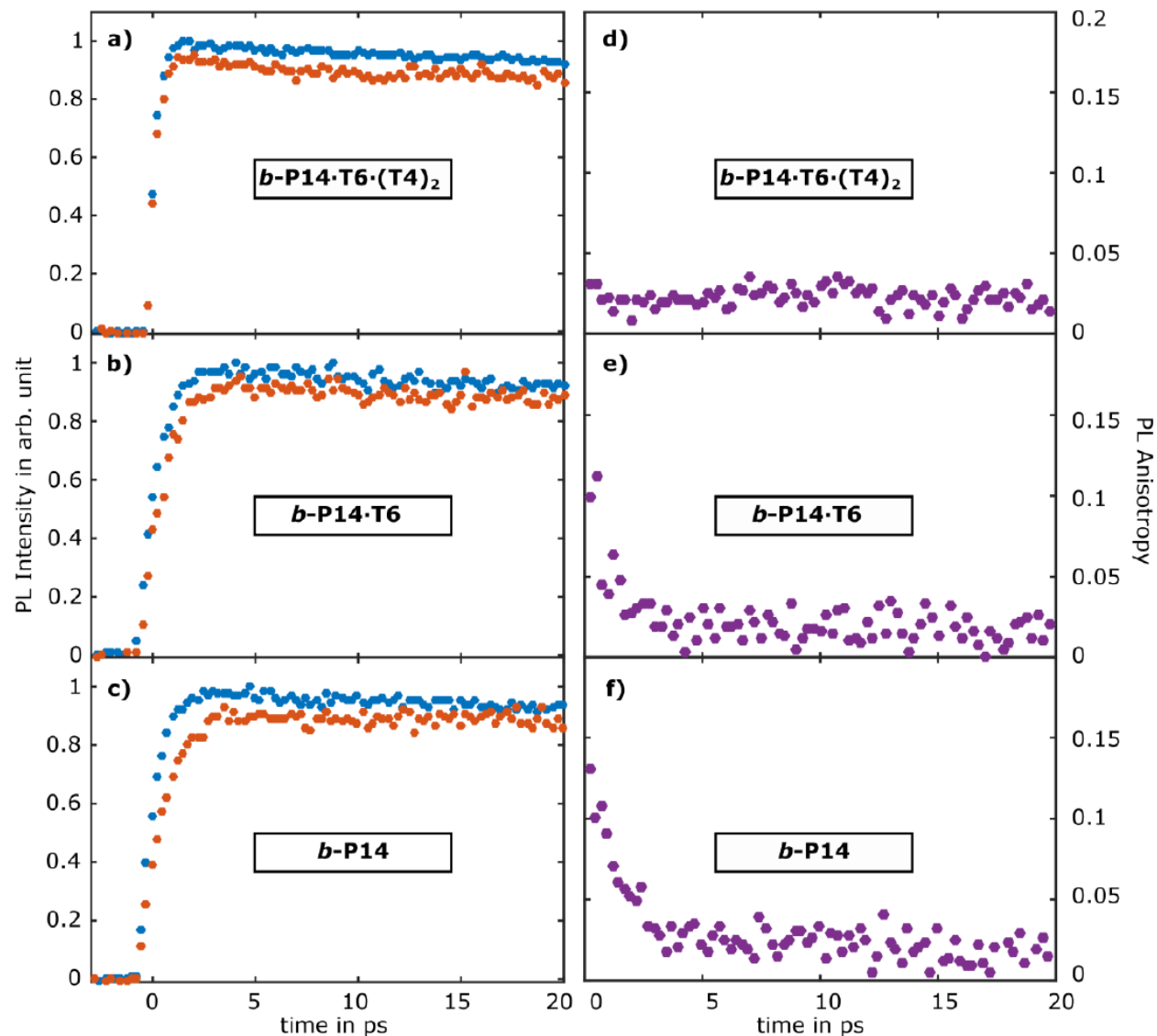| Sample	PL anisotropy
b-P14·T6·(T4)$_2$	0.02 ± 0.01
c-P6·T6	0.10 ± 0.01
c-P10·(T5)$_2$	0.05 ± 0.02
b-P14	0.03 ± 0.01
c-P6 + *c*-P10	0.11 ± 0.01
b-P14·T6	0.03 ± 0.01

Figure S83 (a)-(c) PL decay dynamics of *b*-P14·T6·(T4)$_2$, *b*-P14·T6 and *b*-P14 in toluene for emission polarized parallel (blue) and perpendicular (red) to that of the excitation laser pulse. (d)-(e) PL anisotropy dynamics derived from PL intensities. Samples were excited at 820 nm and the PL was detected at 950 nm.

I. References

(1) Favereau, L.; Cnossen, A.; Kelber, J. B.; Gong, J. Q.; Oetterli, R. M.; Cremers, J.; Herz, L. M.; Anderson, H. L. *J. Am. Chem. Soc.* **2015**, *137*, 14256.
(2) Gong, J. Q.; Favereau, L.; Anderson, H. L.; Herz, L. M. *J. Phys. Chem. Lett.* **2016**, *7*, 332.
(3) Parkinson, P.; Knappke, C. E. I.; Kamonsutthipaijit, N.; Sirithip, K.; Matichak, J. D.; Anderson, H. L.; Herz, L. M. *J. Am. Chem. Soc.* **2014**, *136*, 8217.
(4) Tait, C. E.; Neuhaus, P.; Peeks, M. D.; Anderson, H. L.; Timmel, C. R. *J. Am. Chem. Soc.* **2015**, *137*, 8284.
(5) Hogben, H. J.; Sprafke, J. K.; Hoffmann, M.; Pawlicki, M.; Anderson, H. L. *J. Am. Chem. Soc.* **2011**, *133*, 20962.
(6) Cremers, J.; Richert, S.; Kondratuk, D. V.; Claridge, T. D. W.; Timmel, C. R.; Anderson, H. L. *Chem. Sci.* **2016**, *7*, 6961.
(7) Hunter, C. A.; Anderson, H. L. *Angew. Chem. Int. Ed.* **2009**, *48*, 7488.

(8)   Benson, S. W. *J. Am. Chem. Soc.* **1958**, *80*, 5151.
(9)   Ercolani, G.; Piguet, C.; Borkovec, M.; Hamacek, J. *J. Phys. Chem. B* **2007**, *111*, 12195.
(10)   Peeks, M. D.; Claridge, T. D. W.; Anderson, H. L. *Nature* **2017**, *541*, 200.
(11)   Marques, H. M.; Cukrowski, I. *Phys. Chem. Chem. Phys.* **2003**, *5*, 5499.
(12)   Marques, H. M.; Cukrowski, I. *Phys. Chem. Chem. Phys.* **2002**, *4*, 5878.
(13)   Goldstein, E.; Ma, B.; Lii, J.-H.; Allinger, N. L. *J. Phys. Org. Chem.* **1996**, *9*, 191.
(14)   Jarowski, P. D.; Diederich, F.; Houk, K. N. *J. Org. Chem.* **2005**, *70*, 1671.
(15)   Frisch, M. J.; Trucks, G. W.; Schlegel, H. B.; Scuseria, G. E.; Robb, M. A.; Cheeseman, J. R.; Scalmani, G.; Barone, V.; Petersson, G. A.; Nakatsuji, H.; Li, X.; Caricato, M.; Marenich, A. V.; Bloino, J.; Janesko, B. G.; Gomperts, R.; Mennucci, B.; Hratchian, H. P.; Ortiz, J. V.; Izmaylov, A. F.; Sonnenberg, J. L.; Williams; Ding, F.; Lipparini, F.; Egidi, F.; Goings, J.; Peng, B.; Petrone, A.; Henderson, T.; Ranasinghe, D.; Zakrzewski, V. G.; Gao, J.; Rega, N.; Zheng, G.; Liang, W.; Hada, M.; Ehara, M.; Toyota, K.; Fukuda, R.; Hasegawa, J.; Ishida, M.; Nakajima, T.; Honda, Y.; Kitao, O.; Nakai, H.; Vreven, T.; Throssell, K.; Montgomery Jr., J. A.; Peralta, J. E.; Ogliaro, F.; Bearpark, M. J.; Heyd, J. J.; Brothers, E. N.; Kudin, K. N.; Staroverov, V. N.; Keith, T. A.; Kobayashi, R.; Normand, J.; Raghavachari, K.; Rendell, A. P.; Burant, J. C.; Iyengar, S. S.; Tomasi, J.; Cossi, M.; Millam, J. M.; Klene, M.; Adamo, C.; Cammi, R.; Ochterski, J. W.; Martin, R. L.; Morokuma, K.; Farkas, O.; Foresman, J. B.; Fox, D. J. *Gaussian 09, Revision D.01, software, Wallingford CT* **2013**.
(16)   Becke, A. D. *J. Chem. Phys.* **1993**, *98*, 5648.
(17)   Ditchfield, R.; Hehre, W. J.; Pople, J. A. *J. Chem. Phys.* **1971**, *54*, 724.
(18)   Hehre, W. J.; Ditchfield, R.; Pople, J. A. *J. Chem. Phys.* **1972**, *56*, 2257.
(19)   Hariharan, P. C.; Pople, J. A. *Theor. Chim. Acta* **1973**, *28*, 213.
(20)   Rassolov, V. A.; Pople, J. A.; Ratner, M. A.; Windus, T. L. *J. Chem. Phys.* **1998**, *109*, 1223.
(21)   Grimme, S.; Antony, J.; Ehrlich, S.; Krieg, H. *J. Chem. Phys.* **2010**, *132*, 154104.
(22)   Liu, S.; Kondratuk, D. V.; Rousseaux, S. A. L.; Gil-Ramírez, G.; O'Sullivan, M. C.; Cremers, J.; Claridge, T. D. W.; Anderson, H. L. *Angew. Chem. Int. Ed.* **2015**, *54*, 5355.
(23)   Rousseaux, S. A. L.; Gong, J. Q.; Haver, R.; Odell, B.; Claridge, T. D. W.; Herz, L. M.; Anderson, H. L. *J. Am. Chem. Soc.* **2015**, *137*, 12713.
(24)   Gong, J. Q.; Parkinson, P.; Kondratuk, D. V.; Gil-Ramírez, G.; Anderson, H. L.; Herz, L. M. *J. Phys. Chem. C* **2015**, *119*, 6414.
(25)   Yong, C.-K.; Parkinson, P.; Kondratuk, D. V.; Chen, W.-H.; Stannard, A.; Summerfield, A.; Sprafke, J. K.; O'Sullivan, M. C.; Beton, P. H.; Anderson, H. L.; Herz, L. M. *Chem. Sci.* **2015**, *6*, 181.
(26)   Valeur, B.; Berberan-Santos, M. N. *Molecular fluorescence: principles and applications* **2012** *John Wiley & Sons*.
(27)   Parkinson, P.; Kondratuk, D. V.; Menelaou, C.; Gong, J. Q.; Anderson, H. L.; Herz, L. M. *J. Phys. Chem. Lett.* **2014**, *5*, 4356.
(28)   Neuhaus, P.; Cnossen, A.; Gong, J. Q.; Herz, L. M.; Anderson, H. L. *Angew. Chem. Int. Ed.* **2015**, *54*, 7344.